THE INFLUENCE OF TEMPERING ON THE CORROSION RESISTANCE OF NEWLY DEVELOPED STEELS

by

K.J. JOUBERT

A thesis submitted to the Faculty of Engineering, University of Cape Town in fulfilment of the degree of Master of Science in Applied Science

Department of Materials Engineering, University of Cape Town

September 1988

THE INFLUENCE OF TEMPERING ON THE CORROSION RESISTANCE OF NEWLY DEVELOPED STEELS

K.J.JOUBERT

ABSTRACT

This thesis deals with the effect of heat treatment on the localized corrosion resistance of the low carbon, chromium containing steels, designated 825, 102A and 122 which recently have been developed.

The potentiodynamic polarization technique has been employed to determine the corrosion characteristics of the three steels. The results do not accurately reflect the effect heat treatment has on corrosion rates but scanning electron microscopy of corroded surfaces does allow a characterization.

Both tempering temperature and time at temperature have a significant influence on the corrosion behaviour of chromium steels because the type, size and morphology of carbide precipitates are determined by the temperature and time of tempering.

Localized pitting corrosion predominates for specimens tempered at temperatures below 450°C. Intergranular corrosion together with general corrosion occur after tempering at temperatures in excess of 450°C. The results of hardness tests show that secondary hardening occurs after tempering between 450°C and 600°C. Secondary hardening suggests the presence of chromium carbides which deplete the surrounding matrix of chromium leaving it susceptible to active general corrosion (within the grains) and intergranular corrosion (at grain boundaries).

A model showing the effect that 12% chromium, in comparison to 8% chromium, has on the corrosion resistance, is proposed.

The significance of these results with regard to the application of the steels is discussed.

ACKNOWLEDGEMENTS

I wish to express my appreciation to all who assisted me during the course of this research project, in particular:

Professor A Ball, my supervisor, for his advice;
Mrs P Park-Ross for her invaluable experimental assistance and support;
Mr N Dreze, Mr G Newins and Mr R Hendricks for their technical expertise in the workshop;
Mr B Greeves and Mr J Petersen for their photographic expertise;
Mrs J Geldenhuys, Mrs AC Ball and Mrs H Bohm for their help in the preparation of the final manuscript;
Dr K Barker and Dr D Howarth for their advice;
the staff and my fellow students for their support and encouragement.

The work described in this thesis is part of the collaborative research and development programme of the Research Organisation of the Chamber of Mines of South Africa.

CONTENTS

CHAPTER 1

INTRODUCTION

1.1 MOTIVATION

The cost of mining and processing gold-bearing ore is escalating continually. Conditions in the gold mines are such that severe abrasion and corrosion of equipment occurs resulting in considerable maintenance and replacement costs. Hidden costs include down-time and repetitive replacement of worn parts (Protheroe (1979)).

There is presently a move away from the labour intensive mining methods to mechanized systems. The success of these mechanized mining systems will depend on an overcoming of the effects of severe wear and corrosion on the reliability and economic life of the equipment (Protheroe (1979)). Substantial savings can be achieved by correctly choosing and using available and new materials.

Previous investigations have shown the importance of understanding wear mechanisms (Allen, Protheroe and Ball (1981)), of understanding the role played by corrosion (Noel (1981)) and have highlighted the importance of the composition and microstructure of a steel to be used under these conditions (Harris (1983)).

1.2 THE APPROACH TAKEN TO MATERIALS SELECTION

Protheroe, Ball and Heathcock (1982) recognized the following factors as being important when developing a new alloy for gold mining purposes:

1) A minimum surface hardness of 500HV is a prerequisite because quartzite, the matrix within which gold exists, has a hardness of between 900 and 1300HV.

2) A toughness which would provide a resistance to crack propagation and a Charpy impact energy of at least 30J was specified.

3) Adequate corrosion resistance which dictates a minimum chromium content of greater than 10%.

4) An ability to undergo simple heat treatments and so enable the hardness and toughness to be attained.

5) Desirable fabrication characteristics.

6) The cost should be kept as low as possible.

A range of commercial materials is readily available but none of these materials has yet proved adequate in meeting the combination of requirements. In consequence, an alternative approach through microstructural design has been developed. New alloy compositions have been formulated under the auspices of the Chamber of Mines Research Organisation (COMRO) of South Africa to provide the necessary operational and economic benefits (Protheroe, Ball and Heathcock (1982); Allen, Ball and Noel (1984); Bee, Peters, Atkinson and Garrett (1985)).

These steels are resistant to both corrosion and abrasion and may be utilised universally for pipe work, conveyance systems and machinery.

1.3 OBJECTIVES

This alloy development programme requires testing and evaluation of the new materials as well as an understanding of the mechanisms which control their behaviour. Collaborative work is being done on these new steels to ascertain their properties in different microstructural conditions and under differing abrasive and corrosive conditions. This dissertation assesses the pitting corrosion behaviour of these steels after different tempering treatments.

The specific objectives are:

1) To evaluate, using the potentiodynamic scanning technique, the corrosion performance of three of the new development alloys, designated Alloy 825, Alloy 102A and Alloy 122, in a standard mine water. This involves the definition of the predominant mode of corrosion and an evaluation of pit initiation sites and pit density.

2) To define the optimum heat treatment for these three alloys when exposed to this specific environment. Heat treatment considerations include decarburization and sensitization.

3) To evaluate the corrosion rate of Alloys 825, 102A and 122 after different tempering treatments.

1.4 CONDITIONS WITHIN THE MINES

The principle factors promoting corrosion in underground mines are high relative humidity (90%), high ambient temperature (30°C) and airborne dusts. The mine service-water used in the gold mines may be extremely corrosive. The concentrations of various substances in the water in the dissolved, colloidal or suspended states are low but vary considerably. Table 1.1 summarizes the levels at which important factors are present in mine waters in South African gold mines.

TABLE 1.1 Important constituents in mine waters and the levels at which they are present.

FACTOR	LEVEL/(Concentration in ppm)
Chloride concentration	50 - 2000
Nitrate concentration	50 - 1500
Sulphate concentration	100 - 2000
Dissolved oxygen	Generally saturated
Presence of oxidizers	Traces of Fe^{3+} and Cu^{2+}
Microbes	Suspected to be present
Temperature	30°C average
pH	4 - 9

The following factors can be summarized as the factors affecting the corrosivity of mine waters: -

a) Dissolved gases: These include oxygen, nitrogen and carbon dioxide. The concentration of oxygen has a strong influence on the rate of corrosion. The corrosion rate of iron in water is found to drop to a low value below a certain critical concentration of oxygen. The corrosion effects due to oxygen are much increased in water at low pH.

b) Organic Matter: The types of organic matter vary widely and are found in suspension, or in colloidal or true solution. Very rapid rates of corrosion of mild steel may result when abstracted organic acids are present in water.

c) Microbial Matter: Bacterial action on metals has been classified into the following types (Moreau and Brison (1972)):

   1) those that inhibit corrosion,

   2) those that cause limited attack, and

   3) those that catalyse corrosion reactions.

Thiobacillus produces sulphuric acid, which increases the corrosivity of the water through the oxidation of sulphur. Ferrobacillus ferro-oxydans are usually present with thiobacillus and can cause the accelerated oxidation of pyrite at low pH values. This increases the corrosivity of the water.

These factors will not be taken into account in this thesis.

CHAPTER 2

LITERATURE SURVEY

2.1 INTRODUCTION

Corrosion can be defined as the reaction of a metallic material with its environment. For most metals, corrosion is a result of the metal seeking its energetically preferable state which is the combined oxide state for all non-precious metals. Corrosion of most metals is therefore inevitable and corrosion prevention all but impossible.

Almost all metals, with the exception of gold and to a lesser extent silver, owe much of their usefulness to the existence of a passive state. Passivity is defined by the American Society of Testing and Materials (ASTM G15) as the state of a metal surface characterized by low corrosion rates in a potential region that is strongly oxidising for the metal.

The passive layer in stainless steels is chromium rich and, for the layer to form, a minimum of 12% chromium is required in the alloy. The corrosion resistance of stainless steels is undermined by localised breakdown in the form of pitting and crevice corrosion. It is therefore important to establish the conditions under which pitting occurs.

2.1.1 Basic Electrochemistry and Thermodynamics

Aqueous corrosion is predominantly an electrochemical process combining anodic oxidation, e.g. metal dissolution producing metal ions, and a cathodic reduction, such as oxygen ionization or discharge of hydrogen ions (based on tneories by U.R. Evans and C. Wagner (Sato (1987)).

For corrosion to occur, there must be a negative change in free energy (G).

$$G_{rxn} = G_{red} - G_{oxid}$$

2.1.2 E-pH Diagrams

Pourbaix has summarised the electrochemical conditions for aqueous systems by plotting electrochemical (E-pH) diagrams. Fig. 2.1 represents the two predominant reduction reactions involved in aqueous corrosion - the hydrogen evolution reaction (H.E.R.) and the oxygen reduction reaction (O.R.R.) which may also be expressed by the following equations:

a) H.E.R.

$2H^+ + 2e \longrightarrow H_2$

$E^\circ = 0.00 - 0.59pH$

b) O.R.R.

$O_2 + 4H^+ + 4e \longrightarrow 2H_2O$

$E^\circ = 1.228 - 0.691pH$

Above line b) the evolution of oxygen takes place, below line a) hydrogen evolution occurs and between lines a) and b) water is predicted to be stable (Pourbaix and de Zoubov (1966)).

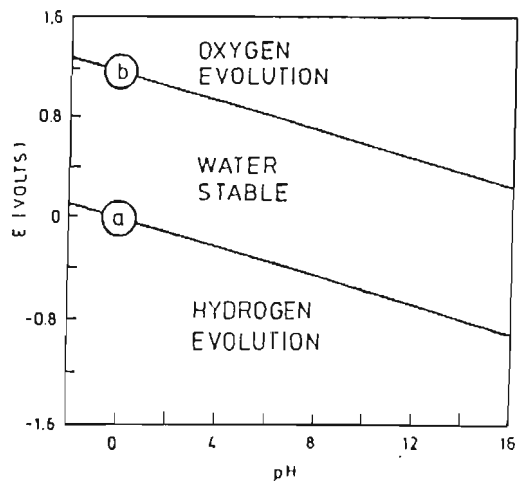

FIGURE 2.1 : Electrochemical equilibrium diagram (E/pH diagrams) for water.

Equilibrium thermodynamics can be used to determine whether or not a particular corrosion reaction is likely to occur. However, if the reaction is shown to be possible, thermodynamic data give no indication whatsoever of the reaction rate. For this, a consideration of electrochemical kinetics is required.

2.1.3 Kinetics of Corrosion

When in equilibrium, the rate of reduction, r_{red}, equals the rate of oxidation, r_{oxid}, and the current flowing is known as the exchange current density, i_o. i_o is related to r_{oxid} and r_{red} by the following equation:

$$r_{oxid} = r_{red} = i_o/nF$$

where i_o = exchange current density
n = number of electrons
F = Faraday's constant

There is no nett current flow and the electrode is at its equilibrium potential, E_{corr}.

As a result of a current flow, the potential of the cathode becomes less positive or more negative, and the potential of the anode less negative or more positive; the anodic and cathodic reactions are said to become mutually polarized. The amount of polarization is referred to as the overpotential.

2.1.4 The Anodic Kinetics of Stainless Steels

Electrochemical techniques have been developed that are capable of defining the conditions under which a given metal environment system is likely to exhibit pitting (Sedricks (1979)). A schematic polarisation curve illustrating the anodic dissolution of a typical stainless steel is shown in fig. 2.2.

The polarization scan begins in the cathodic region where the specimen is polarized to a potential more active than the free corrosion potential, E_{corr}, of the specimen. On increasing the applied potential in the noble direction from E_{corr} the current density increases to a maximum, referred to as the primary passivation potential (E_{pp}), during which time active dissolution of the metal occurs. On further increasing the potential, the current decreases to a minimum known as the passive current density (i_{pass}) and remains at this low value over a wide range of potentials.

The potential range over which the current remains at this low value is termed the passive potential range, and it is this range which defines passivity for a given stainless steel/environment combination. The potential at which the passive layer becomes stable is known as the Flade potential, E_F. On continuing to increase the applied potential in the noble direction, another potential will be reached at which the measured current will again begin to increase - this is known as the breakdown potential, E_b. At this potential, the oxide layer is transformed to a soluble species and the current increases due to transpassive corrosion (Sedricks (1979)). If pitting occurs, the passive film will breakdown at a lower potential E_p, known as the pitting potential.

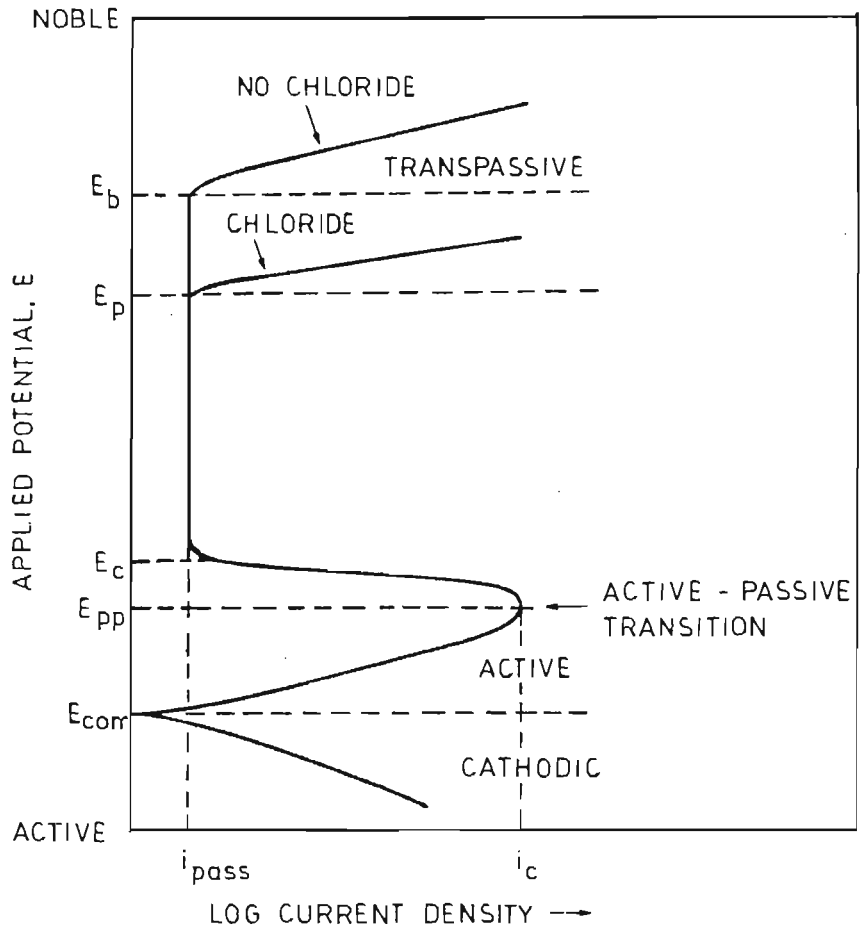

FIGURE 2.2 : A schematic polarization curve for a stainless steel showing passivity in a sulphuric acid solution (Sedricks (1984)).

If localized breakdown by pitting corrosion does occur, reversal of the scan after a specified current density is reached, causes a hysteresis loop to form. The loop meets the passive region of the polarization scan at the protection potential, E_{prot}. The protection potential is the potential below which pits repassivate, and therefore will no longer propagate.

2.2 PITTING CORROSION

Although pitting is well-known as one of the most common forms of corrosion, it remains one of the most difficult forms of corrosion to predict and guard against completely. This is partly because the susceptibility to pitting generally depends upon a combination of alloy composition and environmental conditions but also because small and minor changes in both these compositions and the metal surface integrity may have a major influence on both the initiation and propagation of pitting attack. (Man and Gabe (1981)).

2.2.1 Mechanisms of Pitting Corrosion

The mechanisms proposed by previous workers indicate two main stages:

a) initiation or nucleation of pits on the passivated metal
b) propagation or growth of micropits already formed.

An intermediate stage is the repassivation of the incipient pit or micropit. (Dawson and Ferreira (1985)).

a) Pit Initiation

Kruger and Rhyne have recently reviewed pitting and crevice corrosion and concluded that the following conditions are necessary for the initiation of localized corrosion by pitting:

1) A critical potential, E_p, usually called the pit nucleation or pitting potential must be exceeded. There also exists a critical protection potential, E_{prot}, which is more active than E_p. Corrosion, once initiated, cannot be stopped at potentials more noble than Eprot.

2) Aggressive species, particularly the chloride ion, must be present.

3) There must be an induction period separating the initiation of the breakdown processes, by the introduction of conditions conducive to breakdown, and the completion of the process when pitting commences.

4) There must be breakdown of the surface at localized sites.

Oldfield (1987) proposed four general models which satisfy the above requirements:

I Adsorbed Ion Displacement Model

In this model anionic species such as chloride ions are adsorbed onto the passive film, either singly or in groups, and compete with oxygen in the film. According to Kolotyrkin (1961), pits develop on the spots where oxygen, adsorbed on the metal surface, is displaced by chloride ions. Because the metal surface is not completely homogeneous, an irregular distribution of current does exist on the surface. This allows certain spots to adsorb chloride ions more strongly and hence a more rapid dissolution will occur at these spots. According to this theory the breakdown potential represents the minimum electrode potential value at which the aggressive anions become capable of producing a reversible displacement of the passivating oxygen from the metal surface.

Hoar and Jacob (1967) suggested that this process involves 3-4 chloride ions which jointly adsorb on the oxide film surface around a lattice cation with the resultant formation of a transitional complex of high energy and low probability of formation. Once formed, the complex separates from the film and the cation goes into solution. At increasing potentials more noble than the critical pitting potential, the rate at which the accumulation of chloride ions can occur is accelerated and the induction time for pitting correspondingly reduced.

The inhibitive effect of anions such as hydroxides, nitrates, sulphates and chlorates is explained by the competitive adsorption

theory. The more easily an anion is adsorbed onto the passive surface, and the higher its affinity for the metal surface, the more effectively it will exclude chloride ions and exhibit pitting.

II Ion Migration and Penetration Model

These models assume that anions penetrate the passive film, breakdown being complete when the anion reaches the metal/film interface. These models range from those which assume the existence of pores in the passive film to those which assume penetration by migration through a pore-free film. Heine, Kerr and Pryor (1965) and Hoar, Mears and Rothwell (1965) proposed models falling into this category.

Hoar, Mears and Rothwell assumed that the initiation of pits might be due to the adsorption of aggresive anions on the surface of the oxide film followed by the penetration of ions through the film. The chloride ions are concentrated at certain selected areas such as grain boundaries, dislocations, inclusions and other areas where rapid exchange and substitution is expected. Those areas where chloride concentration is highest will allow metal ions to pass through into solution and thus the oxide layer at that point will be susceptible to enhanced dissolution. The metal ions, on going into solution, will decrease the pH of the area, if they precipitate as hydrated metal oxides. This can cause the localized attack to become macroscopic and the process to become autocatalytic.

III Breakdown-Repair Model

This group is concerned with the chemically induced mechanical disruption of the passive film. The local acidification model in which breakdown occurs via electrochemical or mechanical means,followed by hydrolysis of metal ions to give a reduction in pH, and the salt film model, where a non-protective salt film is formed where the film breaks down, are included in this model.

Hoar (1967) presumes that during anion adsorption of water, molecules are replaced and this causes the lowering of the interfacial tension on the oxide-solution interface by the mutually repulsive forces between charged particles. Eventually the

interfacial tension is so far lowered that a peptization by interfacial charge occurs - the adsorbed anions push one another and the oxide to which they are strongly adsorbed causing slip and forming cracks which then form the nuclei of pits. Any crack or split so produced in the film immediately gets further anions adsorbed on its sides, so that the process is progressive.

Galvele (1976) proposed a model in which hydrolyzing metal ions cause local acidification which leads to the breakdown of passivity. As early as 1937, Hoar proposed a mechanism of "autocatalytic" pit propagation, which considered that the main cause of pitting was the drop of pH inside the pit. The pitting potential is defined as the minimum potential at which localized acidity can be maintained inside the pit. This potential can be reached in pits as small as 10^{-6}cm. This means that a crack in the passivating oxide film would give a diffusion path long enough to reach the critical pH. Such cracks do exist. Galvele is able to explain the effect of aggressive anion concentration, non-aggressive anion concentration, external pH, presence of weak acid salts and alloying elements on pitting through his model.

IV Stochastic Models

In these models pit initiation is treated as a random event, which in some cases leads to a stable pit being established. Williams, Westcott and Fleischmann's (1984) model incorporates both the breakdown-repair model and the stochastic model as does Frankel, Stockert, Hunkeler and Boehni (1987). They used peak counting, passage time, spectral density, ensemble statistics and slope distribution analysis to obtain information. Based on the results, they assumed pitting to be an unpredictable process with regard to the time of initiation and the place of attack. Pits will only be stable if they survive after a critical age.

Oldfield (1987) notes that although the stochastic model can explain many of the observed phenomena, there is no single model which links the stochastic approach to the fundamental models.

Frankel, Stockert, Hunkeler and Boehni (1987) introduce the idea of metastable pits occurring below E_p. Metastable pitting transients exhibited by stainless steels in chloride-containing solutions have a characteristic shape, as displayed in fig. 2.3. The current increases above the background passive current as the pit nucleates and begins to grow. After a short growth period the metastable pits repassivate and the current quickly decreases to the level of the original passive current. The lifetime of these metastable pits can be as long as 15 seconds, but is typically less than 5 seconds. Metastable pits are covered by a porous layer which is a remnant of the passive film. If these covers rupture to form openings, metastable pits repassivate. However, if the pit cover remains intact for a period long enough to allow for salt film precipitation on the pit surface, pit growth is stabilized.

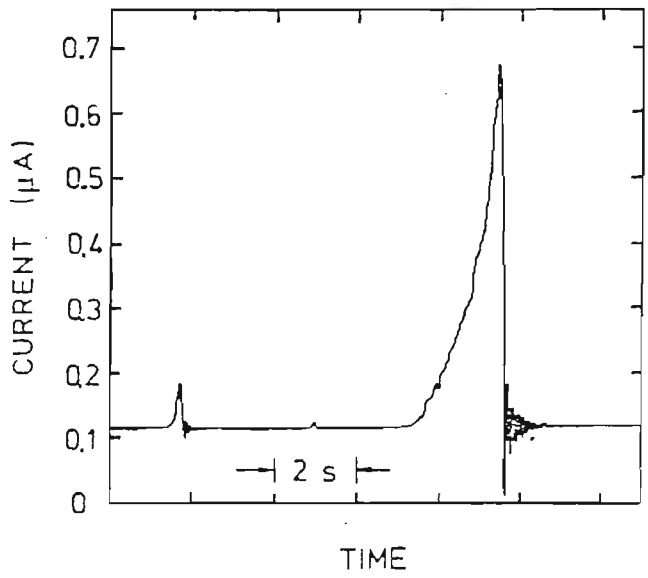

FIGURE 2.3 : Metastable pitting current transients observed on 302 stainless steel in 0.1 M NaCl at 420 mV S.C.E. (Frankel, Stockert, Hunkeler, Boehni (1987)).

b) Pit Propagation

Theories involving pit propagation concern geometry, mass transfer and reaction kinetics. Oldfield (1987) divides the various pit propagation models into three groups.

I Metal Dissolution Hydrolysis

This approach considers the dissolution and hydrolysis of metal ions as a function of pH and potential, and compares them with the Hydrogen Evolution Reaction (H.E.R.).

In Galvele's model (1976) a potential is defined at which the rate of production of hydrogen ions via hydrolysis is equal to their rate of consumption via the H.E.R. Below this potential, passivation is maintained; above it, repassivation does not occur. Galvele proposed that the pH inside the pit has a composition quite different from the bulk solution. He proposes that the bulk solution acts as a supporting electrolyte for the metal ions and the hydrolysis products produced during pit initiation. He concludes that pitting can be explained by transport phenomena and that processes like competitive adsorption, salt formation and film contamination, even though present during the pitting process, do not play a major role in fixing the pitting potential.

II Salt Layer Formation

This model assumes that a highly resistive film, probably a salt film, exists on a growing pit's surface.

Frankenthal and Pickering (1972) found two different types of pits existed on stainless steels in a chloride environment. The first type of pit was not associated with inclusions whilst the second was. The pits associated with inclusions had a lace-like cover which eventually dissolved leaving a large open pit. The pits associated with the inclusions grew to almost any size, whilst those not associated with inclusions became repassivated early in their history. They explained this difference by suggesting that enhanced diffusion and convection in the more open, inclusion-free pits prevent the solution from becoming sufficently concentrated in chloride ion solution and/or hydrogen ion to sustain pitting; thus repassivation occurs. Conversely repassivation is less likely to occur in the covered pits and crevices. In addition, their highly concentrated solutions could be responsible for the absence of crystallographic structure because a viscous layer or a precipitate that limits the dissolution may form.

Vetter and Strehblow (1970) consider this layer to be formed by the cations of the metal and the aggressive ion. The film is considered to be dense and poreless and the rate of pit growth is equivalent to the rate of salt film dissolution.

The work by Frankel et al(1987) already mentioned also assumes the existence of this salt layer.

III Mass Transfer Control

Corrosion in this group of models is thought to be controlled by the mass transfer of species in and out of the pits. Although mass transfer by migration can occur, the assumption is usually made that mass transfer is by diffusion only.

2.2.2 Factors Affecting Pitting Corrosion

According to Oldfield (1987), alloy composition, passive film characteristics, electrochemical reactions, mass transport, bulk solution composition and geometry all play an important role in pitting corrosion.

a) Alloy Composition

The main effect of alloy composition is that it controls the stability of the protective film. Once propagation commences it is the alloy composition and its dissolution characteristics which determine the maximum rate of corrosion.

b) Passive Film Characteristics

The stability of a passive film determines an alloy's inherent resistance to pitting and crevice corrosion. Hultquist and Leygraf (1981) found the resistance to initiation of crevice corrosion increased approximately linearly with the chromium content of the protective film. Thus, the composition of the passive film, too, is important as is surface finish, heat-treatment and cold working.

c) Bulk Solution Environment

Temperature, flow rates and volume effects are all important aspects of pitting corrosion. Chance, Schreiber and Francis (1975) found the corrosion rates generally increased with temperature. However, there were some interesting exceptions, such as iron in oxygenated water and zinc in distilled water; in both cases a corrosion rate maximum occurs. On studying the effects of temperature on type 409 stainless steel he found that the corrosion rate increased up to 49°C but thereafter decreased radically until a low value was reached at 65°C which was essentially unaffected by temperature up to 90°C. From this it was concluded that the nature of the protective film changes with temperature.

d) Bulk Solution Composition

The ingredients of the bulk solution, such as chloride ion level, pH, pollutants and oxygen level determine its basic corrosivity.

1) Effect of Chloride Ions

The decrease in the pitting potential with increased chloride ion concentration is a well documented fact as illustrated by fig. 2.2. Mankowski and Szklarska-Smialowska (1975) found that the concentration of chloride ions within the pits was much higher than that in the bulk solution. Szauer and Jakobs (1976) found a higher inclination to pit formation in alloyed steels in corrosive environments containing chlorides. They found that when the amounts of chloride ion solution were small, the tendency of the examined steels to pitting attack was more dependent on metallurgical factors such as metal composition and texture. When the corrosive environment contained higher amounts of chlorides, corrosion attack was determined more by the aggressiveness of the solution. Lee et al (1981) proposed a general diagram of the effect of chloride ions on a carbon steel (Fig. 2.4).

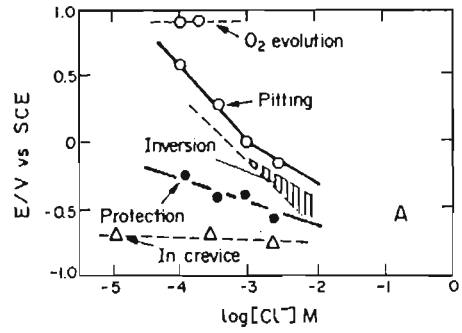

FIGURE 2.4 : The pitting, inversion and protection potentials of a carbon steel as a function of the bulk concentration of chloride ions (Lee et al (1981)).

Janik-Czachor (1981) showed, too, that E_p decreased as the concentration of aggressive ions Cx^- increased. He found the decrease depended upon the particular anion.

Atrens (1983) too found that both the pitting potential and the protection potential varied with the logarithm of the choride ion concentration in a 12% Cr martensitic stainless steel in chloride solutions at 80°C.

2) Effect of Sulphate Ions

As cited by Chance, Schreiber and France (1975), Shatalov et al showed that corrosion rates increased with temperature in solutions with relatively high concentrations of sulphate; by contrast, Florianovich (1965) found a maximum corrosion rate with temperature in solutions with relatively low concentrations of sulphate. From this, Chance et al (1975) reasoned that sulphate ions contributed to the corrosion rate-temperature phenomenon differently at different concentrations and temperatures.

It is generally accepted, however, that sulphates reduce the tendency to pitting when in a chloride environment (Sedricks 1979). Fig. 2.5 illustrates work done by Man and Gabe (1981) on the effect of sulphate concentration on the pitting potential of 317L, 316, 304 and a high alloy stainless steel in 3% NaCl solution.

Greater ennobling occurred with higher molybdenum content of the steel. In this particular solution the inhibitive effect of the sulphate was not particularly pronounced.

However, in work done by Palumbo et al (1987) on Alloy 800 (45.9 wt % Fe, 29.1 wt % Ni, 22.8 wt % Cr and balance Al, Ti and Si) in a chloride sulphate media the effect was most pronounced. Work done by Cotterell (1988) too substantiates this as illustrated in fig. 2.6.

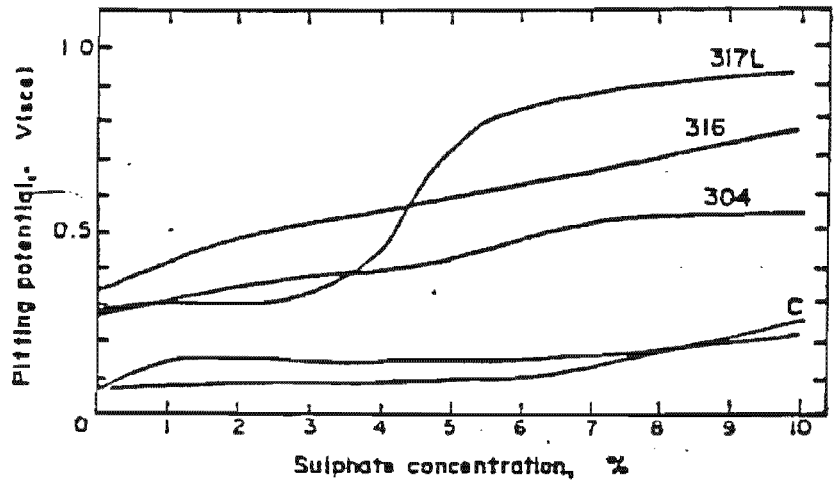

FIGURE 2.5 : Effect of sulphate concentration (%) on the pitting potential of steels in NaCl solutions. C refers to a high alloy steel. (Man and Gabe (1981)).

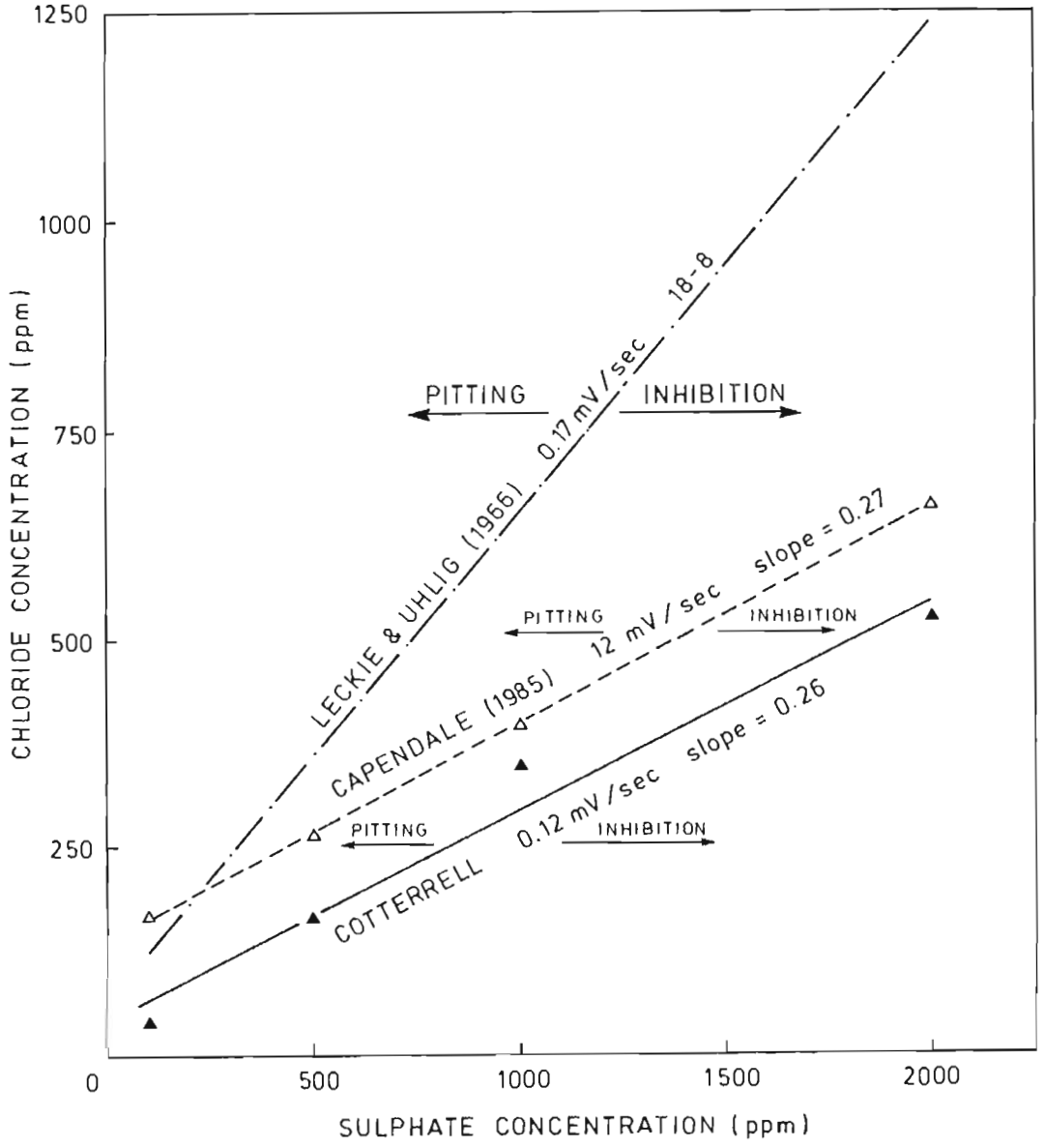

FIGURE 2.6 : Chloride concentration plotted as a function of sulphate concentration. (Cotterrell (1988)).

e) Heat Treatment

Work done by Truman and Pirt (1976) on a 13% Cr steel showed that there was a loss of corrosion resistance with certain tempering temperatures due to the precipitation of chromium carbides at the grain boundaries. This causes a depletion in the chromium adjacent to the grain boundaries and so increased attack occurs in this region. A review of the relevant work follows.

2.2.3 The Influence of Metallurgical Aspects on Pitting

2.2.3.1 Microstructural Changes through Tempering

On quenching a steel containing between 0.1% and 1.0% C, martensite is formed. The martensite transformation is a diffusionless transformation during which carbon and other alloying elements remain locked in the positions they occupied in the parent austenite (Chadwick (1972)). This results in a supersaturated metastable structure, with much internal stress. On tempering there is therefore a strong driving force for precipitation to occur.

TABLE 2.1 : Summary of the various changes which occur during the tempering of ferrous martensites at temperatures up to 700°C. (Porter and Easterling (1980)).

Temperature/°C	Transformation	Remarks
25–100	Carbon segregation to dislocations; pre-precipitation clustering	Clustering predominant in high-carbon steels
100–250	Epsilon-carbide precipitation (first stage of tempering)	May be absent in low-carbon, low-alloy steels
200–300	Retained austenite transforms to bainite (second stage)	Occurs only in medium-carbon and high-carbon steels
250–350	Lath-like Fe_3C precipitation (third stage)	
400–600	Recovery of dislocation substructure. Lath-like Fe_3C agglomerates to form spheroidal Fe_3C	Lath structure maintained
500–600	Formation of alloy carbides. (secondary hardening or fourth stage)	Occurs only in steels containing Ti, Cr, Mo, V, Nb, or W; Fe_3C may dissolve
600–700	Recrystallization and grain growth; coarsening of spheroidal Fe_3C	Recrystallization inhibited in medium-carbon and high-carbon steels; equiaxed ferrite formed

2.2.3.2 Alloying Elements and Tempering

If there are no carbide formers, low carbon steels soften rapidly with increasing tempering temperatures. This softening is due to rapid coarsening of cementite with increasing temperature which removes carbon from the martensite matrix, a process dependent on the diffusion of carbon and iron. Carbide formers not only retard softening after tempering at lower temperatures but also form fine alloy carbides that produce a hardness increase after tempering at higher temperatures (500° to 600°C) - known as secondary hardening. These secondary hardening peaks develop only at high temperatures because alloy carbide formation is dependent on the diffusion of the carbide-forming elements. As a result, not only is a finer dispersion of particles produced, but once formed, the alloy carbides are quite resistant to coarsening (Krauss (1980)). Fig. 2.7 illustrates the effect of increasing the alloy content on secondary hardening during tempering of steels with various molybdenum content.

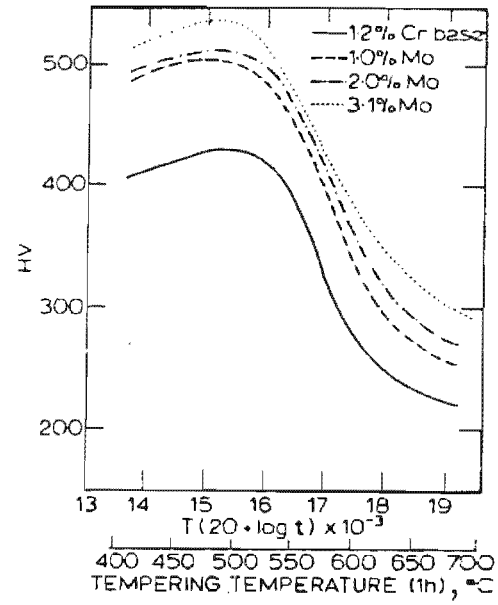

FIGURE 2.7 : Retardation of softening and secondary hardening during tempering of 0.1% C, 12% Cr steels with various molybdenum contents (Pickering (1978)).

The effectiveness of the carbides as strengtheners depends on the fineness of the dispersion and the volume fraction precipitated. Elements in order of their tendency to form carbides, are Mn<Cr<W<Mo<Va<Ti. (Reed-Hill (1964)).

2.2.3.3. The Effect of Carbides on Corrosion

Payer and Staehle (1975) reported on the behaviour of $Cr_{23}C_6$ in AISI 304 stainless steels. They found that in the temperature range 450° to 850°C, precipitation of carbides was promoted. The presence of the chromium carbides in grain boundaries rendered the alloy more susceptible to intergranular corrosion. This phenomenon is also known as sensitization. However, on comparing the polarization behaviour of AISI 304 steel in the sensitized and stabilized state, the chromium carbide had no significant effect upon it as shown in fig. 2.8. They thus concluded that anodic polarization curves could not be used as a test for sensitization and therefore could not be used as a measure of the change in corrosion rates when carbides were involved.

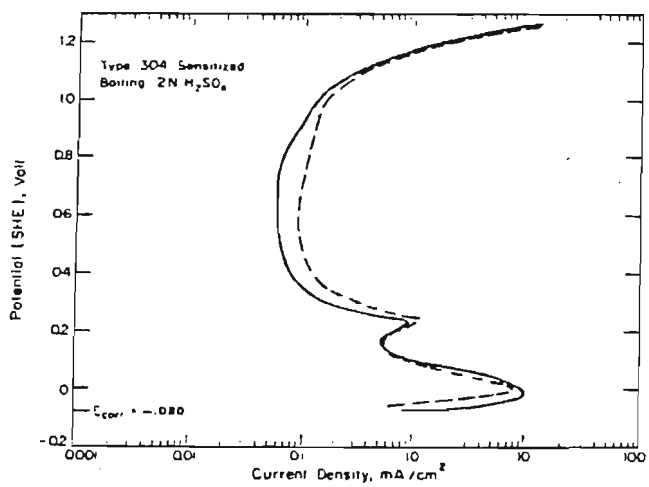

FIGURE 2.8 : Anodic polarization curve for sensitized steel in boiling 2N H_2SO_4, (101°C). Dashed curve for solution treated AISI 304 steel (Payer and Staehle (1975)).

Truman (1976) did work on the corrosion resistance of 13% Cr steels as influenced by tempering treatments. He found, by weight loss tests, that a maximum corrosion rate existed on tempering between 560°C and 600°C (2.5 hr tempers in aerated tap water) as illustrated in fig. 2.9.

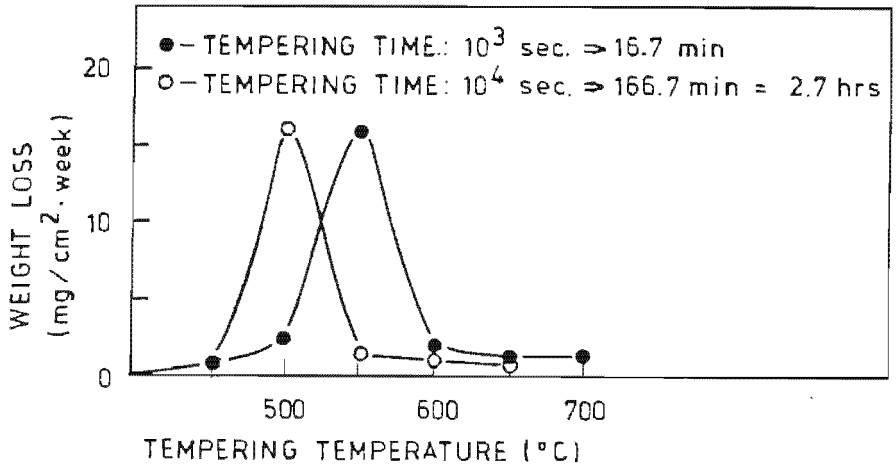

FIGURE 2.9 : The corrosion rate after tempering at various temperatures (of a 13% Cr steel) (Truman (1976)).

He proposed three reasons for the loss of corrosion resistance within a certain tempering temperature range, all involving precipitated carbides. Truman's first hypothesis involves the formation of iron carbides which themselves have poor corrosion resistance. Progressive selective attack could occur, for instance, if there was a cluster of iron carbides, resulting in a maximum loss of corrosion resistance. Increasing the time of treatment or treating at higher temperatures leads to spheroidization and, in some cases, alters the iron carbide to a chromium-rich carbide and thus increases the corrosion resistance. This hypothesis therefore does not take the resulting matrix into consideration but only the type of carbide.

Truman's second hypothesis proposed that the carbides are chromium-rich and therefore more resistant to corrosion than the surrounding matrix. Here it is proposed that the chromium carbides are more noble than the surrounding matrix, which acts as the cathode, and thus selective attack occurs adjacent to the matrix. This mechanism therefore takes the relative polarity of the carbide and matrix into account.

The third mechanism also proposes that the carbides causing reduced corrosion resistance are chromium-rich but that the decrease in corrosion resistance is due to the reduction in chromium immediately adjacent to the growing carbides resulting in chromium-depleted zones. Selective corrosion can result if the distribution and morphology of the carbides is such that their zones of influence overlap, for example, because of especially dense precipitation along the prior-austenite grain boundaries. This latter mechanism is very similar to that accepted as giving rise to intergranular cracking with austenitic stainless steels.

Devine, Ritter and Drummond (1981), when discussing the influence of heat treatment on the sensitization of 18Cr-2Mo-Ti stabilized ferritic stainless steel found that during low temperature ageing (550°C),(Ti,Cr)(C,N) grew and a chromium depleted zone was created adjacent to the grain boundary precipitates which caused the alloy to become susceptible to severe intergranular cracking. During longer time ageing treatments, chromium is rejected from the grain boundary $M_{23}C_6$ into the chromium depleted zone. Chromium also diffuses from the matrix into the grain boundary depleted zone and susceptibility to intergranular cracking is removed. A paper by Devine and Ritter (1983) substantiates the results.

Tomlinson and Giles (1983) found the corrosion rate from weight loss measurements, followed qualitatively the surface area of the carbide in a 0.79C alloy tempered in the range 100° - 700°C. It was supposed that the corrosion rate was related to the carbide area at the alloy/solution interface available for the reaction. A maximum corrosion rate was found in the range 200° - 500°C.

Lee, Cragnolino and MacDonald (1985) experimented on the effect of heat treatment on the caustic cracking of Inconel 600. Fig. 2.10 shows the development of carbides from the solution annealed treatment through to a temperature of 700°C for 24 hours. Increasing the length of the heat treatment time at 700°C changed the carbide precipitation

morphology at the grain boundaries from thin and semi-continuous to thick and cluster-like, and also induced precipitation inside the grain, which is clearly noticeable after heat treatment of 10 hours.

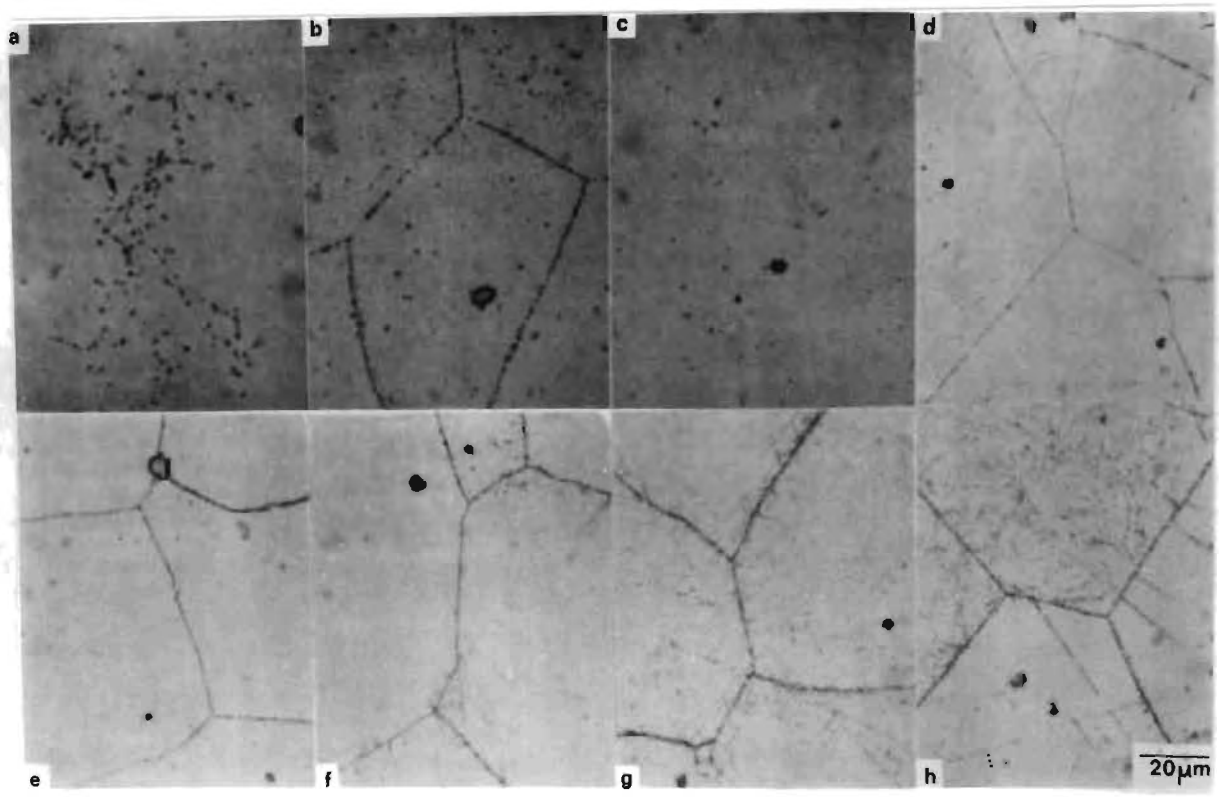

FIGURE 2.10 : Carbide precipitation in Inconel 600 (phosphoric acid etch):

a) as received (ML);
b) annealed at 1100°C for 1 hour;
c) annealed at 1200°C for 15 minutes (SA);
d) SA + 700°C, 20 min.;
e) SA + 700°C, 1 hour;
f) SA + 700°C, 3 hours;
g) SA + 700°C, 10 hours;
h) SA + 700°C, 24 hours (Lee, Cragnolino and MacDonald (1985)).

Grobler and Mostert (1988) did work on the effects of tempering temperature on Alloy 927. It was found that with increasing tempering temperature, hardness values gradually dropped and then increased at 500°C where secondary hardening took place. Further increases in tempering temperature caused a substantial lowering in hardness as illustrated in fig. 2.11. To ascertain the influence of tempering on corrosion resistance, salt spray and potentiodynamic testing in simulated mild and aggressive mine waters was carried out. It was found that for a tempering time of 1 hour, tempering temperatures higher than 600°C caused a marked drop in corrosion resistance (fig. 2.11). It was found that above 500°C M_2C and M_7C_3 carbides over-age rapidly and are mostly replaced by the equilibrium carbide $M_{23}C_6$ at temperatures above 600°C. The precipitation, growth and coarsening of alloy carbides such as $M_{23}C_6$ are associated with partitioning of carbide-forming alloying elements such as chromium and molybdenum to the carbide. A depletion of the ferrite martrix of these elements therefore takes place, leading to a lower corrosion resistance.

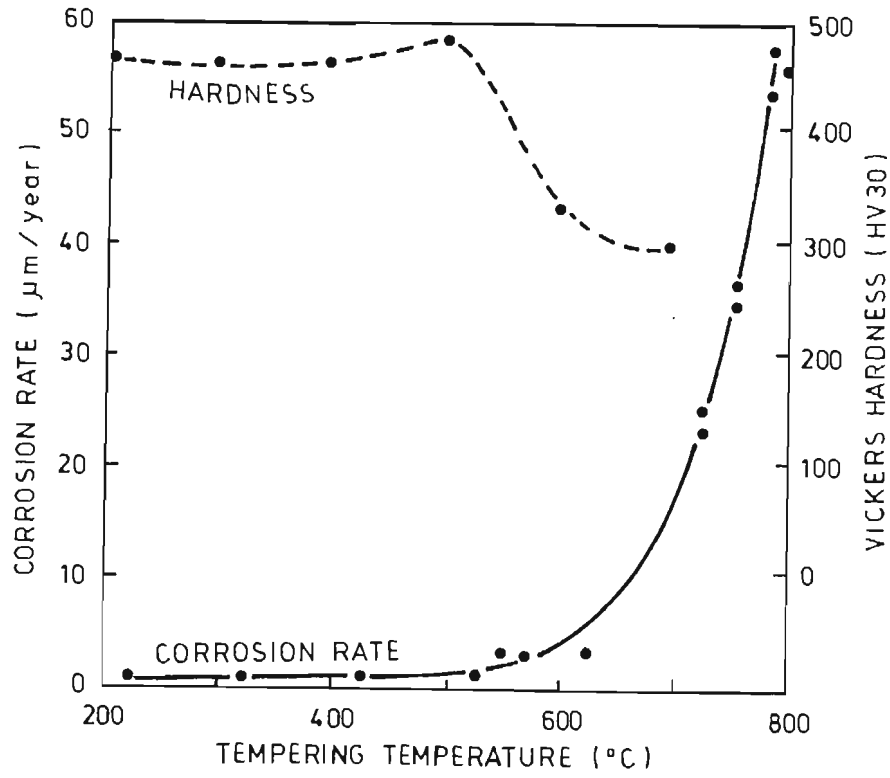

FIGURE 2.11 : Corrosion rate and hardness as a function of tempering temperature in simulated mine water. Samples temperd for 1 hour (Grobler and Mostert (1988)).

2.2.3.4 The Influence of Non-Metallic Inclusions on the Pitting Corrosion Resistance

Residual impurities from steel making practices can often have a pronounced effect on the corrosion resistance of the product. Sedricks (1984) notes that manganese sulphide inclusions are the most favourable sites for pit initiation in stainless steels.

Wilde and Armijo (1967) found that as the sulphur content increased, the corrosion rate increased thus substantiating what had been reported.

Scotto, Ventura and Traverso (1979) found that pitting attack on austenitic stainless steels always nucleated on sulphides and mixed inclusions. It was postulated that the dissolution of these sulphides was necessary but not sufficient for pit nucleation. The probability of pit nucleation was thought to be influenced by the shape of the inclusions and not only by their composition. Frankenthal and Pickering (1972) suggested that those pits not associated with inclusions do not grow to an appreciable size due to the pit cavity being exposed to the bulk solution which facilitates the repassivation of the steel. Section 2.2.1b discussed this concept more fully.

2.2.3.5 The Effect of Solid Solution Alloying

a) Chromium

Stainless steels basically derive their passive characteristics from alloying with chromium. Much work has been done in order to decrease the chromium content as chromium has been identified as one of the materials which are classified in the critical material shortage category. However, decreasing the chromium content has a definite detrimental effect on the corrosion resistance of a material.

Brigham (1975) used the critical pitting temperature (C.P.T.) as a basis for evaluation of the quantitative effects of chromium additions. The C.P.T. is defined as that temperature below which pitting will not initiate and above which pits will initiate. Brigham found that chromium additions in the 18-26% range produce a dominant and progressive beneficial effect on the pit initiation resistance of austenitic stainless steels.

Hashimoto et al (1979) found that the amount of chromium necessary for spontaneous passivation was dependent upon the base metal and metalloid. It was found that an increase in the chromium content of an alloy leads to a continuous increase in the corrosion potential and chromium content in the surface film and to a continuous decrease in the anodic current density. Thus the addition of chromium moves E_{pp} in the active direction therefore increasing the passive potential range. Once the chromium content of the alloy reaches a certain amount, spontaneous passivation takes place.

Chen and Stephens (1979) found that incrementally reducing the chromium content in 304 stainless steels from the normal 18% level to approximately 8% had a marked influence on the shape of the s-shaped potentiodynamic anodic polarization curves shown in fig. 2.12. In particluar, I_c increases over two orders of magnitude as a result of this chromium reduction.

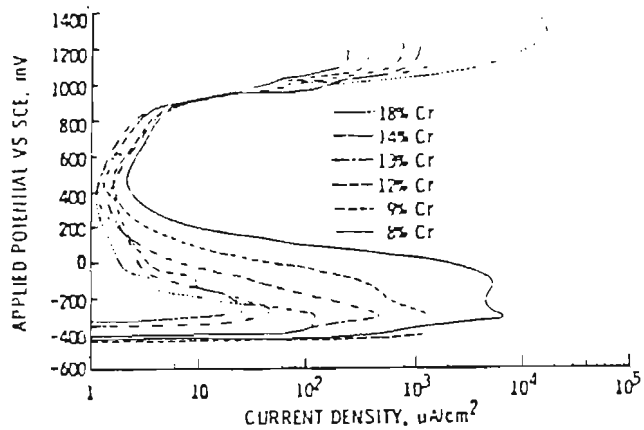

FIGURE 2.12 : Effect of Cr content on potentiodynamic anodic polarization curves of Cr modified 304 stainless steel alloys in H_2SO_4. (Chen and Stephens (1979)).

b) Molybdenum

It is well known that for a given chromium content in a stainless steel the addition of molybdenum has a strong beneficial influence on passivity (fig. 2.13). Molybdenum moves the pitting potential in the noble direction thereby extending the passive potential range. The mechanism of the combined effect of molybdenum and chromium is still a problem to be clarified (Yang, Ni and Hua (1984)).

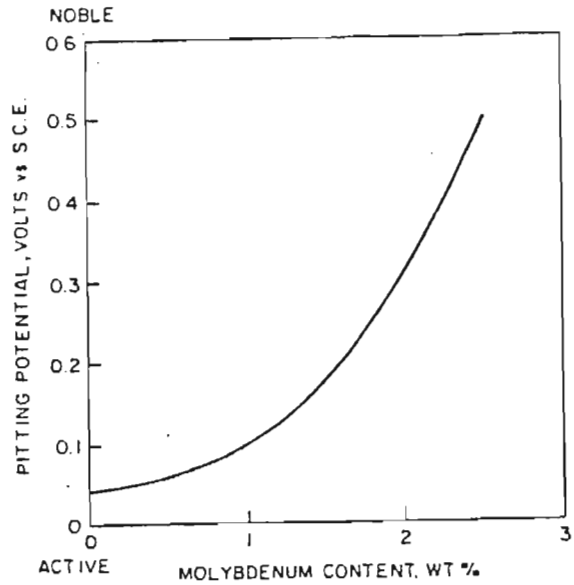

FIGURE 2.13 : Effect of molybdenum content on pitting potential of Fe-15Cr-13Ni alloys in a deaerated 0.1N NaCl solution at 25°C. (After Horvath and Uhlig as cited by Sedricks (1979).

It is clear that molybdenum and chromium act co-operatively; for below a certain chromium content molybdenum ceases to be beneficial and may indeed be detrimental. Molybdenum, nevertheless, appears to play a different role to chromium in that it does not so unambiguously enter the passive film. X-ray proton spectroscopy work found molybdenum in passive films, but significantly molybdenum does not appear in the fully developed passive film at high potentials. It was thus postulated that molybdenum had a transitory presence in the film during a critical stage of the latter's formation (Wanklyn (1981)).

c) Other Alloying Elements

Among other elements that move the pitting potential in the noble direction thereby extending the passive potential range are nickel, vanadium, silicon and tungsten. The effects of the various alloying elements are shown in fig. 2.14.

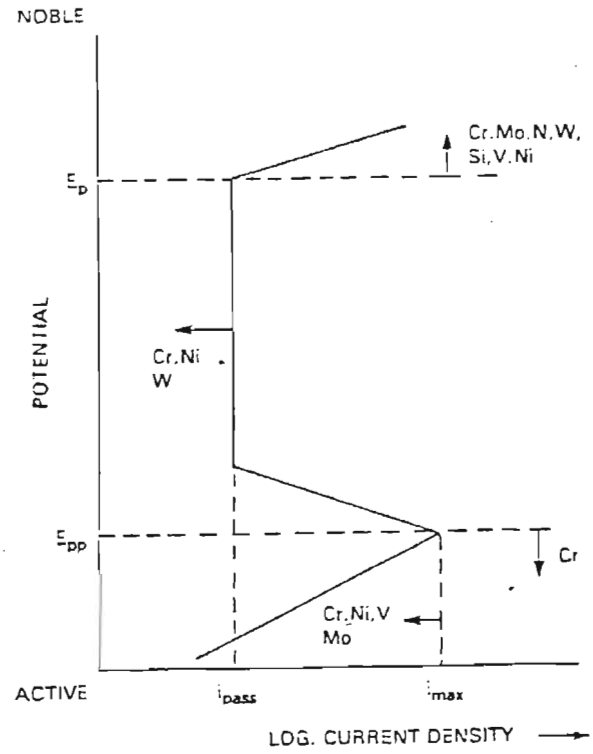

FIGURE 2.14 : Schematic summary of the effect of alloying elements in stainless steels on the anodic polarization curve. (Sedricks (1984)).

CHAPTER 3

EXPERIMENTAL TECHNIQUES

3.1 SPECIMEN PREPARATION

For each alloy a single bar of material was used in order to prevent any variation in composition. The bar, which was 15.8mm in diameter, wassoaked at 1100°C for 15 minutes in a Naber box-type furnace which has a volume of 11 litres and a temperature range of up to 1100°C. After being oil-quenched, the bars were then sectioned into 4mm thick disc-shaped specimens. These specimens were then ground on silicon carbide pads and one of each alloy tempered at tempering temperatures ranging from 150°C to 600°C with 50° intervals for two hours. A double tempering treatment involved repeating this process. Finally the specimens were polished to a 3μm diamond finish. The diamond polish finish ensured a smooth surface which allowed easier microscopic examination of the corroded surface. Once polished, the specimens were degreased in an ultrasonic bath.

3.2 SPECIMEN MOUNTING TECHNIQUES

Capendale(1985) considered the following three techniques for specimen mounting during potentiodynamic testing:

a) Hot mounting resin.
b) Heat shrunk polytetrafluoroethylene (P.T.F.E.).
c) Compression gasket specimen holder.

The three techniques have the following in common:

1) 1 cm^2 of specimen is exposed allowing easy determination of current density ($\mu A/cm^2$).
2) The specimen is the only reactive surface.
3) The specimen can be re-used by removing any surface corrosion effect by regrinding and repolishing.

Capendale (1985) found crevice corrosion to be a serious problem when applying techniques a) and b) due to the cleaning technique which requires the whole mount to be polished as one unit.

The compression gasket specimen holder technique, however, enables the removal of the specimen which can then be polished and cleaned independently of the mounting medium. Crevice corrosion did occur using this technique but was not as serious and was often the result of a worn P.T.F.E. gasket. This technique, too, allowed for easy access to the specimen for microscopic viewing and was thus selected as the specimen holder for specimen mounting. The Stern-Makrides gasket recommended by the ASTM Standard G5-78 (ASTM (1980) was regarded as being impractical due to the difficulty involved in specimen manufacture and polishing.

Cotterrell (1988), too, selected to use the compression gasket specimen holder to allow direct comparison with Capendale's work. This technique was selected for specimen mounting by the author as it has been found to be the most suitable technique for comparative work and is shown in fig. 3.1.

The holder is made from crystalline polyester to provide rigidity while P.T.F.E. is used for the circular gasket and bolt. A seal is created between the gasket and specimen on tightening.

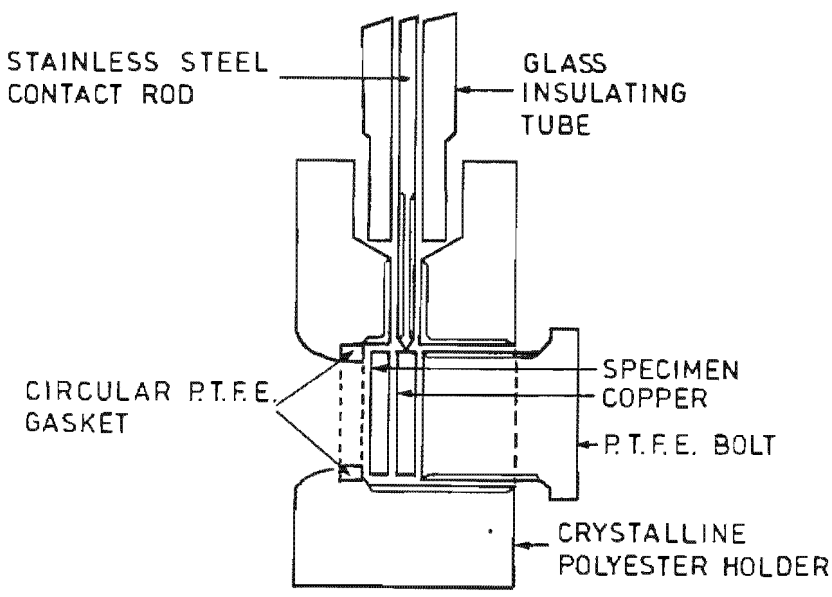

FIGURE 3.1 : The compression gasket specimen holder.

3.3 PREPARATION OF SOLUTIONS

Analytical reagent grade chemicals were used at all times to ensure accuracy and consistency. Caution was taken to avoid any contamination of the solution and the cleaning procedures were stringent. Solutions were prepared in 20 litre batches in order to avoid any variation in a specific series of tests. A constant pH was maintained and monitored by a Schott Gerate pH meter.

The simulated mine water used in all experimental work consisted of:

$CaCl_2$	1040mg	665ppm Cl^-
Mg_2SO_4	200mg	409ppm SO^{2-}_4
NaCl	1375mg	834ppm Cl^-
Na_2SO_4	1215mg	821ppm SO^{2-}_4

Thus a total of 1500ppm Cl^- and 1200ppm SO^{2-}_4 ions were present in the solution which was aerated, held at a neutral pH and kept at ambient temperature (30°C).

3.4 INSTRUMENTATION

Two self-contained potentiostat testing systems were utilised to obtain polarization experiments.

3.4.1 E.G. and G. Princeton Applied Research Potentiostat

An E.G. and G. Princeton Applied Research Model 173 potentiostat/ galvanostat was used for the polarisation experiments. Conversion of current density to logarithm of current density was performed by a Model 376 logarithmic convertor. The reference electrode, a saturated calomel electrode, (S.C.E.), was monitored by a Model 178 electrometer probe. Two high density non-permeable graphite rods were used as the counter electrode and an alloy specimen as the test electrode. A Model 178/41 noise filter eliminated the possible pick-up of noise in the power lines at the cell. Potentiodynamic scanning was accomplished by an Elscint Model ABA-26 external baseline automatic advance. The potential and logarithm of the current were plotted using a Houston Omnigraphic S-200 X-Y plotter.

Figure 3.2 shows the instrumentation used during testing.

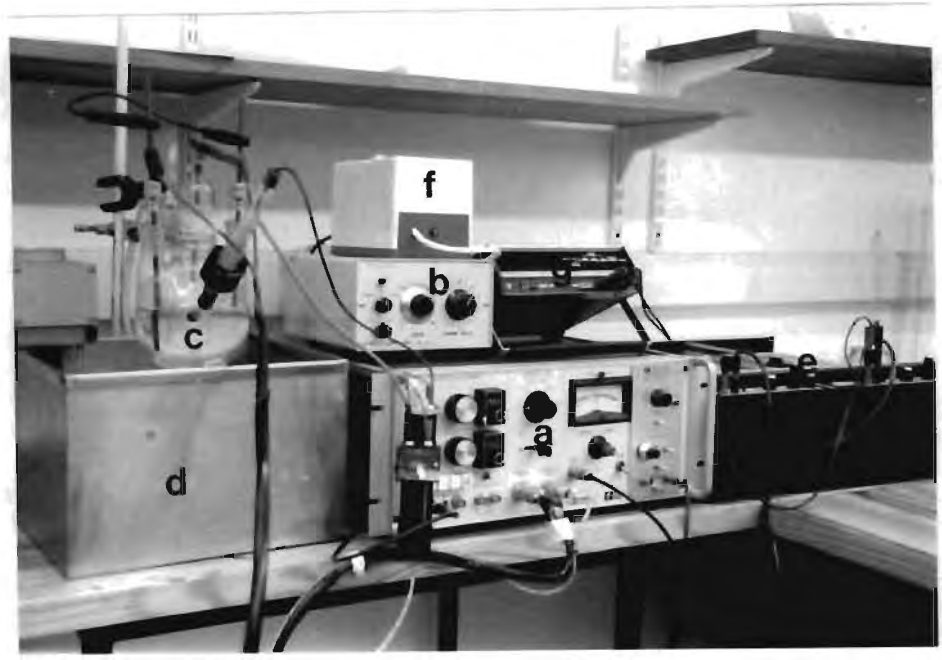

FIGURE 3.2 : A photograph of the Princeton potentiodynamic testing instrumentation showing a) potentiostat and logarithmic current convertor, b) scan generator, c) corrosion flask, d) thermoregulated water bath, e) X-Y recorder, f) automatic switch-off trigger g) the voltmeter.

3.4.2 Wenking Model LT-78 Potentiostat

A Wenking Model LT-78 potentiostat was used for determining free corrosion versus time scans. The current output from the potentiostat was a voltage which is proportional to the current scale selected, and ranges from -200mV to +200mV. This voltage is amplified using a 20dB gain and a Philips Model PM5171 amplifier/logarithmic convertor obtains the logarithm of the amplified signal. The resulting output, for this particular application, was to an EPR-200A Electron Polyrecorder which records voltage (mV) against time. A scan rate of 2cm/hr is maintained. A Standard Calomel Electrode was used as the reference electrode. Figure 3.3 shows the Wenking instrumentation.

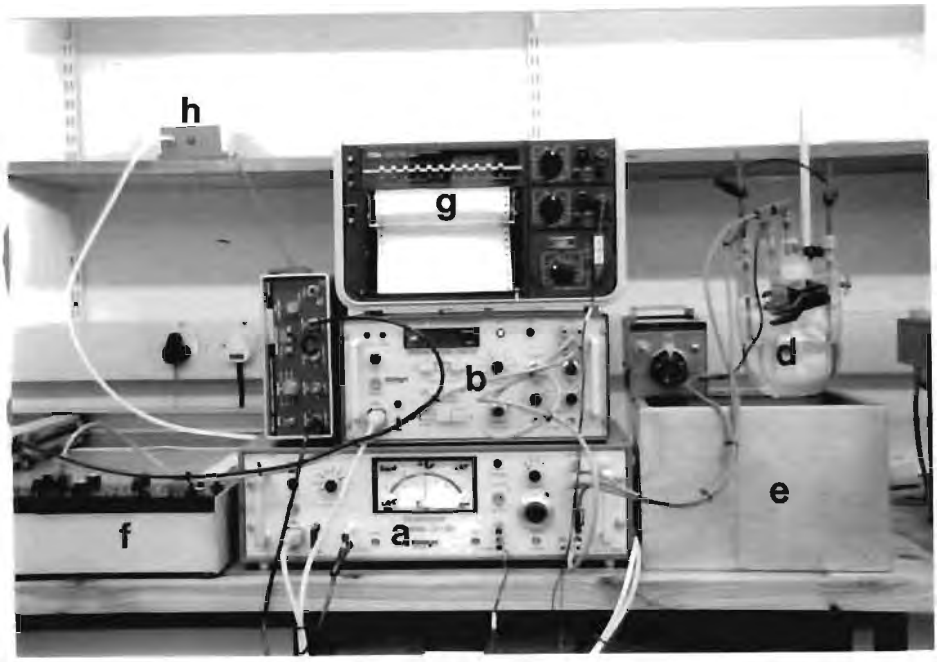

FIGURE 3.3 : A photograph of the Wenking poteniodynamic polarization testing equipment showing:

a) potentiostat, b) scan generator,
c) logarithmic current convertor,
d) corrosion flask, e) thermoregulated water bath,
f) X-Y recorder, g) two pen recorder,
h) the automatic switch-off trigger.

3.4.3 The Corrosion Cell

The same corrosion cell was used for both systems, based on the Princeton Applied Research Cell. All experiments were conducted in the glass corrosion flask which provides reproducible conditions from one experiment to another to allow a rational comparison between specimens and/or environments to be drawn. A saturated calomel electrode was used as a reference electrode - it has a potential of 0.241V with reference to the standard hydrogen electrode.

3.4.4 Dilatometry

A dilatometer was used to obtain the transformation temperatures Ms, the martensite start temperature, Mf, the martensite finish temperature, Al, the reaustenite start temperature and A3, the reaustenite finish temperature, of the three alloys. These transformation temperatures were determined from the onset of a discontinuity in a plot of thermal expansion versus temperature for both the heating and cooling cycles. The heating rate was 3°C/min and cooling was effected by switching off the furnace. The cooling rate varies with temperature as is illustrated in fig. 3.4.

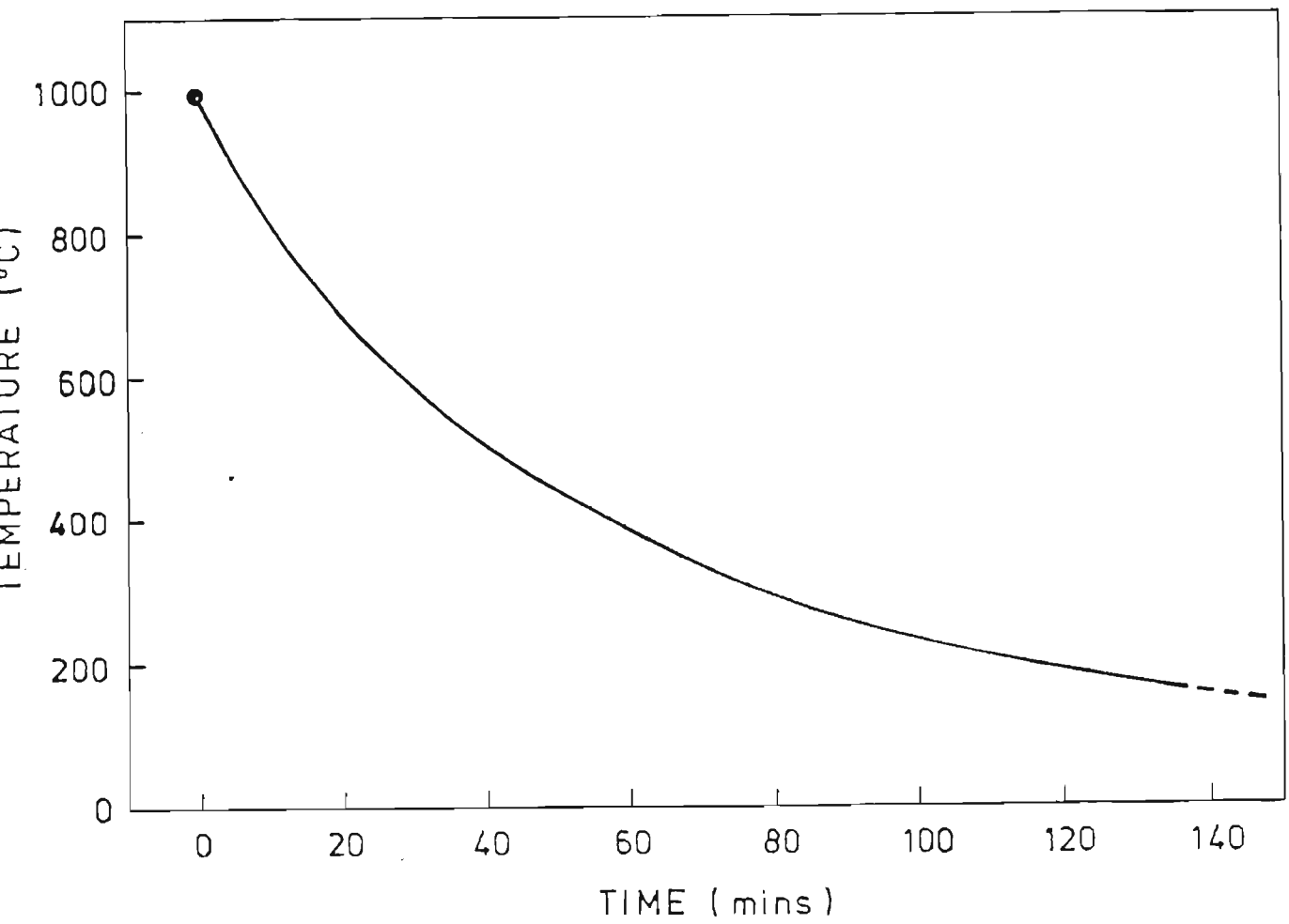

FIGURE 3.4 : Variation of cooling rate during specimen cooling.

A typical scan showing the start and finish temperatures for the transformation between the austenite and martensite phases under controlled heating and cooling conditions is given in fig. 3.5.

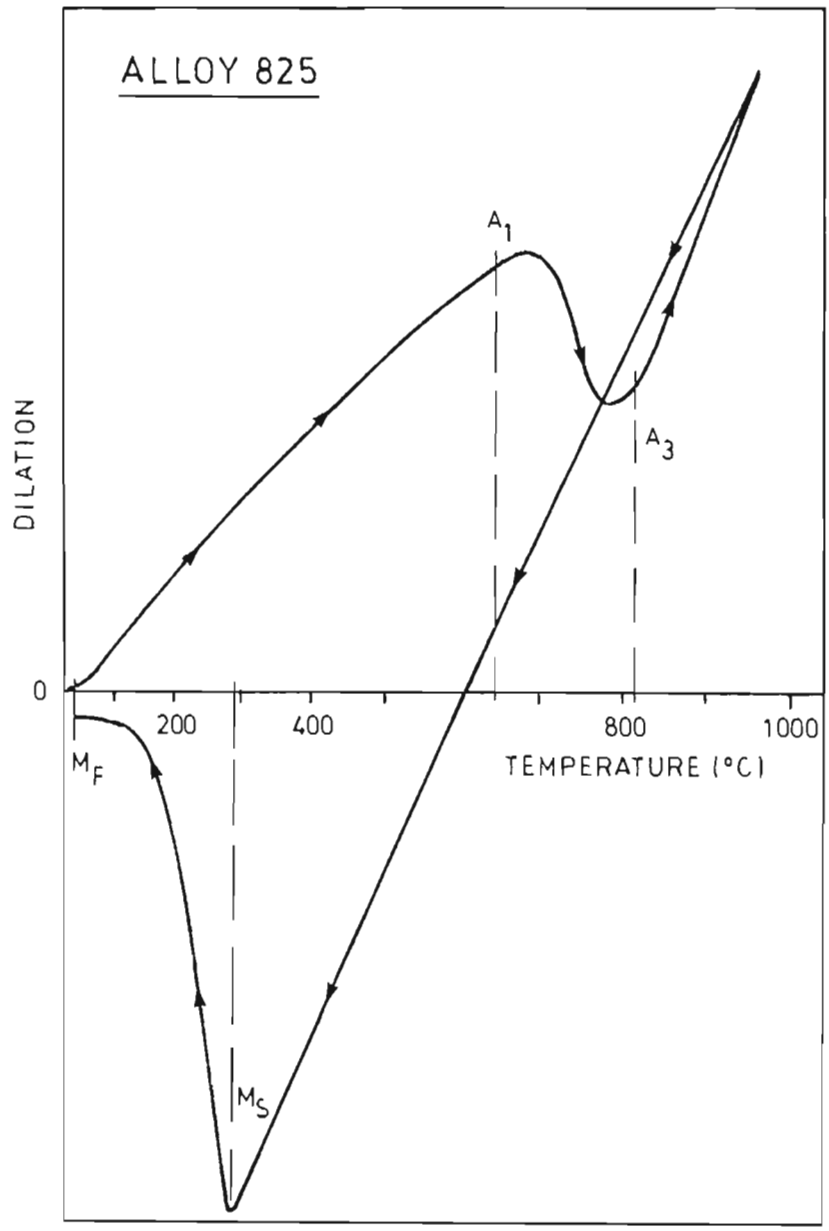

FIGURE 3.5 : The dilatometer scan of Alloy 825.

3.5 TESTING PROCEDURE

3.5.1 Standard Test

To ensure that the potentiostat was functioning correctly, a test was performed on AISI 430 in 1N H_2SO_4 according to ASTM standard G5-78 (ASTM (1980). Figure 3.6 shows that the potentiodynamic curve obtained corresponds well to the ASTM standard reference curve as well as to the curve Capendale obtained.

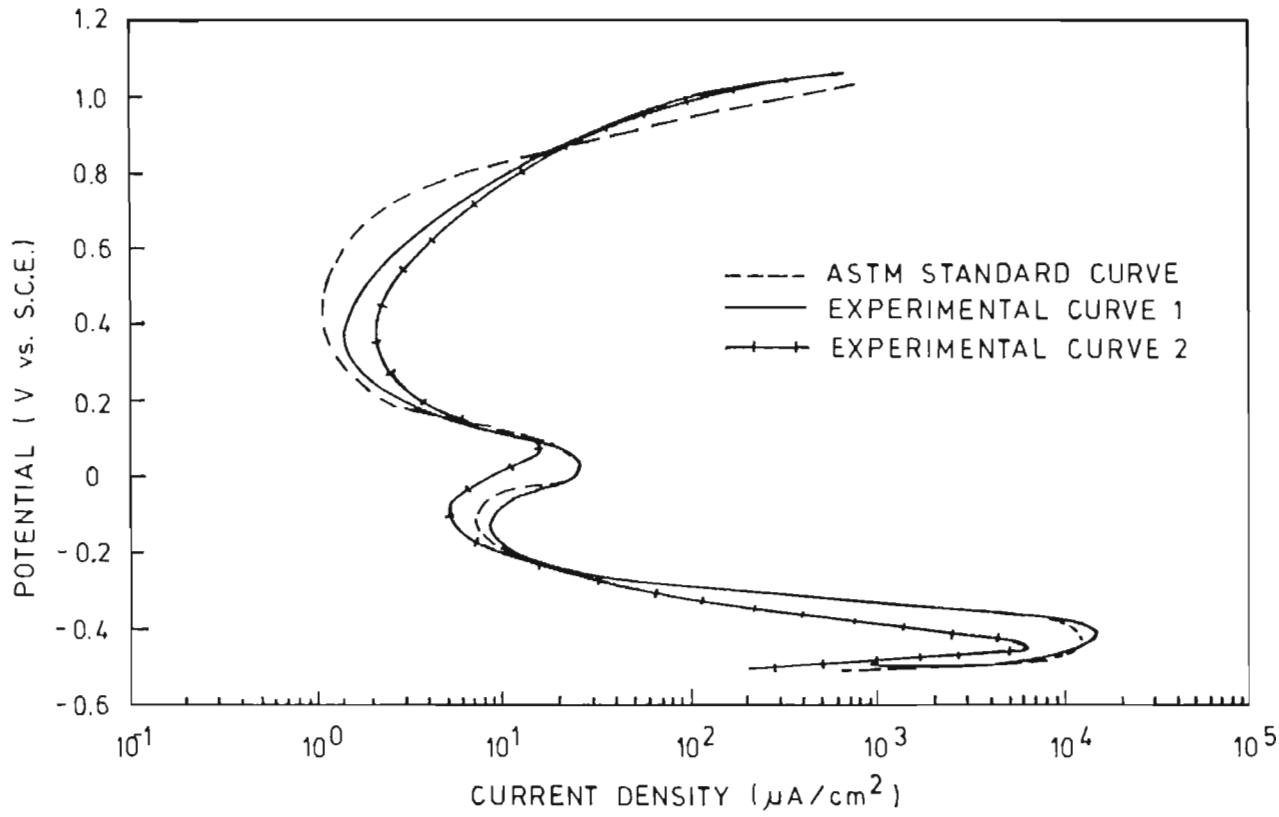

FIGURE 3.6 : Potentiodynamic scan of AISI 431 in 1N H_2SO_4.
Experimental Curve 1 obtained by Capendale.
Experimental Curve 2 obtained by Joubert.

3.5.2 Pitting Corrosion Tests

The solution was aerated by bubbling oxygen through it for 30 minutes prior to the sample being placed in it. The temperature was maintained at 30°C by placing the corrosion cell in a thermo-regulated water bath.

The potentiodynamic scan rate was 0.12mV/sec in the anodic direction. The pitting potential, E_p, or the breakdown potential, E_b, was identified as that potential at which there was a sudden increase in current density. Once the current density had reached $100\mu A/cm^2$, the scan was reversed until it crossed either the passive region or the cathodic region of the scan at which stage it was terminated.

Figure 3.7 is of a typical scan obtained showing the protection potential, E_{prot}, the breakdown potential, E_b (or the pitting potential, E_p, if pits were obtained) and the free corrosion potential, E_{corr}.

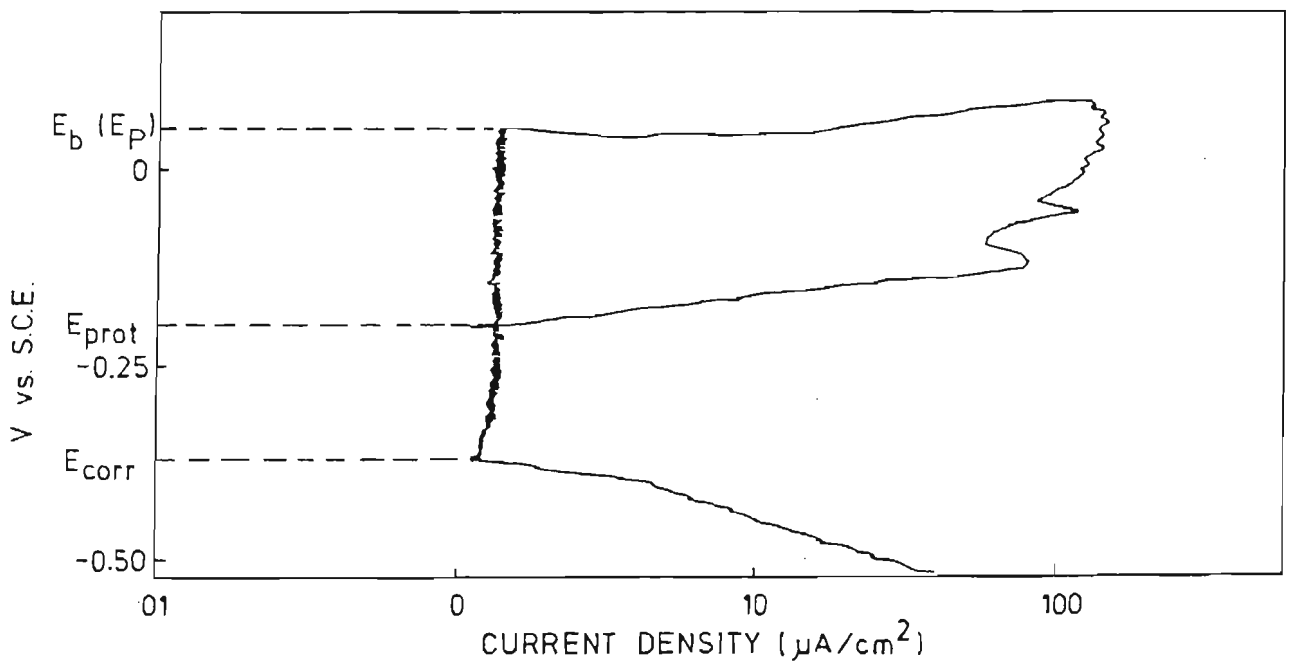

FIGURE 3.7 : A typical potentiodynamic scan obtained from the Princeton.

When a passive region existed, i_{pass} was used in the corrosion rate equation (equation A1). When there was no passive region, i_{corr} was used in the rate equation (equation A1). A derivation of this equation is given in appendix A. An explanation of why i_{pass} is used in certain circumstances and i_{corr} in other circumstances is also given.

3.5.3 Free Corrosion Potential versus Time Tests

An Ecorr vs time test was done, over a period of 48 hours for each steel, using specimens which had been tempered at 250°C. The standard solution was used, fully aerated and at a temperature of 30°C. The corrosion potential was monitored on a pen recorder at a scan rate of 2cm/hr.

3.6 THE MATERIALS

The three steels which were investigated have been designated Alloys 825, 102A and 122 by the COMRO. The chemical compositions of these alloys are shown in Table 3.1.

TABLE 3.1 : Compositions of Alloys, 825, 102A and 122.

% COMPOSITION	ALLOY 825	ALLOY 102A	ALLOY 122
Carbon	0.240	0.212	0.211
Chromium	8.050	10.030	11.980
Nickel	2.950	0.240	0.110
Nitrogen	0.024	0.080	0.032
Sulphur	0.006	0.003	0.011
Mangenese	0.410	0.990	0.920
Molybdenum	0.148	0.013	0.000
Cobalt	0.134	0.014	0.033
Aluminium	0.034	0.430	0.013
Phosphorus	0.019	0.035	0.017
Titanium	0.003	0.005	0.001
Niobium	0.005	0.003	0.003
Silicon	0.460	0.450	0.330
Copper	0.082	0.080	0.016

The data obtained by dilatometry of the transformation temperatures for the three steels is given in Table 3.2.

TABLE 3.2 : Transformation temperatures of Alloys 825, 102A and 122.

ALLOY	A1	A3	M_S	Mf
825	656	818	283	20
102A	800	891	312	83.3
122	827	881	376	197

All materials were solution annealed at 1100°C for 30 minutes and then oil quenched. Typical microstructures are shown of the materials having undergone a 200°C double temper where the material is kept at 200°C for 2 hours, allowed to air cool and then reheated for a further 2 hours and air cooled.

3.6.1 Alloy 825

Alloy 825 has a clean, tempered martensitic structure typical of a low carbon alloy steel (fig. 3.8). The prior austenite grains are large (± 60 μm). Work done by Barker (1988) using the TEM showed the martensitic laths to be highly dislocated and no retained austenite to be present. A hardness value of 568HV was obtained for the as-quenched condition while a hardness of 502HV was obtained for the 200°C double temper (2 hours per temper).

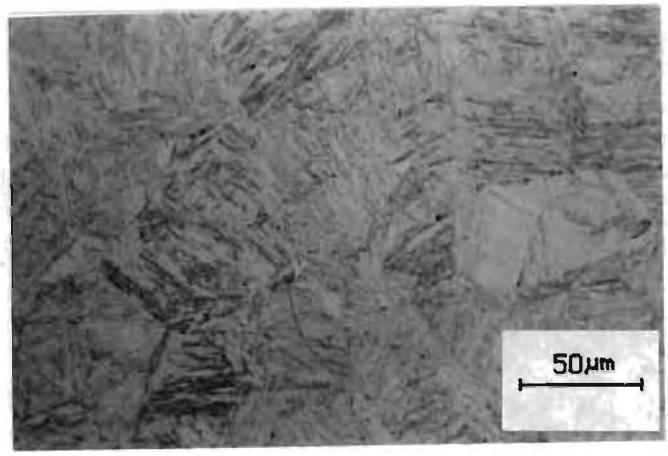

FIGURE 3.8 : The microstructure of Alloy 825 after heating to 1100°C for 30 minutes, quenching and double tempering at 200°C (2 hours each temper). Specimen etched in 5g $FeCl_3$ + 15ml conc. HCl + 15 ml EtOH + 20 ml water + 5 drops HNO_3 for 8 seconds at room temperature.

3.6.2 Alloy 102A

Alloy 102A has a clean lath martenistic structure with few inclusions or precipitates present (fig. 3.9). The prior austenite grains are large and have an average size of 75μm. No retained austenite was detected. A hardness value of 520HV was obtained for the as-quenched condition while a hardness of 496HV was obtained for the 200°C double temper (2 hours per temper).

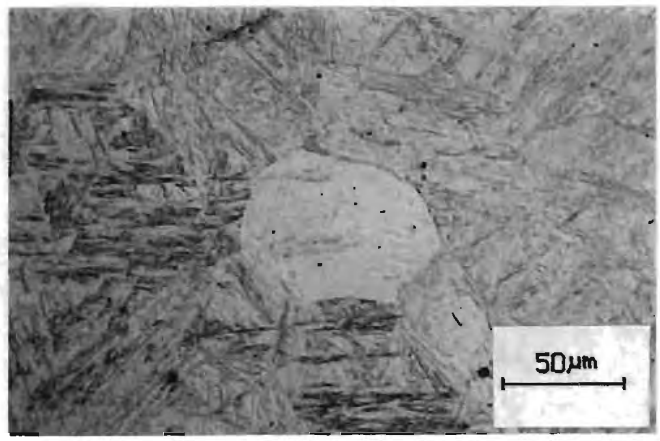

FIGURE 3.9 : The microstructure of Alloy 102A after heating to 1100°C for 30 minutes, quenching and double tempering at 200°C (2 hours each temper). Specimen etched in 5 g $FeCl_3$ + 15 ml conc. HCl + 15 ml EtOH + 20 ml water + 5 drops HNO_3 for 12 seconds at room temperature.

3.6.3 Alloy 122

Alloy 122 has a lath martensitic structure with many inclusions and precipitates visible under optical examinations (fig. 3.10). The prior austenite grains are large (± 70μm). No retained austenite was detected. A hardness value of 554HV was obtained for the as-quenched condition while a hardness of 435HV was obtained for the 200°C double temper (2 hours per temper). This alloy was thus most softened by the temper.

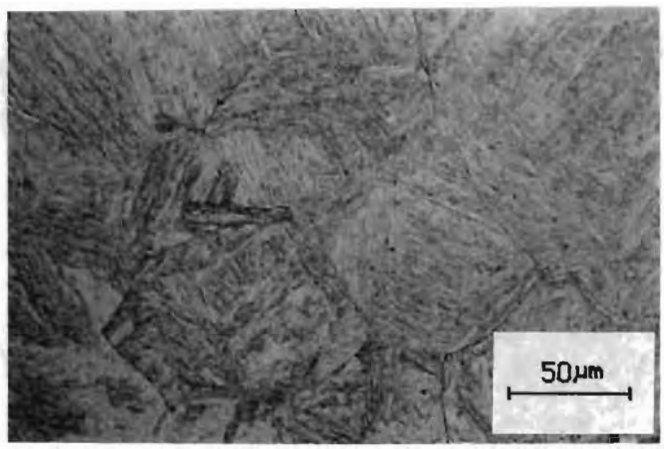

FIGURE 3.10 : The microstructure of Alloy 122 after heating to 1100°C for 30 minutes, quenching then double tempering at 200°C (2 hours per temper). Specimen etched in 5g $FeCl_3$ + 15 ml conc. HCl + 15 ml EtOH + 20 ml water + 5 drops HNO_3 for 10 seconds at room temperature.

CHAPTER 4

RESULTS

The results for each alloy are presented separately within three sections. These sections show the effect a change in tempering temperature has on the hardness and microstructure, the electrochemical properties and the surface corrosion of each alloy.

A single temper was achieved by placing the specimen in the furnace, which was already at temperature, for two hours and then allowing the specimen to air cool. For a double temper the process was repeated.

4.1 HARDNESS AND MICROSTRUCTURE

4.1.1 Alloy 825

The effect of tempering temperature on hardness for Alloy 825, in the double and single tempered states, is shown in fig. 4.1. The hardness of the as-quenched material was 568 HV. An increase in the tempering temperature resulted in a decrease in hardness values. These reached a minimum at 350°C. The hardness then increased with tempering temperature, reaching a secondary hardening peak between 450° and 500°C. A noticeable decrease in hardness is found on tempering at still higher temperatures.

The effect of tempering temperature and time of tempering on microstructure is illustrated in fig. 4.2. At the lower tempering temperatures (150°C to 450°C) many intragranular precipitates can be seen. At tempering temperatures above 500°C (fig. 4.2b) the secondary precipitation of solid solution carbon as FeC_3 within the martensite has resulted in a more textured etch. Further precipitation of iron and chromium carbides at grain boundaries results in grain boundary definition.

After tempering above 650°C no grain boundary precipitation can be observed but there is intragranular precipitation (fig. 4.2c).

A sample tempered at 700°C for 15 minutes is shown in fig 4.2d. Grain boundary as well as intragranular precipitation is evident. The grain boundary precipitation became less evident after higher tempering temperatures. After tempering for 15 minutes at 1000°C, no grain boundary precipitation could be observed.

Alloy 825, double tempered at 500°C is shown in fig. 4.2e. Intragranular precipitation is observed but no grain boundaries have been decorated.

Alloy 825

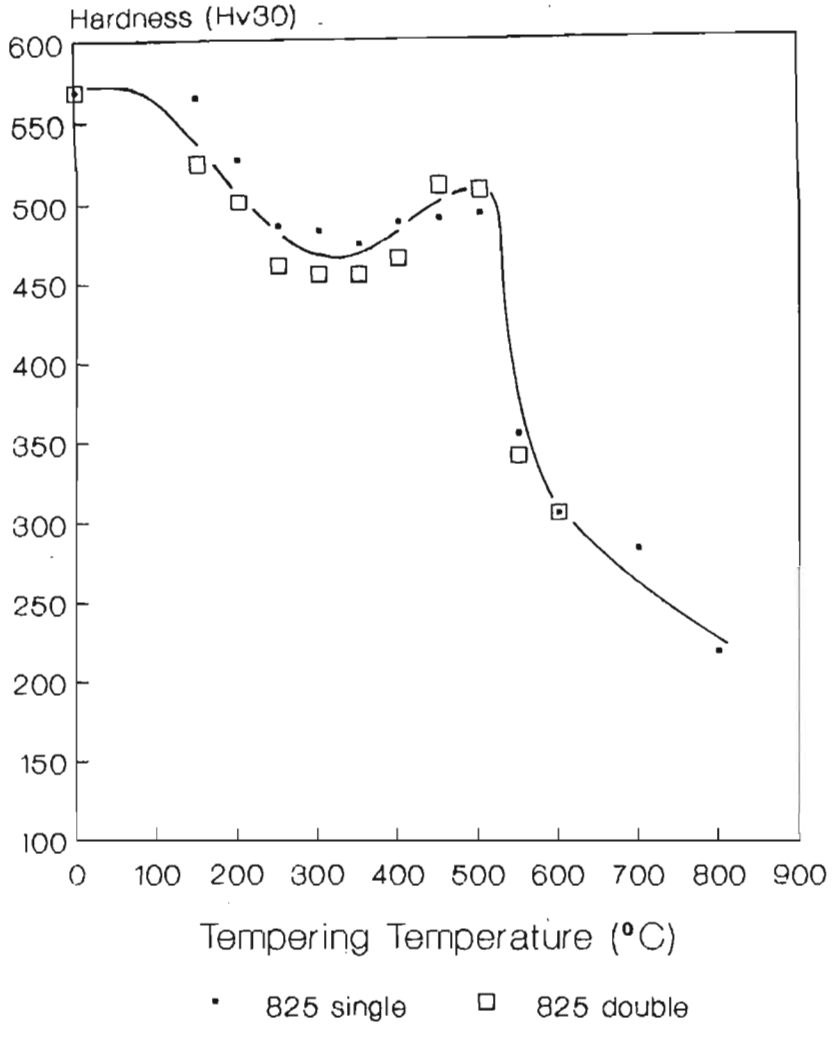

FIGURE 4.1 : Hardness versus tempering temperature.
Single tempering time - 2 hours.
Double tempering time - total of 4 hours.

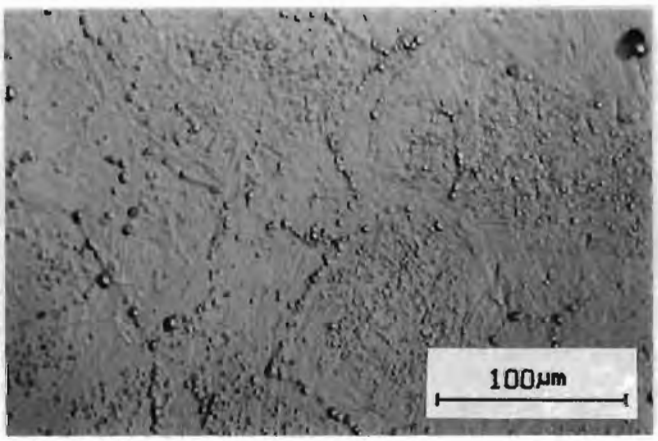

FIGURE 4.2a : Tempered at 250°C for 2 hours. Shows intergranular precipitation.

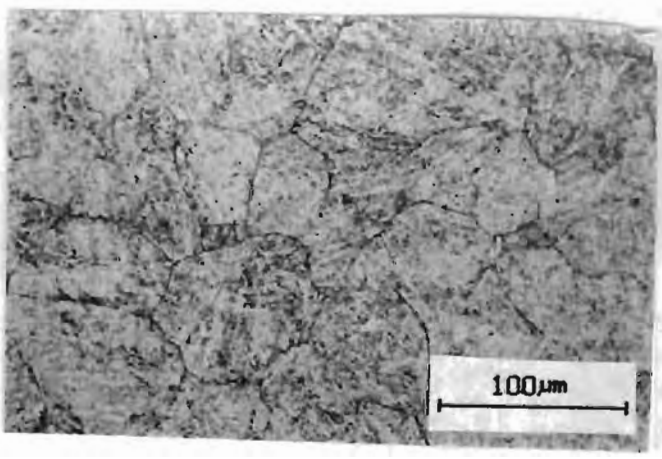

b) Tempered at 550°C.for 2 hours. Grain boundary and intragranular precipitation.

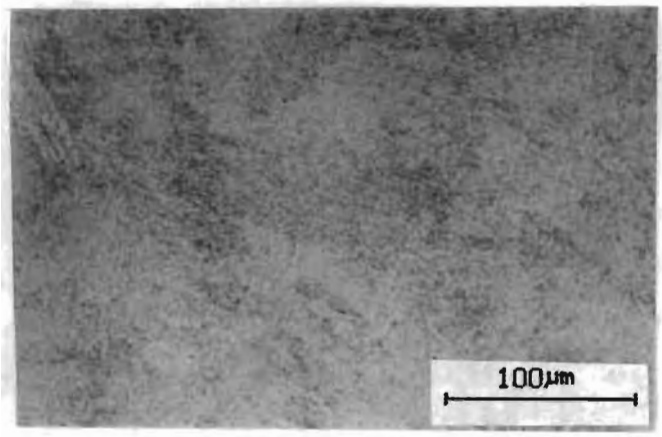

c) Tempered at 700°C for 2 hours. Shows intragranular precipitation.

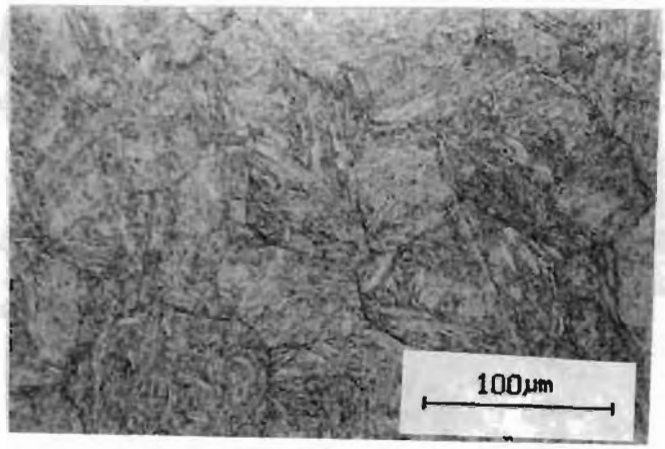

d) Tempered at 700°C for 15 minutes. Shows grain boundary as well as intragranular preciptation.

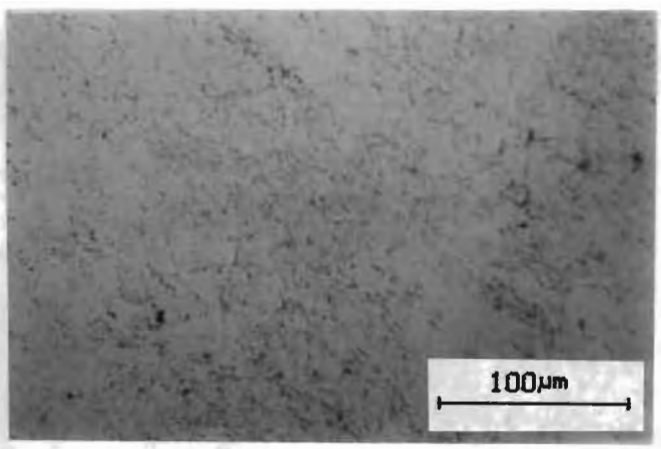

e) Double tempered at 500°C for a total of 4 hours. Intragranular precipitation is evident.

4.1.2 Alloy 102A

In the quenched condition, the hardness was measured as 520HV which increased slightly after tempering at 150°C. A steady decrease in hardness then followed up to a tempering temperature of 350°C (fig. 4.3). A steady increase in hardness with increasing tempering temperature then followed and a secondary hardness peak was reached at 500°C. A rapid decrease in hardness occurred on increasing the tempering temperature further to 600°C. The hardness of the double tempered samples was consistently lower than that of the single tempered samples.

The effect of tempering temperature and time on microstructure is illustrated in fig. 4.4. After lower tempering temperatures (150°C to 500°C) many intragranular precipitates can be seen with no grain boundary definition. At tempering temperatures above 500°C, heterogenous chromium-carbide precipitation results in grain boundary definition (fig. 4.4b). Intragranular precipitation, too, is still present. After tempering above 650°C, intragranular precipitation is observed but no grain boundary precipitation is observed (fig. 4.4c). The microstrucure of a fifteen minute temper after 700°C is shown in fig. 4.4.d Definite grain boundaries can be observed as well as intragranular precipitation. After tempering at higher temperatures, the grain boundaries become less well defined and after tempering at 1000°C are no longer optically visible.

A sample double tempered at 500°C is shown in fig. 4.4.e. Intragranular precipitation is observed and there is evidence of discontinuous grain boundary precipitation.

Alloy 102A

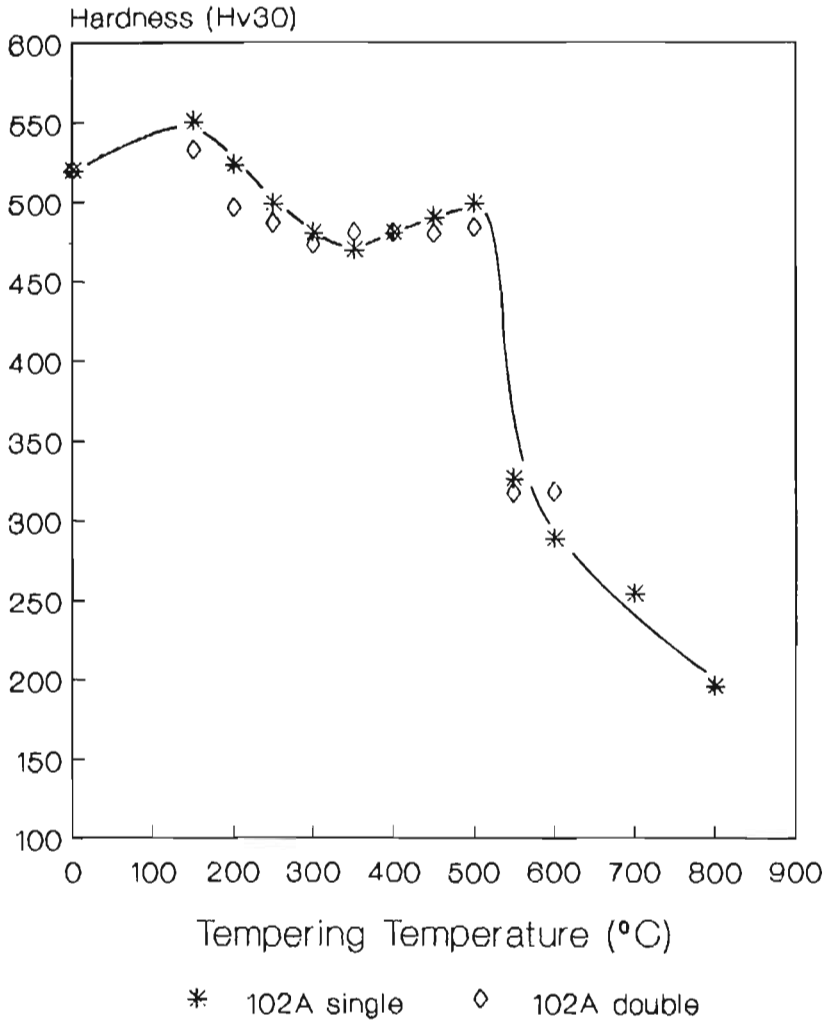

FIGURE 4.3 : Hardness versus tempering temperature.
Single tempering time - 2 hours.
Double tempering time - a total of 4 hours.

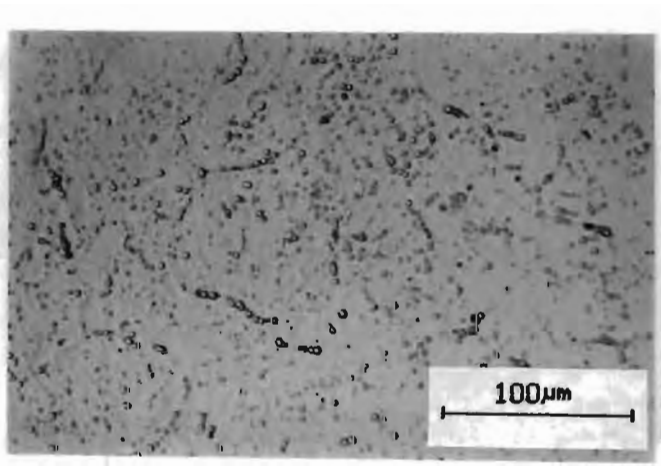

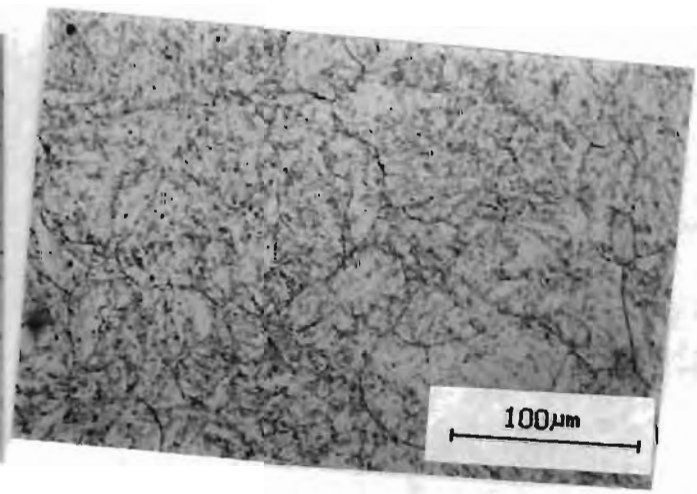

FIGURE 4.4a : Tempered at 300°C for 2 hours. Shows random intragranular precipitation.

b) Tempered at 550°C for 2 hours. Grain boundary and intragranular precipitation can be observed.

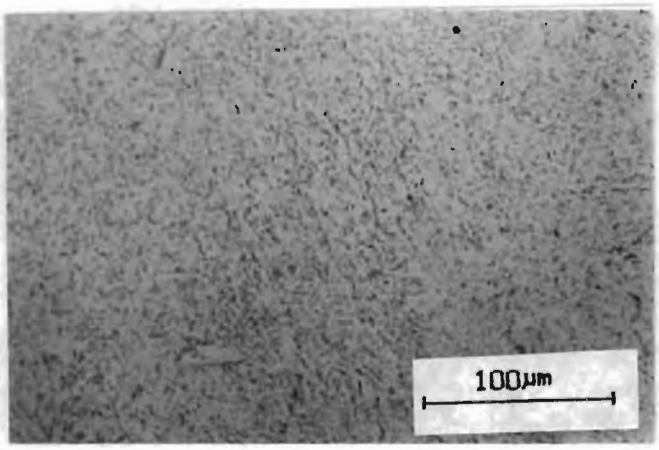

c) Tempered at 800°C for 2 hours. Intragranular precipitation can be observed but no grain boundary precipitation.

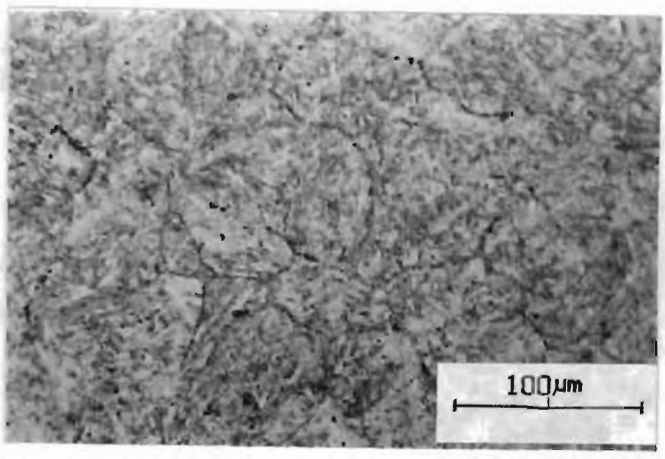

d) Tempered at 700°C for 15 minutes. Grain boundary as well as intra-intragranular precipitation is evident.

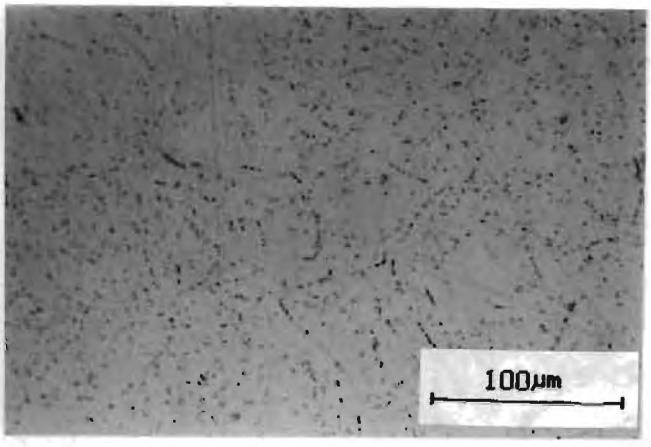

e) Double tempered at 500°C for a total of 4 hours. Intragranular precipitation and intergranular precipitation can be observed.

4.1.3 Alloy 122

The effect of tempering temperature on hardness for alloy 122, in the single and double tempered states, is shown in fig. 4.5. Both the single and double tempers show a decrease in hardness on increasing the tempering temperature from the quenched condition to tempering temperatures of 350°C to 400°C. Hardness then increases reaching a secondary hardening peak between 450°C and 500°C. There follows a significant decrease in bulk hardness on tempering at temperatures greater than 500°C for both the single and double tempers.

The effect of tempering temperature and time on microstructure is shown in fig. 4.6. After tempering below 500°C, clustered intragranular precipitates are observed (fig. 4.6a). After tempering above 500°C, grain boundary precipitation as well as intragranular precipitation is observed (fig. 4.6b). After tempering above 650°C, no grain boundary precipitation can be observed but much intragranular precipitation is evident (fig.4.6c).

The microstructure of a fifteen minute temper after 700°C is shown in fig. 4.6d. Grain boundary precipitation is evident which becomes less evident with increasing tempering temperature. After tempering at 900°C for 15 minutes the intragranular precipitates become clustered.

A sample which has been double tempered at 500°C is shown in fig. 4.6e. Intragranular precipitation is evident.

Alloy 122

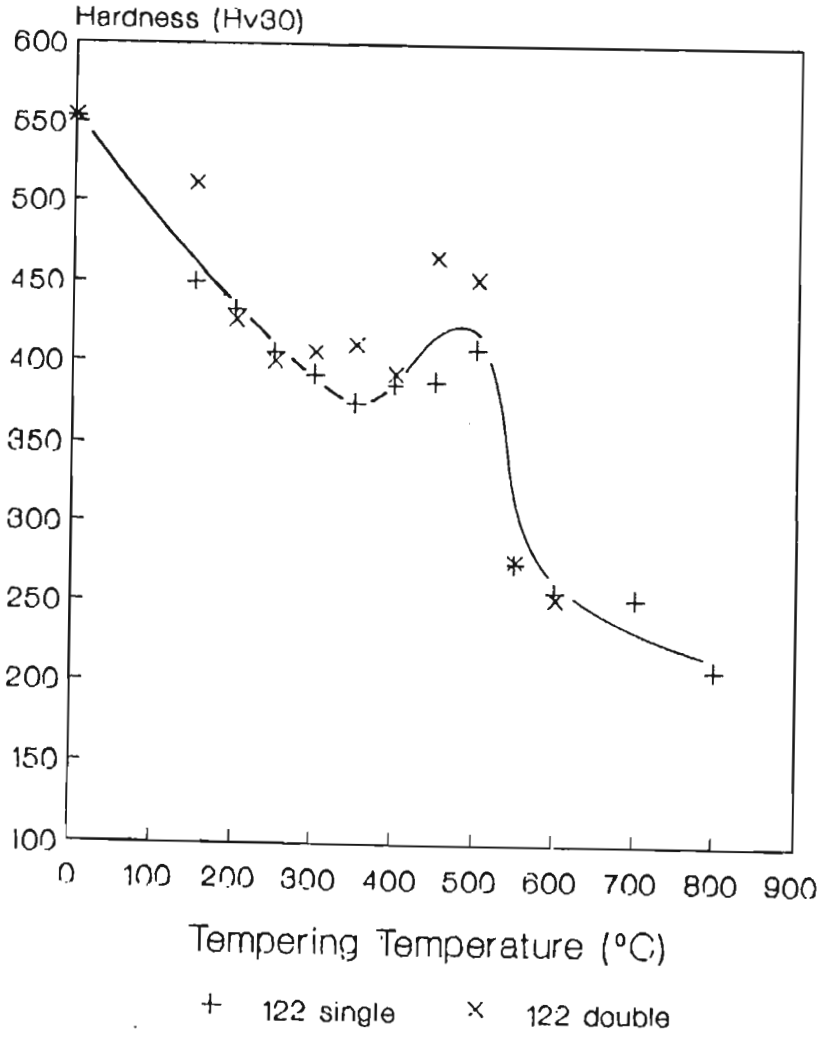

FIGURE 4.5 : Hardness versus tempering temperature.
Single tempering time - 2 hours.
Double tempering time - a total of 4 hours.

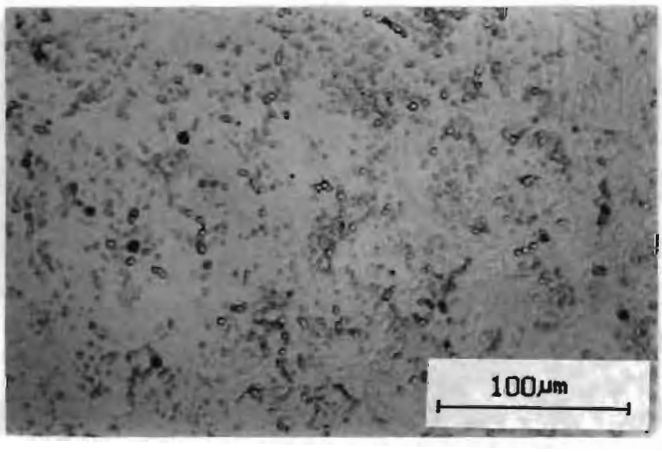

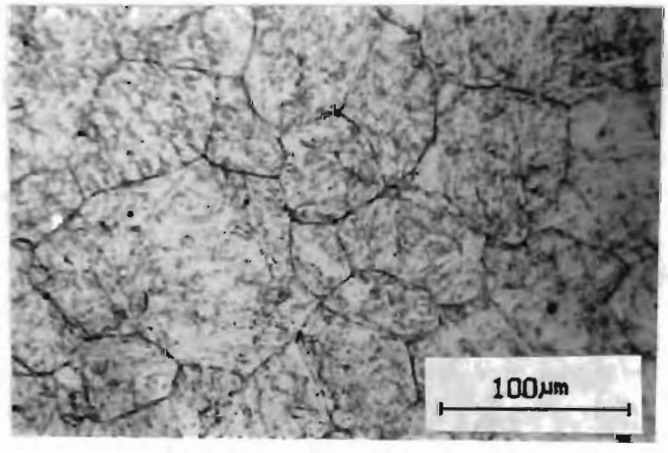

FIGURE 4.6a : Tempered at 250°C for 2 hours. Clustered intragranular precipitates are observed.

b) Tempered at 550°C for 2 hours. Grain boundary as well as intragranular (but not clustered)precipitation can be observed.

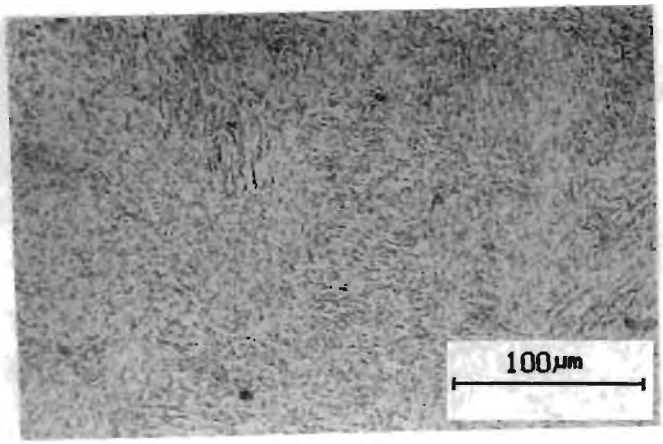

c) Tempered at 800°C for 2 hours. Intragranular precipitation is evident.

d) Tempered at 700°C for 15 minutes. Grain boundary and clustered intragranular precipitates are observed.

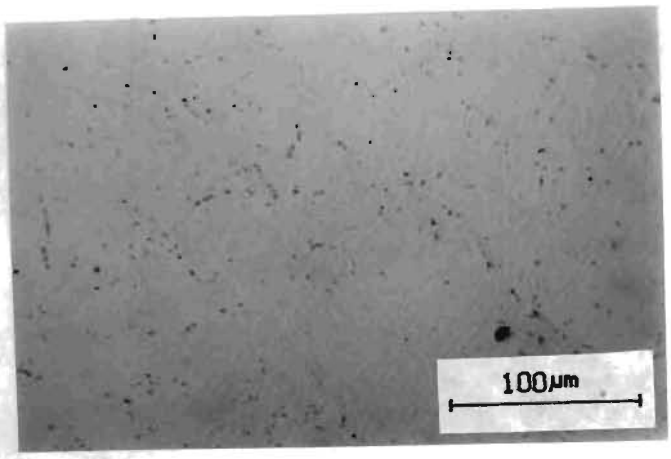

e) Double tempered at 500°C for a total of 4 hours. Intragranular precipitation, but not grain boundary precipitation, is shown.

4.1.4 A Comparison between the Three Alloys

Figures 4.7a and b compare the effect tempering temperature has on hardness for the three alloys in the single and double tempered states respectively. The three alloys follow similar trends experiencing a decrease in hardness with increasing tempering temperature from 0°C to 350°C and reaching a maximum hardness after tempering at 500°C. A subsequent decrease in hardness results after tempering at higher temperatures.

Alloys 825 and 102A show similar hardness values but Alloy 122 is on average about 100HV softer for each tempering temperature. In the double tempered state however, the hardness values of the three alloys fall within a narrower range.

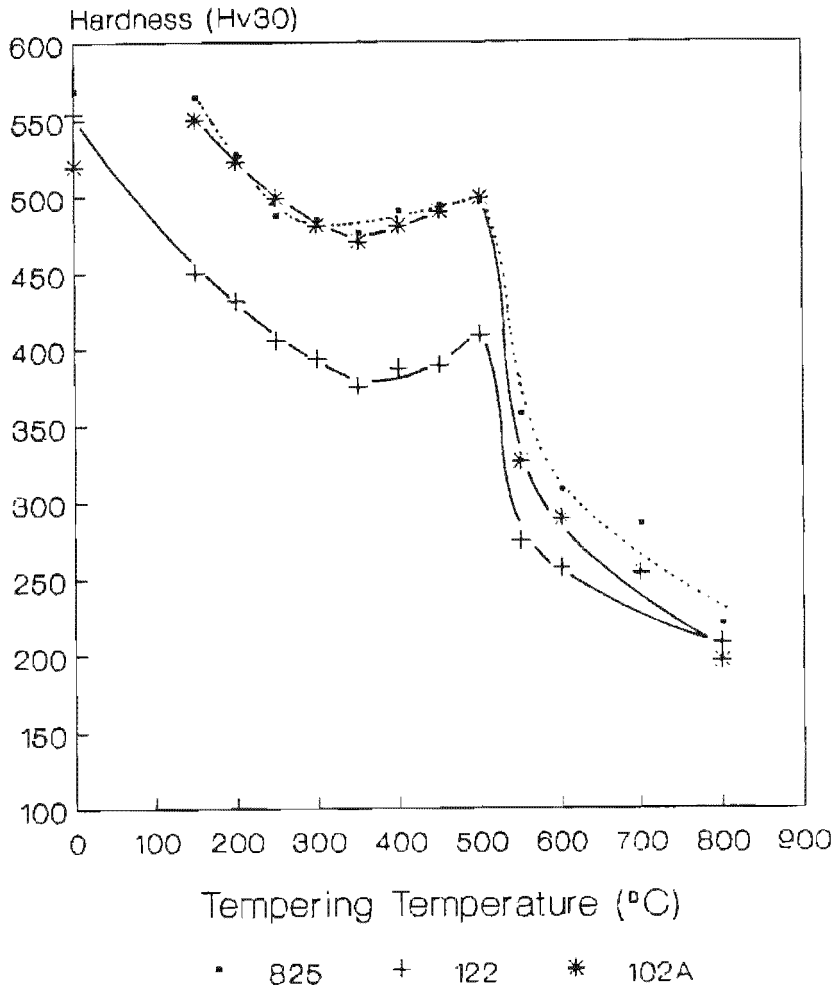

FIGURE 4.7a : Hardness versus tempering temperature.
Tempering time - 2 hours.

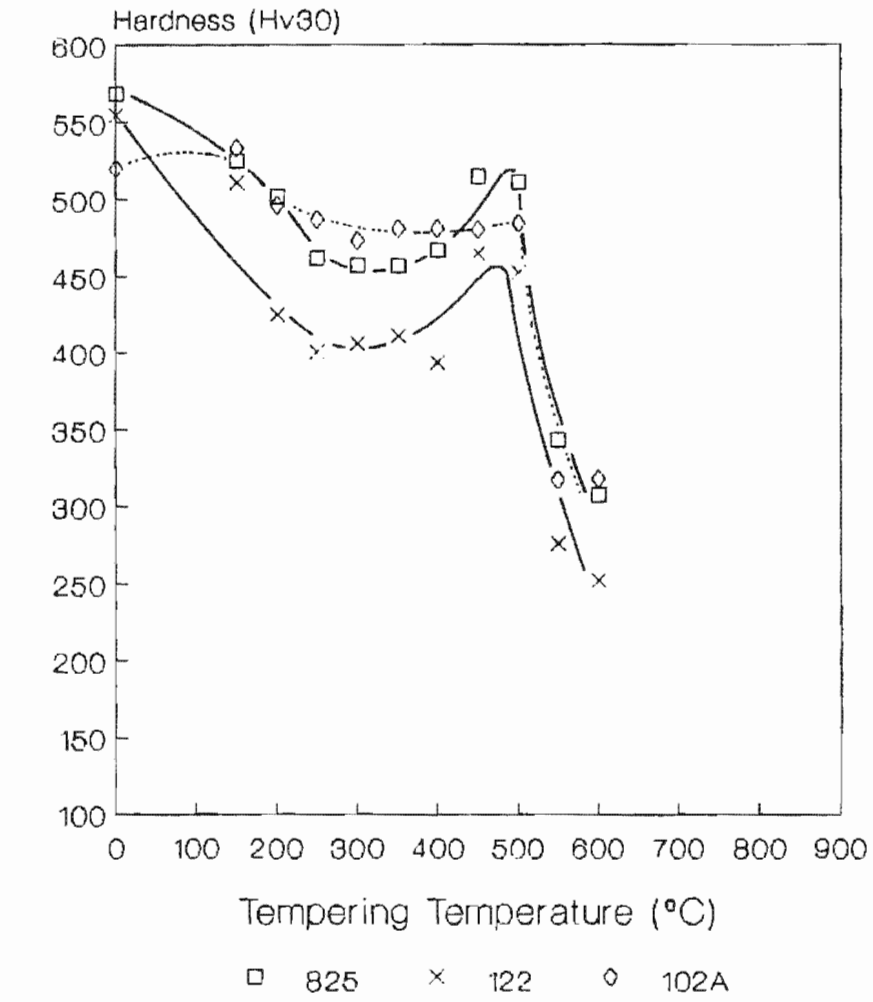

FIGURE 4.7b : Hardness versus tempering temperature.
Tempering time - a total of 4 hours.

4.2 ELECTROCHEMICAL PROPERTIES

Potentiodynamic polarization scans were carried out on samples, encompassing the full range of heat treatments carried out. Fresh samples were used for each tempering treatment. The surface of the specimens were polished to a 3μm finish. All tests were carried out in aerated minewater containing 1500ppm chloride ions and 1200ppm sulphate ions and maintained at 30°C.

Corrosion rates were calculated from the potentiodynamic scans obtained according to the method outlined in Appendix A. When a passive region existed in the potentiodynamic scan, i_{pass} was used to calculate the corrosion rates. If there was no passive region, i_{corr} was used.

Free corrosion potential versus time plots were carried out on one sample for each material. Samples for these tests were tempered for 2 hours at 300°C.

4.2.1 Alloy 825

Free Corrosion Potential Versus Time

The variation of free corrosion potential with time, is plotted in fig. 4.8. The value of the free corrosion potential becomes gradually more cathodic (active) throughout the duration of the test. An initial potential of -300mV decreased with time and eventually reached a relatively stable value of -450mV after 30 hours.

Corrosion Rates

The corrosion rates, calculated using i_{corr} in the corrosion rate equation (equation A1), versus tempering temperature are shown in fig. 4.9a. In both the single and double tempered conditions, the corrosion rate increased with increasing tempering temperature and reached a peak at a tempering temperature between 450°C and 550°C.

The variation of the corrosion rate, calculated using i_{pass} in the rate equation (equation A1), with tempering temperature is plotted in fig. 4.9b. In both the single and double tempered conditions, a

constant corrosion rate of approximately 0.02mm/yr is observed. A combination of figs. 4.9a and b is plotted in fig. 4.9c. When a passive region existed on the potentiodynamic scan, i_{pass} was used to calculate the corrosion rate. If there was no passive region, i_{corr} was used to calculate the corrosion rate. For the single temper, a maximum corrosion rate is reached after tempering at 500°C and in the case of the double temper, a maximum corrosion rate is reached after tempering at 550°C.

Breakdown Potential and Passive Region Range

The variation of breakdown potential with tempering temperature is plotted in fig. 4.10. Those samples which underwent single tempers broke down earlier than those that underwent double tempering treatments. The range of the passive region versus tempering temperature is plotted in fig. 4.11. A double tempering treatment consistently increased the passive region range.

For tempering temperatures below 400°C, both the breakdown potential and the passive region range are random. For tempering temperatures above 400°C, both the breakdown potential and the passive region range decreased and became near constant.

Protected Passive Region

The protected passive region, defined as the protection potential subtracted from the breakdown potential for each tempering temperature, is plotted against tempering temperature in fig. 4.12. It is observed that, under single tempering conditions, Alloy 825 has a protected region only after tempering at 150°but not after tempering at higher temperatures. Under double tempering conditions Alloy 825 has a protected region when tempering up to temperatures of 350°C. Thus, it is observed that the double temper extends the tempering temperature range over which a protected passive region exists. For tempering temperatures above 350°C, the protection potential was always below the free corrosion potential and did not join the anodic curve within the passive range and in these cases there is no anodic potential range within which the material could safely perform without the danger of pitting.

Alloy 825

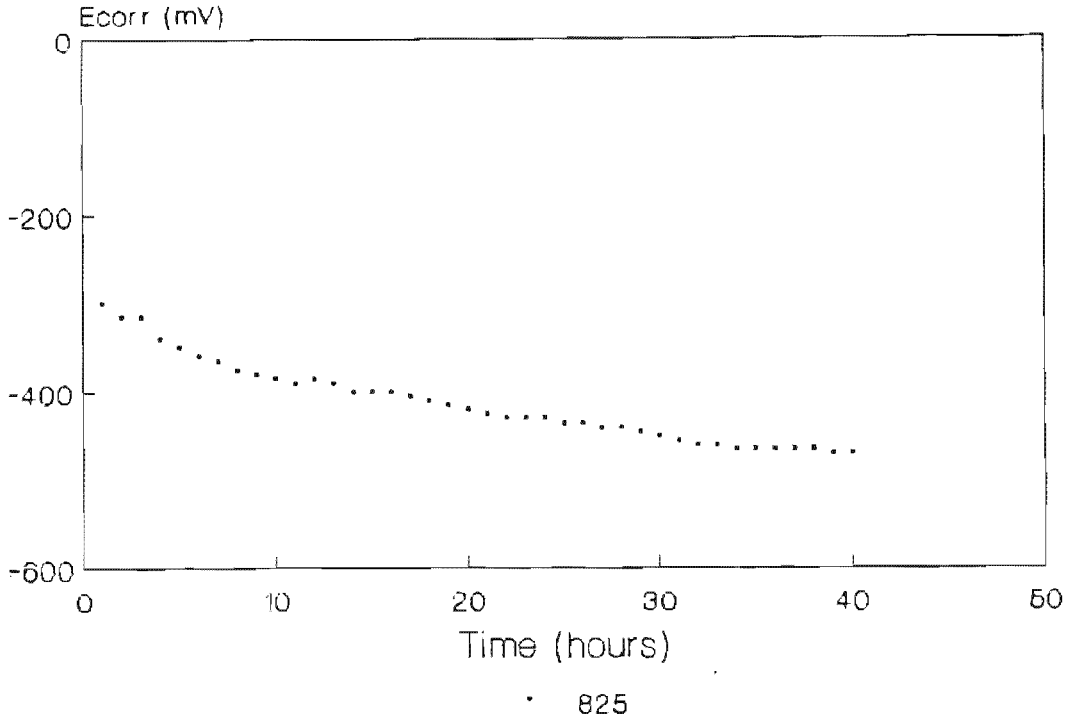

Tempering temperature 300°C

FIGURE 4.8 : Free corrosion potential versus time for Alloy 825.

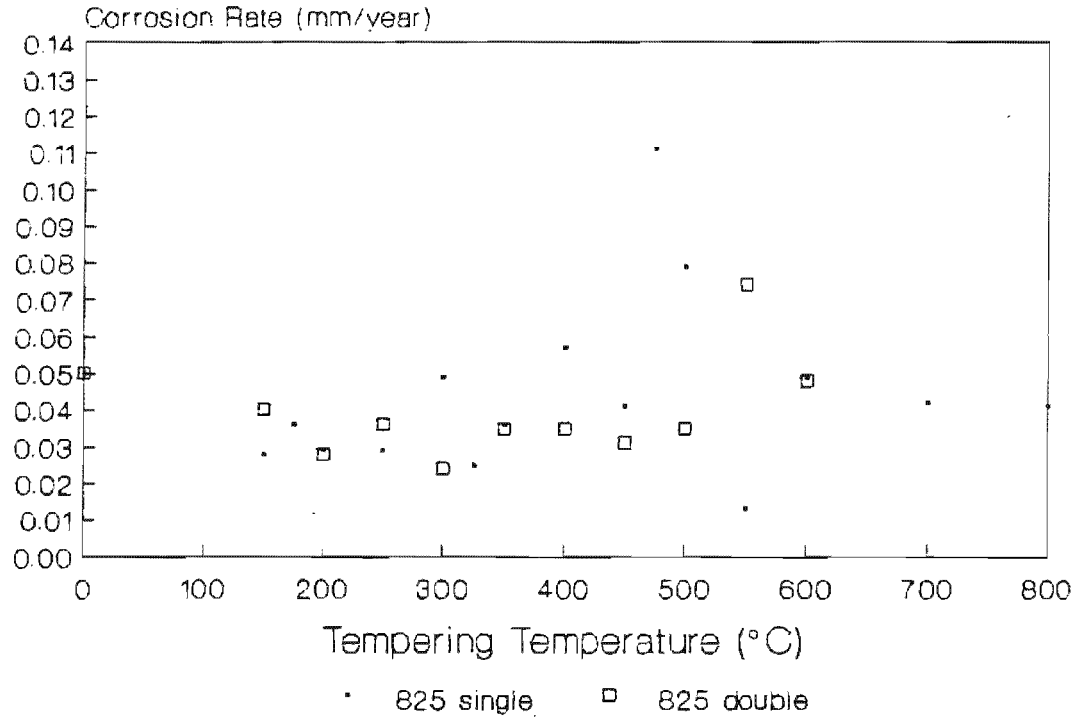

Corrosion rate calculated using icorr

FIGURE 4.9a : Corrosion rate versus tempering temperature for Alloy 825.

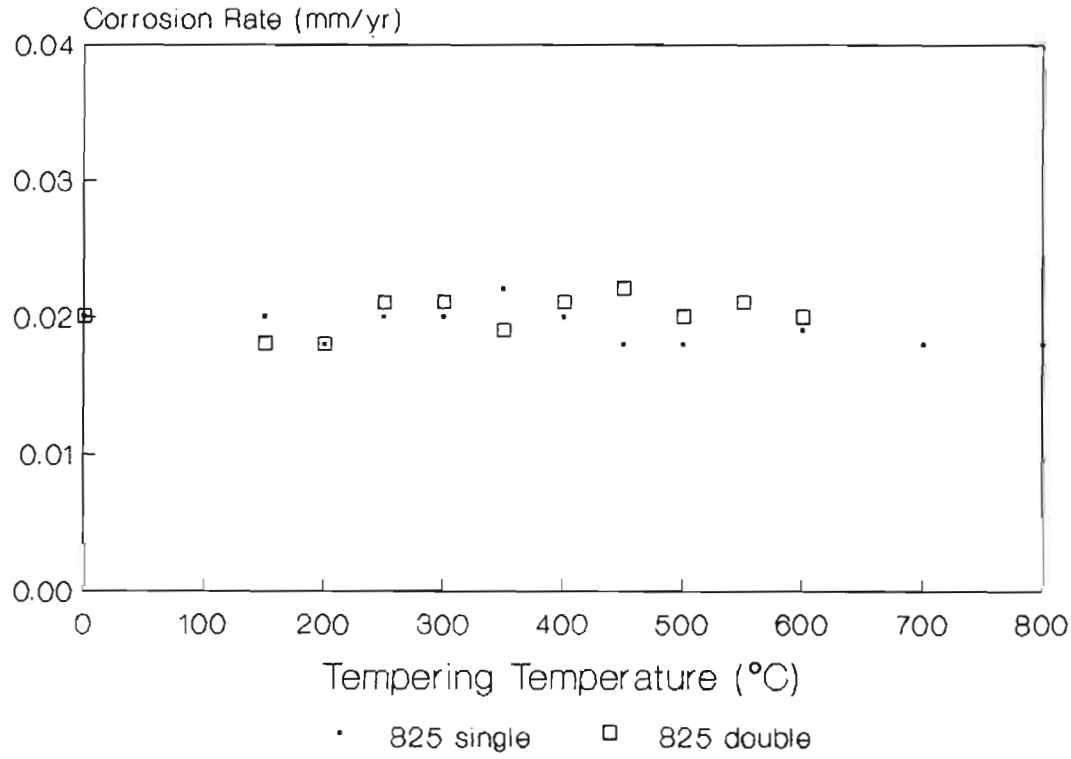

Corrosion rate calculated using ipass

FIGURE 4.9b : Corrosion rate versus tempering temperature for Alloy 825.

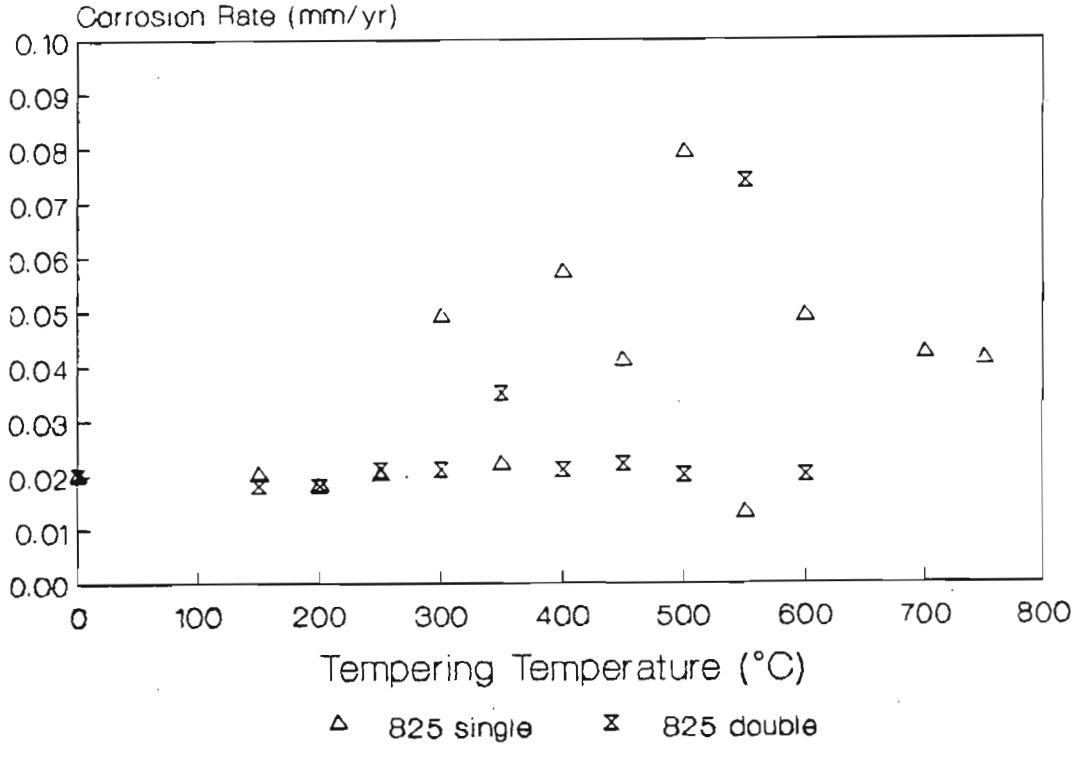

Combination of icorr and ipass

FIGURE 4.9c : Corrosion rate versus tempering temperature for Alloy 825.

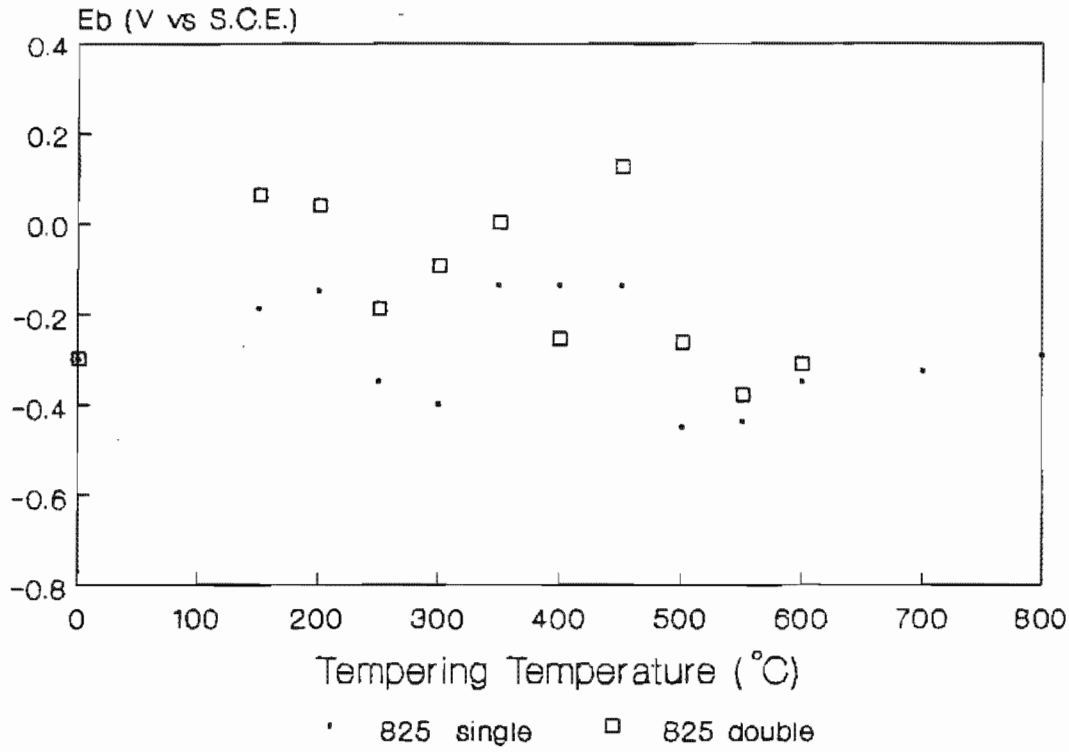

FIGURE 4.10 : Breakdown potential versus tempering temperature for Alloy 825.

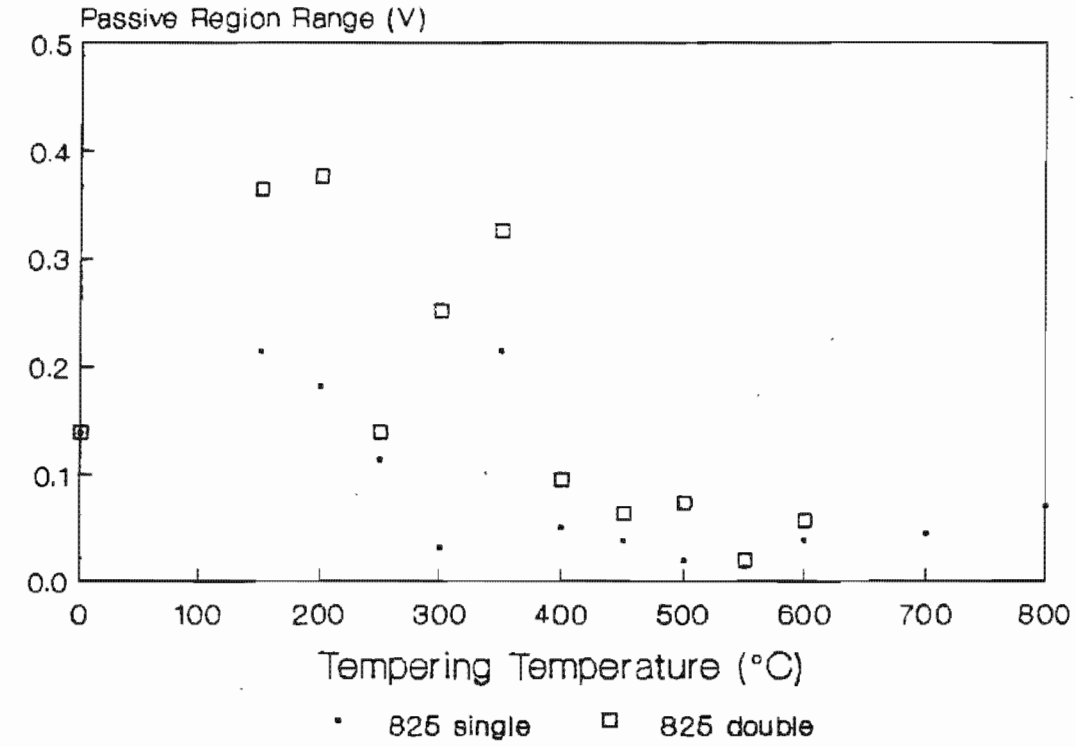

FIGURE 4.11 : Passive region range versus tempering temperature for Alloy 825.

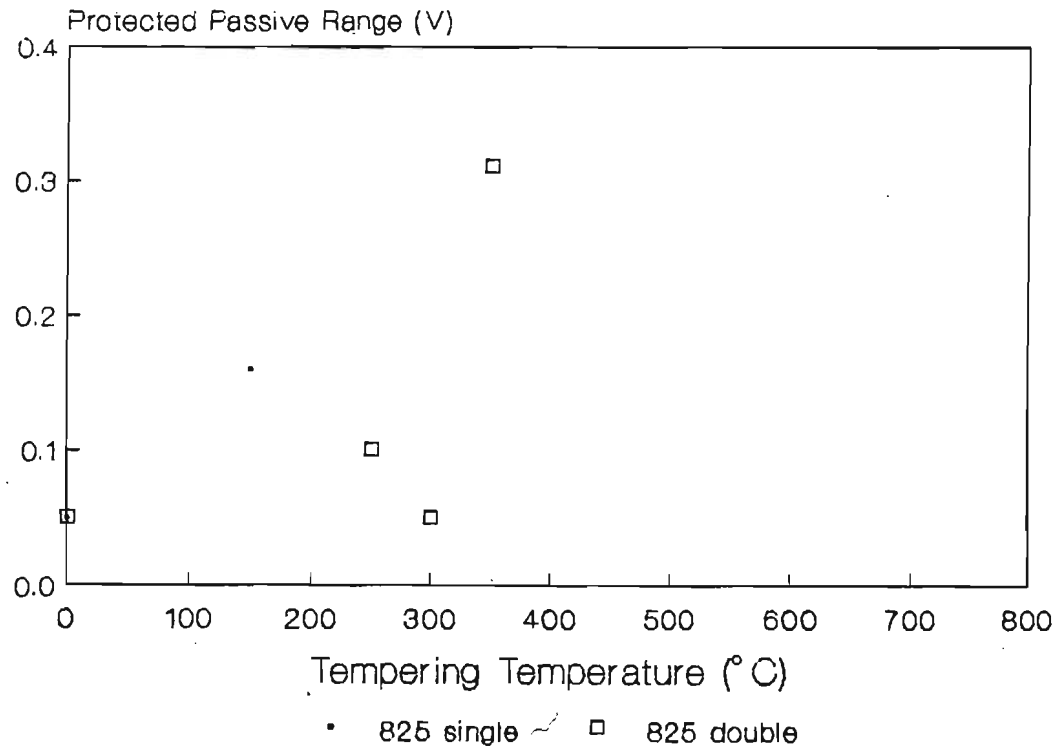

FIGURE 4.12 : Protected passive range versus tempering temperature for Alloy 825.

4.2.2 Alloy 102A

Free Corrosion Potential Versus Time

The variation of free corrosion potential with time is plotted in fig. 4.13. This steel, which contains a higher percentage of chromium than alloy 825, has an initial voltage of -350mV which increased rapidly within the first ten hours to reach a stable potential of -100mV.

Corrosion Rates

The corrosion rate, calculated using i_{corr} in the corrosion rate equation (equation A1), is plotted against tempering temperature in fig. 4.14a. A steady, but small, increase in corrosion rate can be observed with each successive tempering temperature, reaching a maximum after tempering at 500°C.

The variation of corrosion rate, calculated using i_{pass} in the corrosion rate equation (equation A1), with tempering temperature is plotted in fig. 4.14b. The double temper has a consistently lower corrosion rate than the single temper. The single tempered samples have an average corrosion rate of 0.020mm/yr while the double tempered samples have an average corrosion rate of 0.018mm/yr.

Breakdown Potential and Passive Region Range

The breakdown potential and the passive region range plotted against tempering temperature (figs. 4.15 and 4.16 respectively) show similar trends for both the single and double tempered conditions allowing for experimental error.

Both the breakdown potential and the passive region range show random instability. Both increase on increasing the tempering temperature from the as-quenched condition to a 250°C temper. A minimum is reached on further increasing the tempering temperature with a trough existing after tempering between 400°C and 550°C. After a further increase in tempering temperature, the breakdown potential and passive region range both increase.

Protected Passive Range

Alloy 102A has a maximum protected passive range after tempering at 300°C as can be observed in fig. 4.17. No protected region is observed after tempering at 400°C or higher. The double tempering treatment extends the tempering temperature range over which a protected region exists from 350°C (single temper) to 400°C (double temper).

Alloy 102A

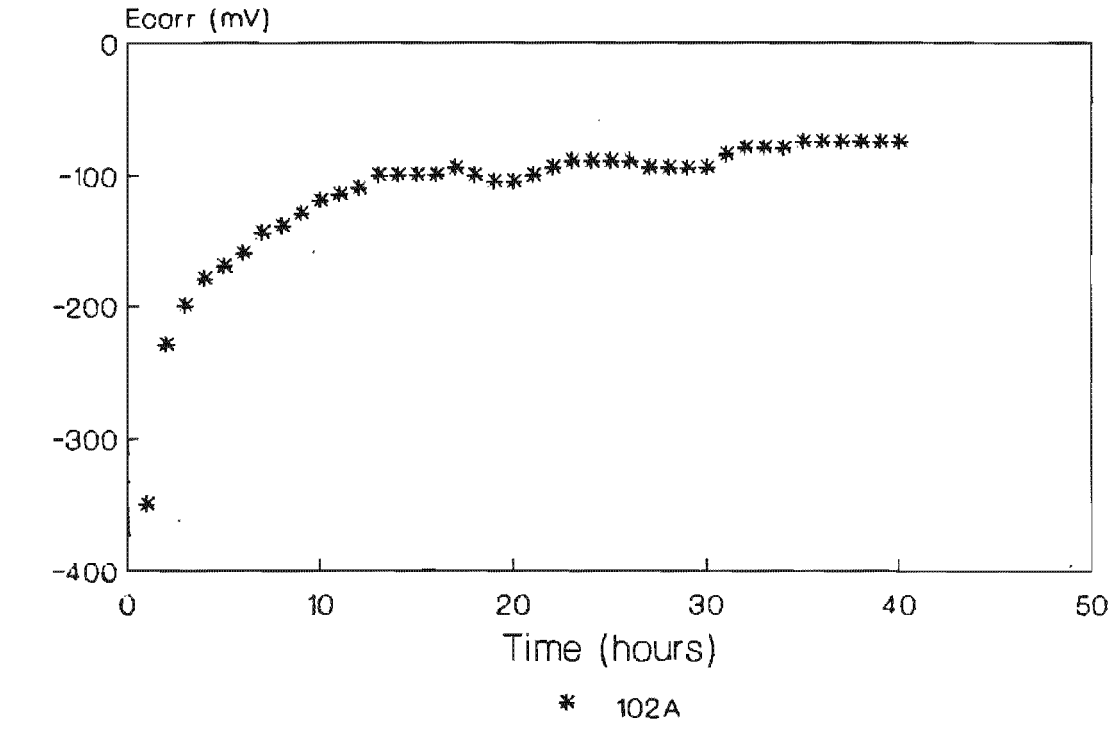

FIGURE 4.13 : Free corrosion potential versus time for Alloy 102A.

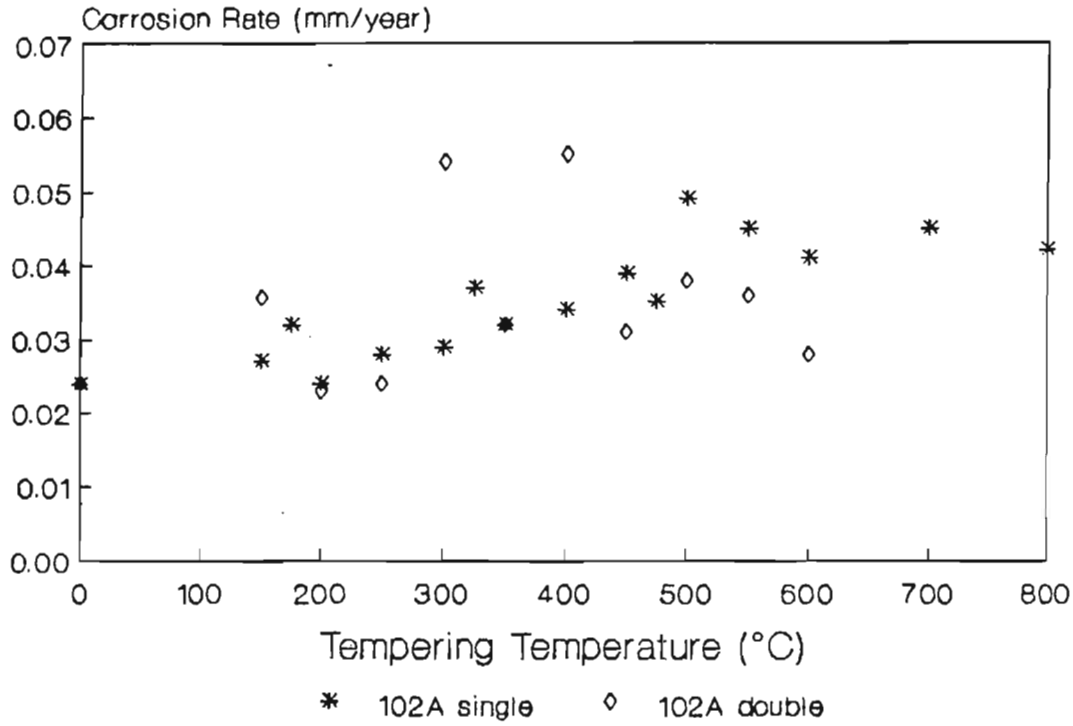

Corrosion rate calculated using icorr

FIGURE 4.14a : Corrosion rate versus tempering temperature for Alloy 102A.

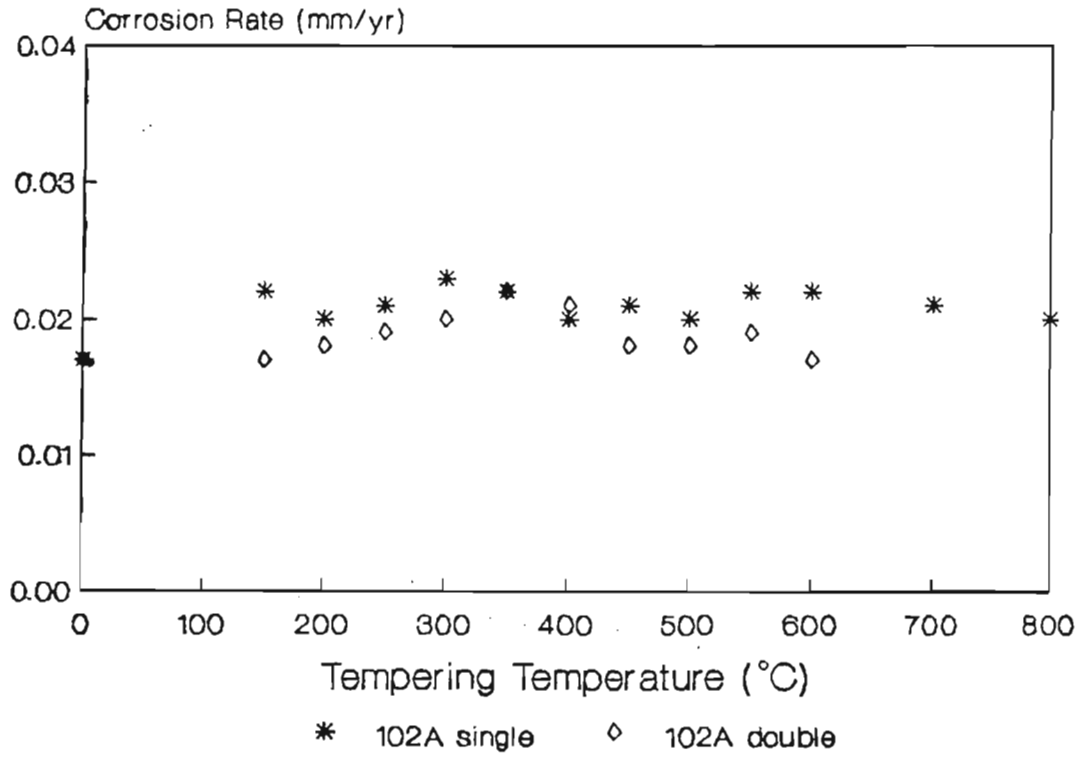

Corrosion rate calculated using ipass

FIGURE 4.14b : Corrosion rate versus tempering temperature for Alloy 102A.

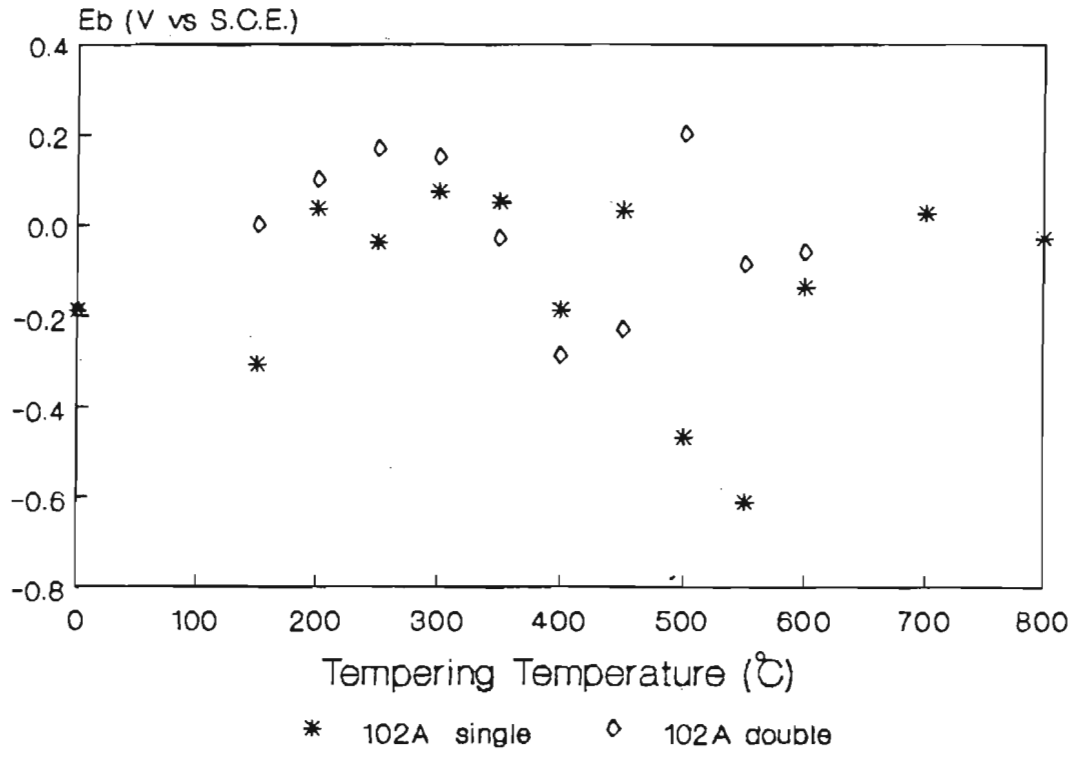

FIGURE 4.15 : Breakdown potential versus tempering temperature for Alloy 102A.

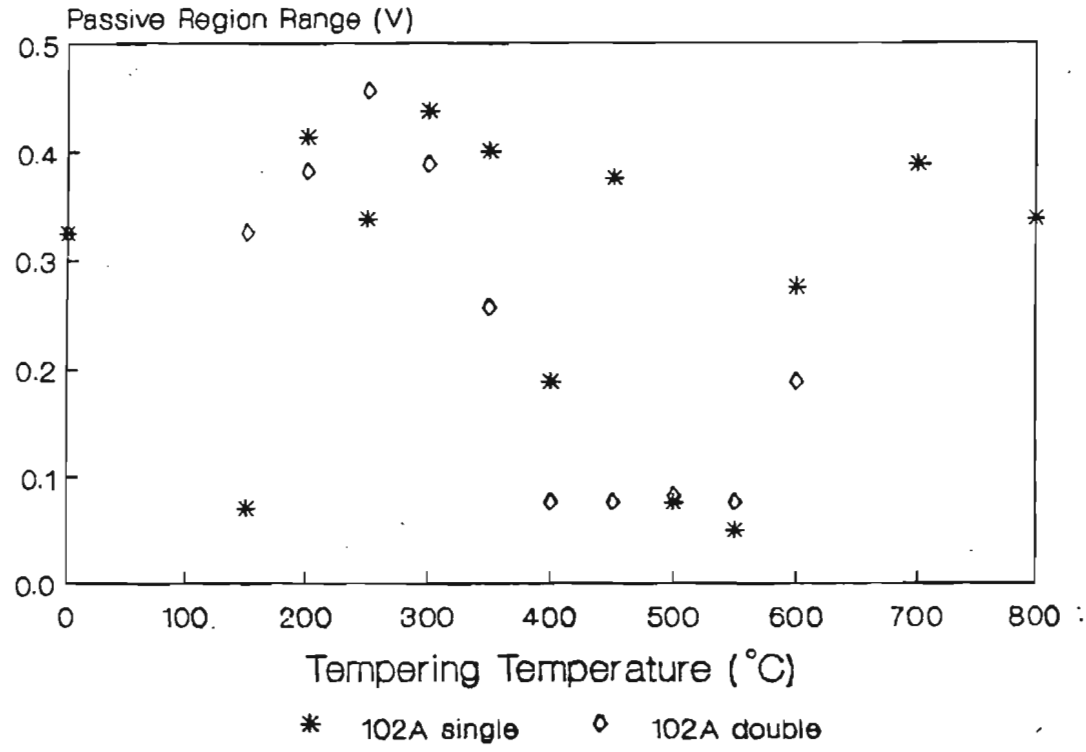

FIGURE 4.16 : Passive region range versus tempering temperature for Alloy 102A.

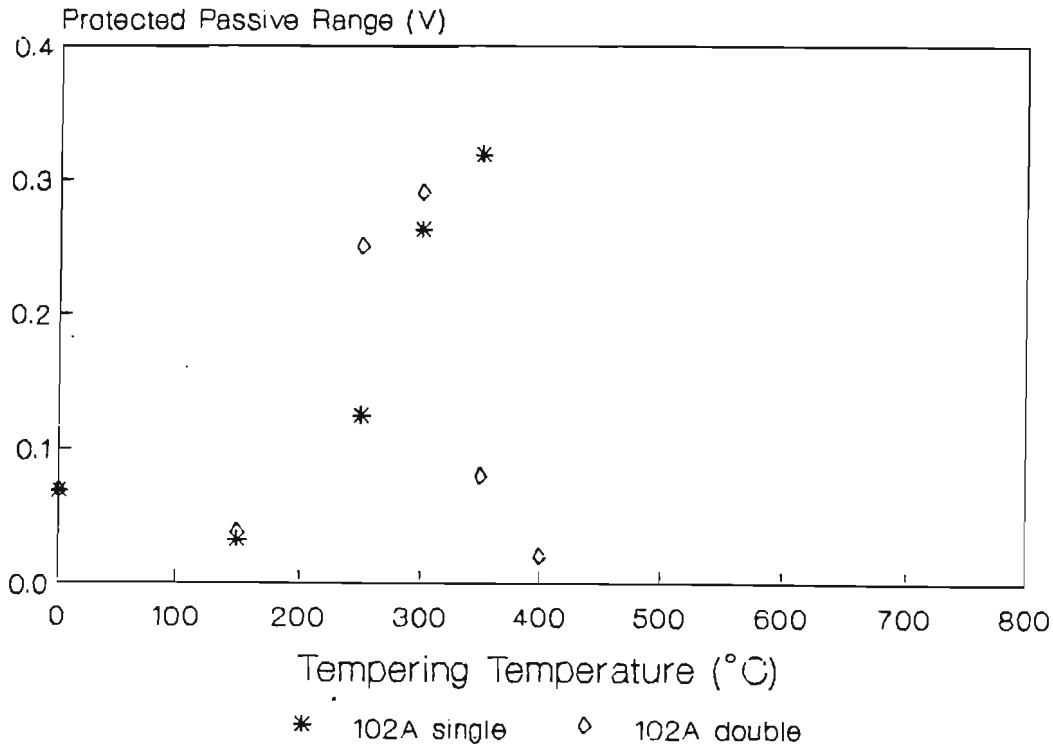

FIGURE 4.17 : Protected passive range versus tempering temperature for Alloy 102A.

4.2.3 Alloy 122

. Free Corrosion Potential Versus Time

The variation of free corrosion potential with time is plotted in fig. 4.18. The free corrosion potential becomes gradually more anodic throughout the duration of the test. An initial potential of -150mV increases with time to reach 50mV after 40 hours.

Corrosion Rates

The corrosion rate, calculated using i_{corr} in the corrosion rate equation (equation A1) is plotted against tempering temperature in fig. 4.19a. In both the single and double tempered conditions, the corrosion rate decreases with increasing tempering temperature reaching a minimum at 250°C. Samples tempered at 350°C show maximum corrosion rates.

The variation of corrosion rate, calculated using i_{pass} in equation A1, is plotted in fig. 4.19b. A steady corrosion rate of approximately 0.016 mm/yr can be observed with a small increase in the corrosion rate between 400°C and 500°C.

Breakdown Potential and Passive Region Range

The breakdown potential and the passive region range (figs. 4.20 and 4.21 respectively) are near constant when tempering between 150°C and 400°C. Samples tempered at temperatures above 400°C show a decrease, which increases with an increase in tempering temperature, in the breakdown potential and the passive region range.

Protected Passive Range

The variation of the protected passive range with tempering temperature is shown in fig. 4.22. In the single tempered condition, a maximum is reached after tempering at 250°C. After tempering at temperatures above 450°C, the protected passive range tends to zero. The double tempered samples show a near constant protected range throughout the tempering temperature range.

Alloy 122

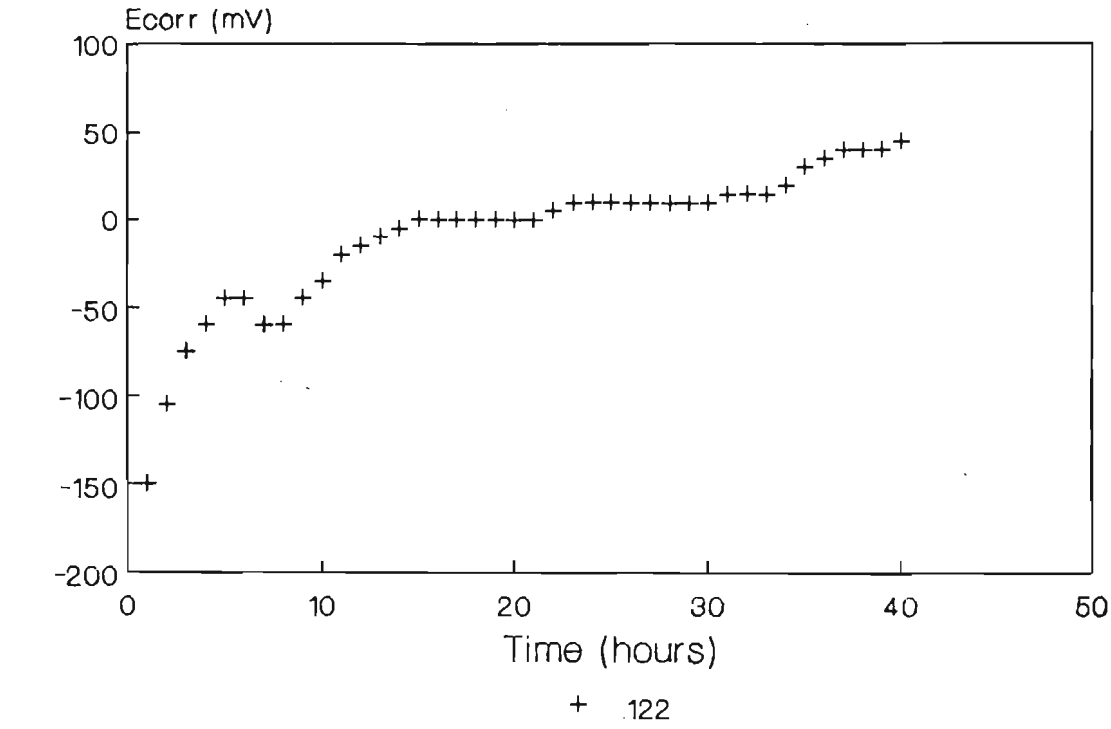

Tempering temperature 300°C

FIGURE 4.18 : Free corrosion potential versus time for Alloy 122.

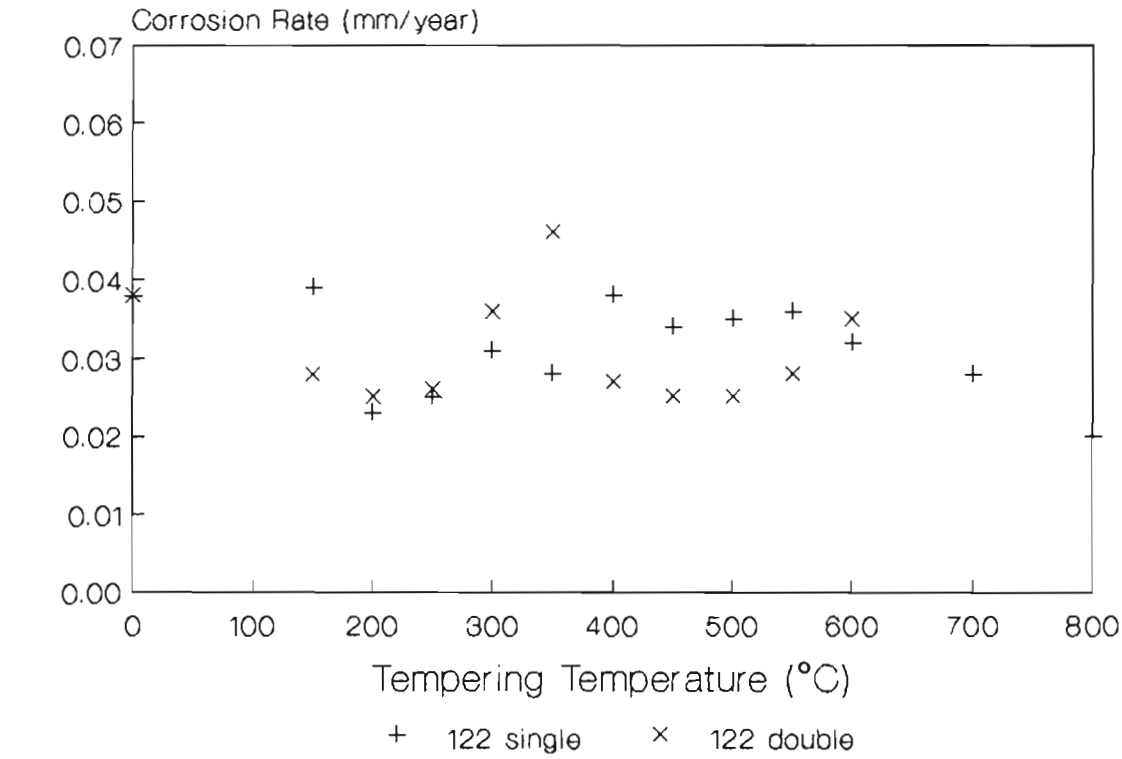

Corrosion rate calculated using icorr

FIGURE 4.19a : Corrosion rate versus tempering temperature for Alloy 122.

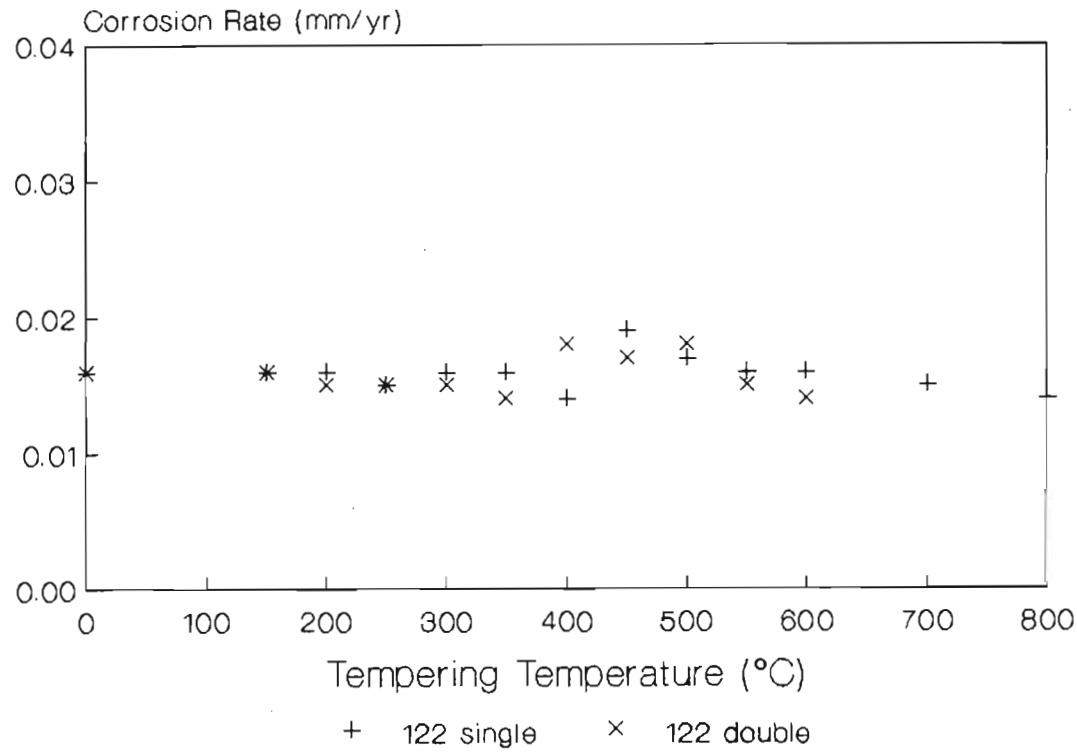

Corrosion rate calculated using ipass

FIGURE 4.19b : Corrosion rate versus tempering temperature for Alloy 122.

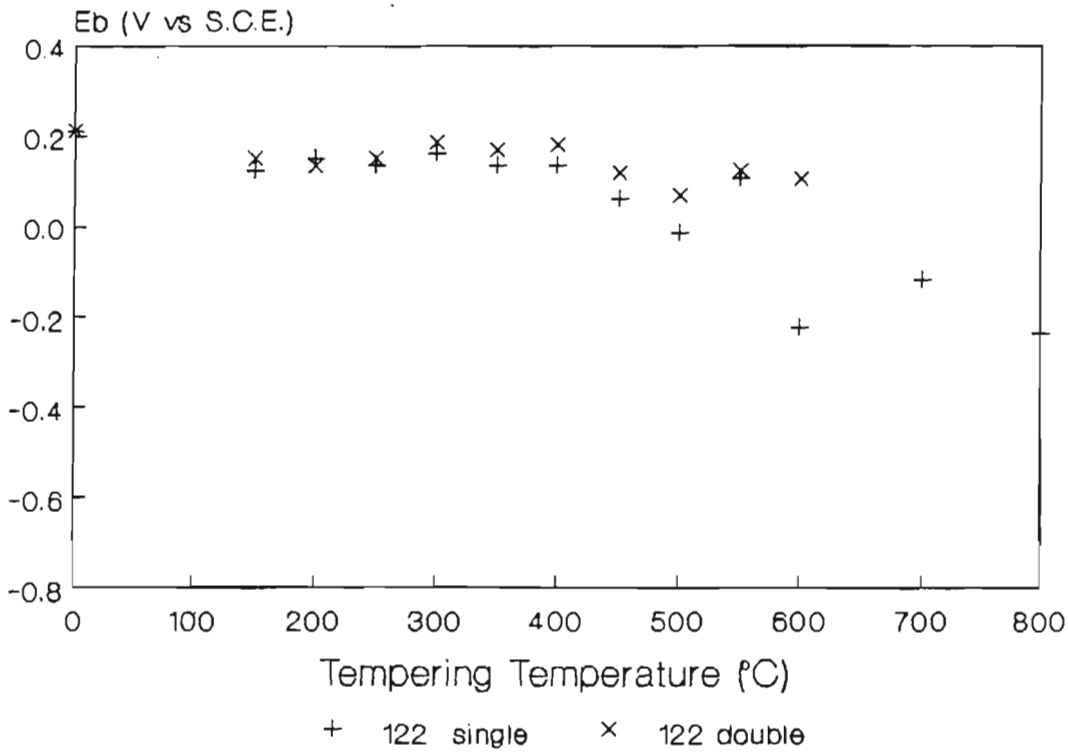

FIGURE 4.20 : Breakdown potential versus tempering temperature for Alloy 122.

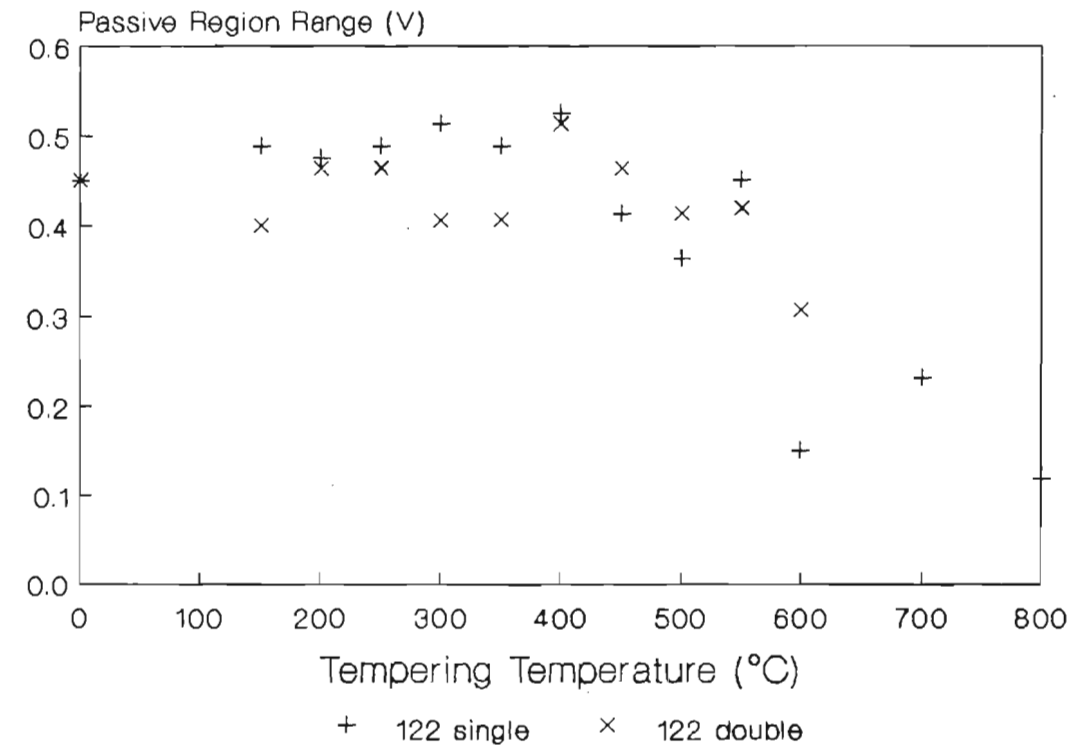

FIGURE 4.21 : Passive region range versus tempering temperature for Alloy 122.

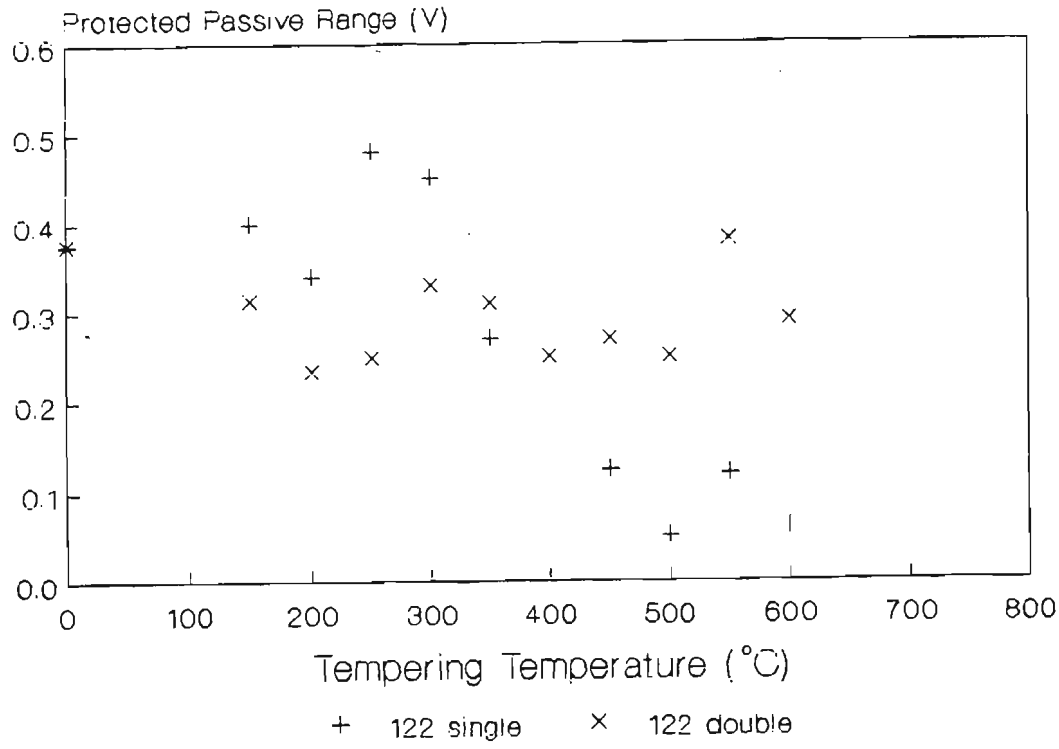

FIGURE 4.22 : Protected passive range versus tempering temperature for Alloy 122.

4.2.4 A Comparison Between The Three Alloys

A comparison of the free corrosion potential of each alloy versus time is given in fig. 4.23. The free corrosion potential of Alloys 102A and 122 both become more noble with time whereas the free corrosion potential of Alloy 825 becomes more active with time. Alloy 122, containing the highest percentage of chromium has the most noble free corrosion potential. Alloy 825, containing the lowest percentage of chromium, has the least noble free corrosion potential.

The variation of the protected passive range with tempering temperature, for alloys having undergone the single tempering treatment is plotted in fig. 4.24a and for alloys having undergone the double tempering treatment in fig. 4.24b. It is evident that with an increase in chromium content, the highest tempering temperature for which a stable protected passive range exists increases. It is apparent that the double temper also increases the tempering temperature range over which a stable protection potential exists.

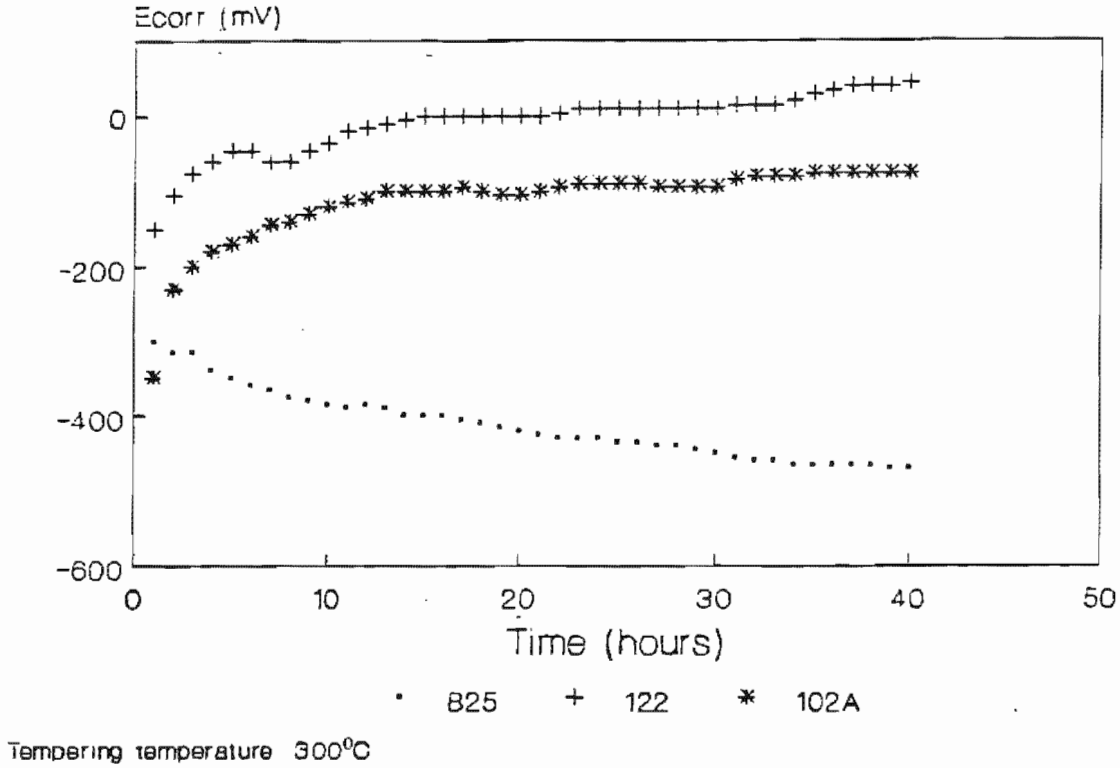

FIGURE 4.23 : Free corrosion potential versus time for Alloys 825, 102A and 122.

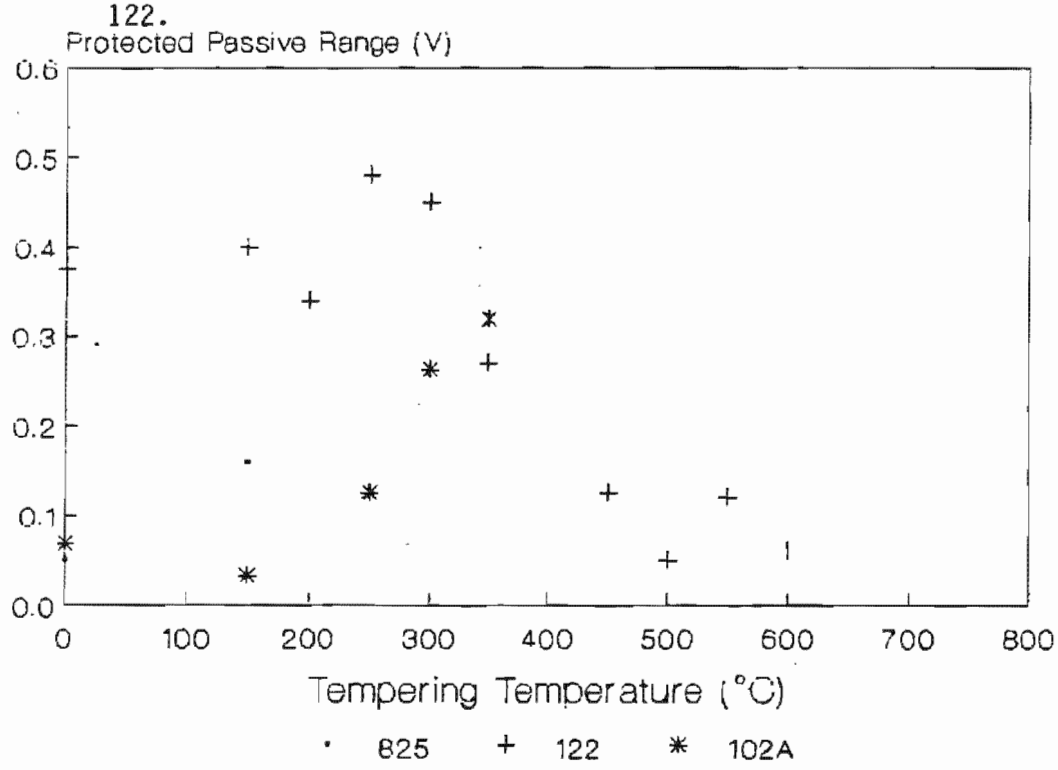

Single Temper

FIGURE 4.24a : Protected passive range versus tempering temperature for Alloys 825, 102A and 122.

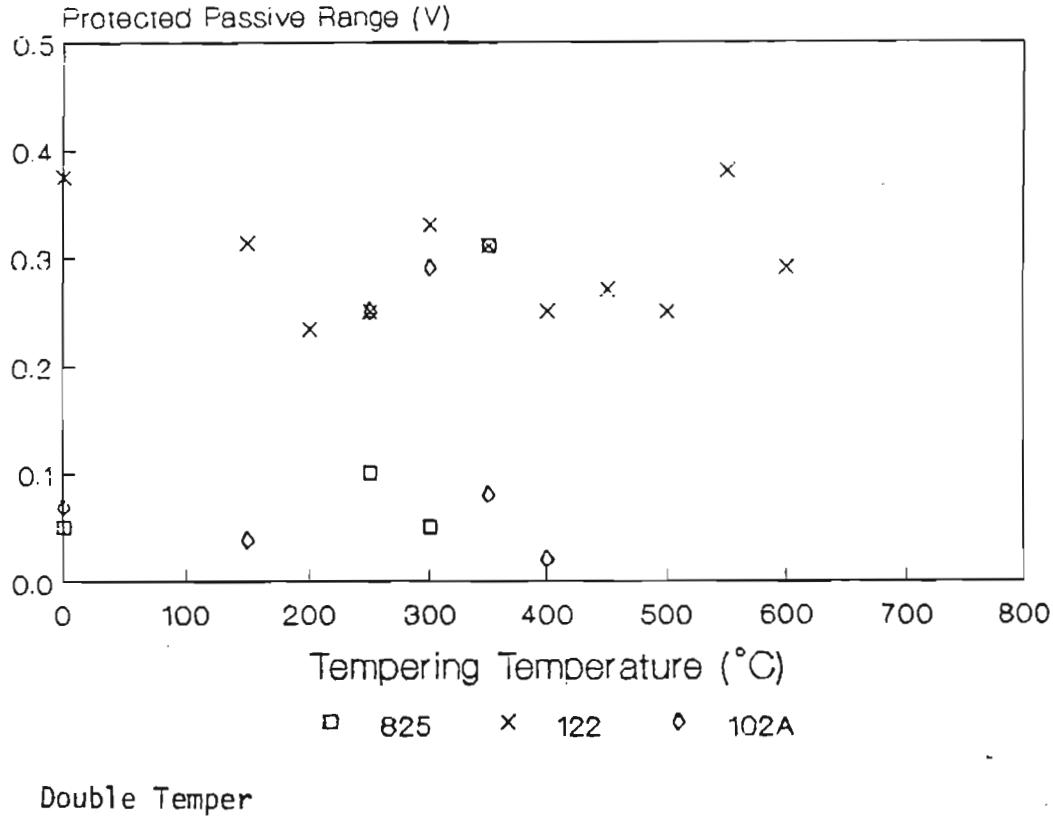

FIGURE 4.24b : Protected passive range versus tempering temperature for Alloys 825, 102A and 122.

4.3 THE NATURE OF THE CORROSIVE ATTACK FOR ALLOYS 825, 102A AND 122

An optical examination of the surfaces, having undergone potentiodynamic tests in a solution containing 200ppm Chloride ions showed inclusions to be present. Typical inclusions are shown in fig. 4.25. An Energy Dispersive System (EDS) analysis of a typical inclusion in alloy 122, is given in fig. 4.26. It is evident that the inclusions are aluminium oxide inclusions, having studied the EDS analysis, morphology and size (Kiessling, 1978).

A pit density analysis of the corroded surfaces revealed a random count over the tempering temperature range. No trend was evident.

A S.E.M. examination of the effect of tempering temperature on the mode of surface corrosion is illustrated in fig. 4.27. After tempering at lower temperatures (150°C to 400°C) the alloys undergo pitting corrosion and the surface outside the pits maintains passivity. After tempering at higher temperatures, the alloys are still subject to pitting corrosion but more general breakdown of the passivity also occurs. Each alloy displays the change in mode of corrosion at a different temperature. Alloy 825 starts to show a general breakdown of passivity as well as pitting after tempering at 350°C. After tempering at 450°C, the predominant modes of attack are general and intergranular corrosion. Alloy 102A shows the beginning of general breakdown of passivity after tempering at 450°C. After tempering at 500°C, the predominant modes of attack are general and intergranularcorrosion. Alloy 122, however, only shows a general breakdown of passivity after tempering in excess of 700°C. A schematic diagram illustrating these factors is given in fig. 4.28.

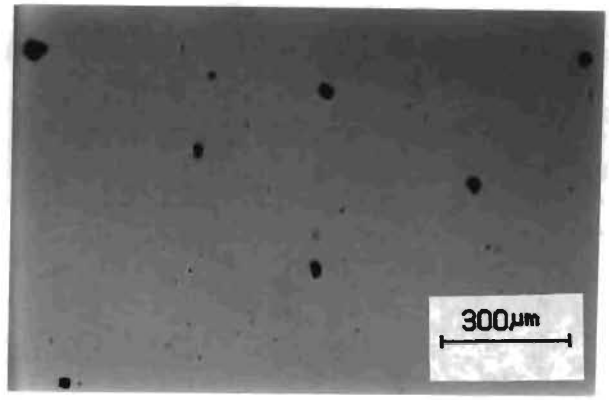

FIGURE 4.25 : Aluminium oxide inclusions on the surface of Alloy 122.

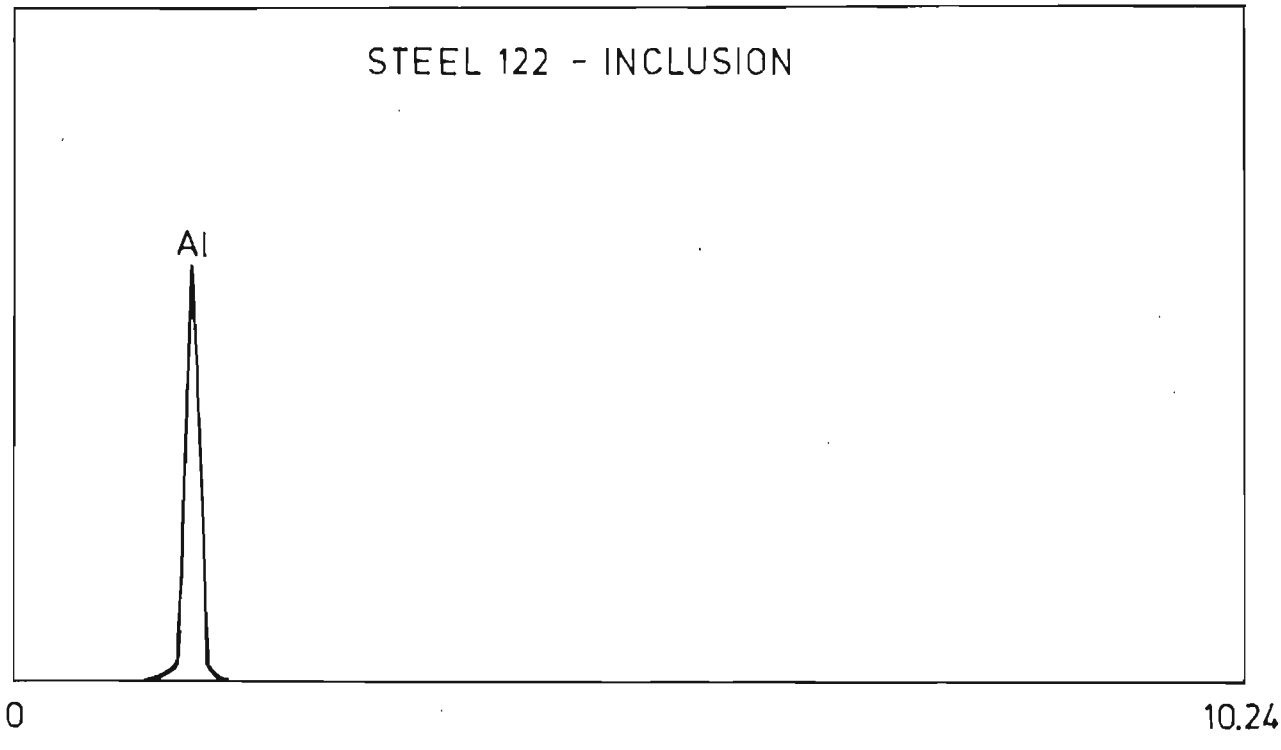

FIGURE 4.26 : An EDS analysis of a typical inclusion in Alloy 122.

FIGURE 4.27 :

a) Alloy 825 - tempering time 2 hours

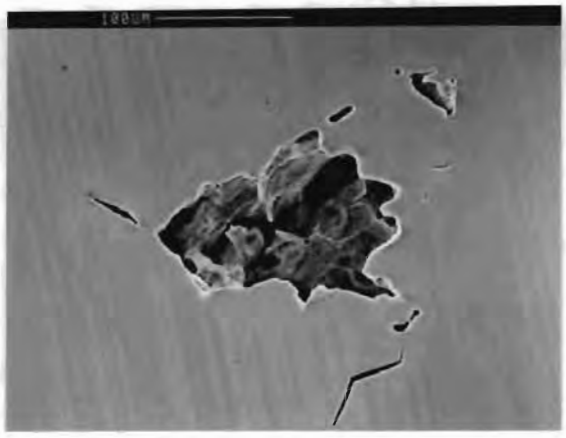

Tempered at 200°C. Predominant mode of corrosion is pitting corrosion.

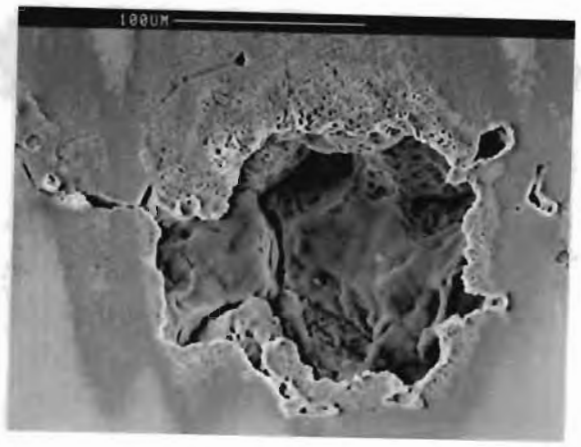

Tempered at 400°C. Predominantly pitting corrosion, but corrosion attack surrounding pits evident.

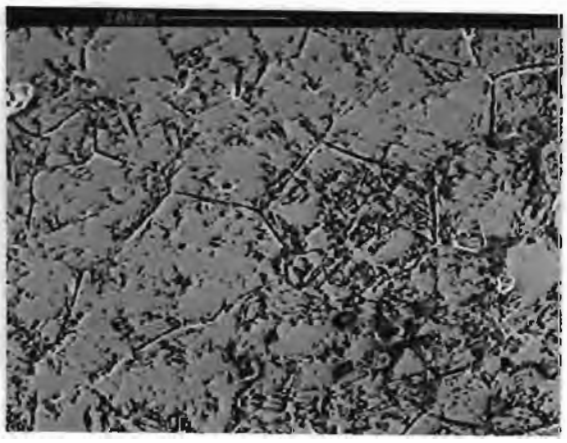

Tempered at 500°C. The predominant modes of corrosion are general and intergranular.

Tempered at 550°C. Pitting, general and intergranular attack is evident.

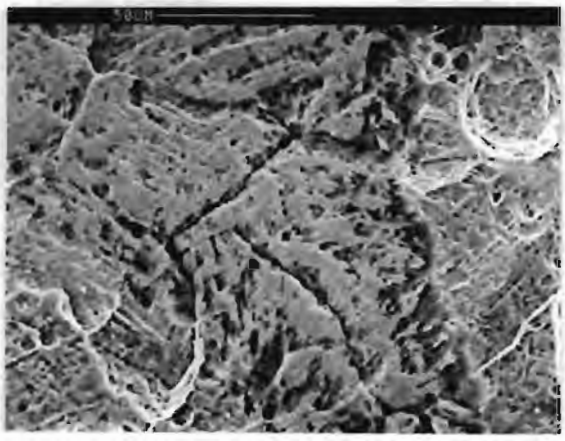

Tempered at 700°C. General and intergranular attack is evident.

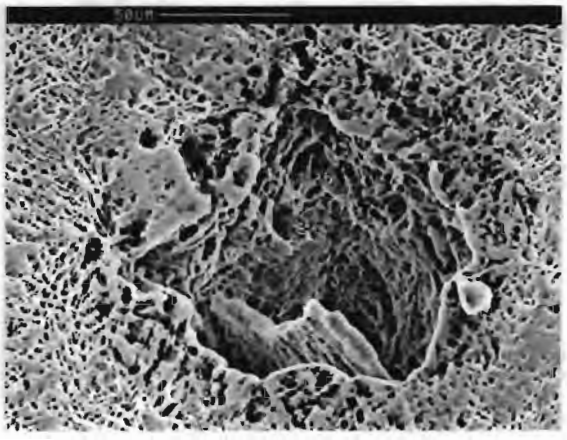

Tempered at 800°C. Shows general and pitting corrosion.

b) Alloy 102A - tempering time 2 hours

As quenched. Predominant mode of corrosion is pitting corrosion.

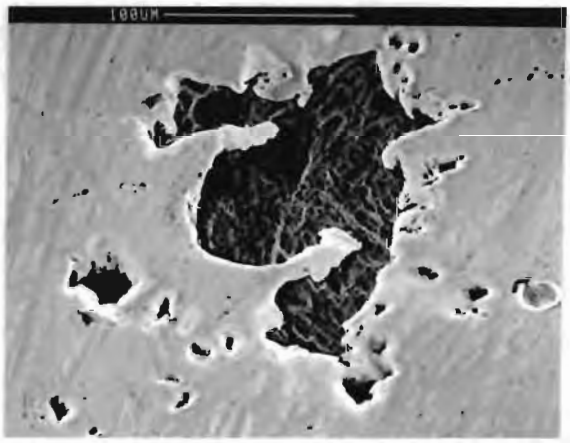

Tempered at 450°C. Shows some general attack associated with pits.

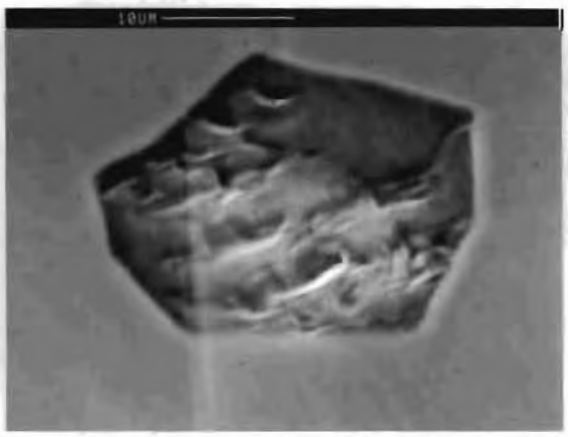

Tempered at 500°C. Shows pit initiation.

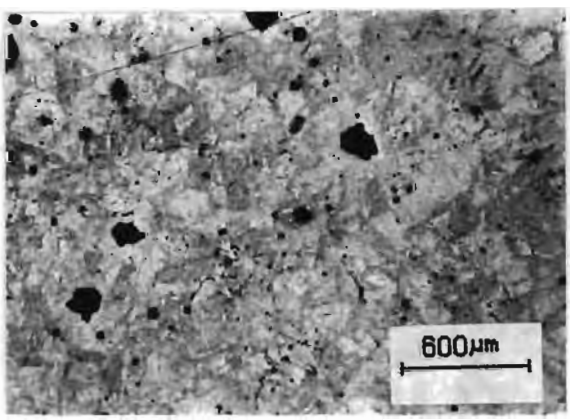

Tempered at 550°C. Shows general and pitting corrosion.

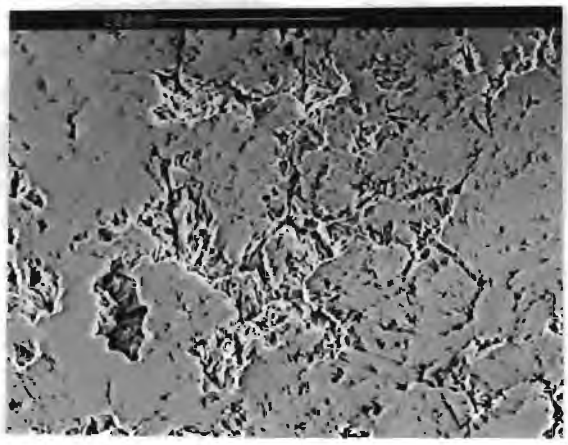

Tempered at 550°C. Predominant modes of corrosion are general and intergranular.

Tempered at 600°C. Shows intergranular attack associated with a pit. Pieces of oxide are evident within the pit.

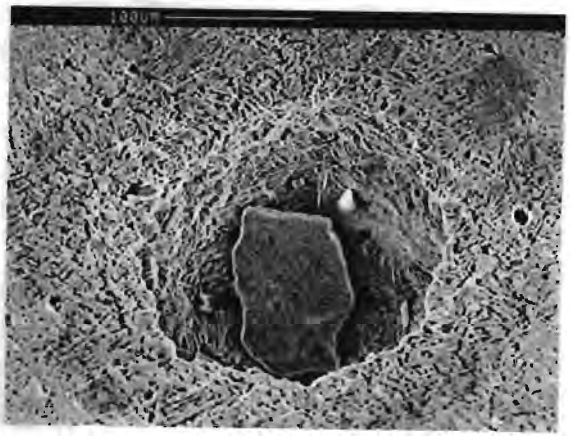

Tempered at 700°C. Shows pit surrounded by general corrosion. An oxide platelet is evident within the pit.

c) Alloy 122 - tempering time 2 hours

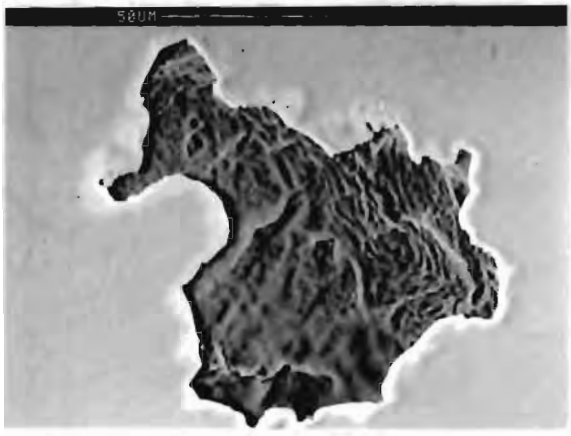

Tempered at 300°C. Curling up of oxide layer can be seen on edge of pit.

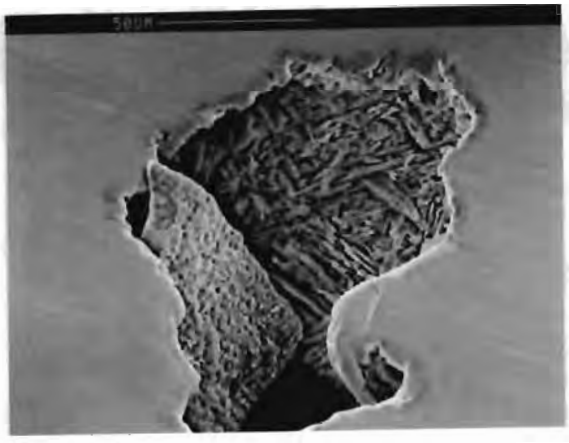

Tempered at 600°C. Shows martensitic laths within pit.

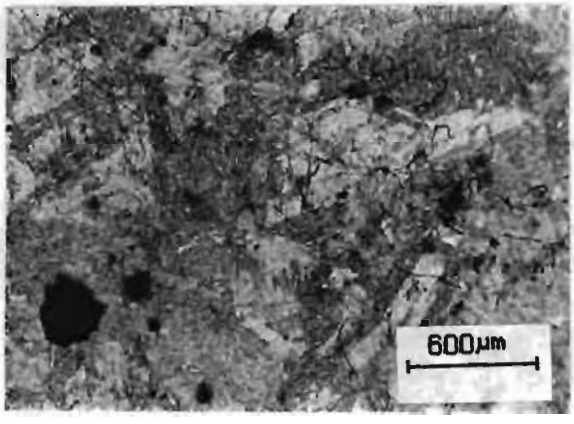

Tempered at 700°C. Shows general and pitting corrosion.

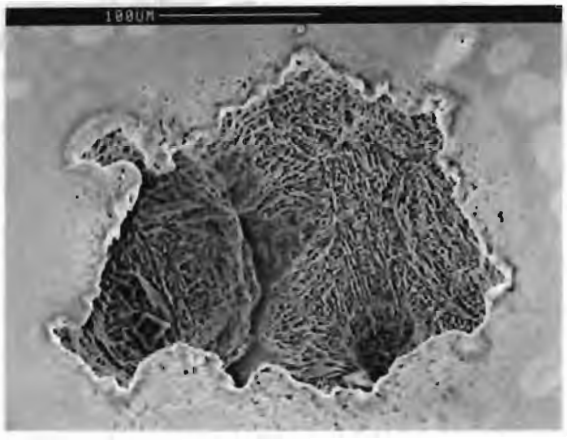

Tempered at 700°C. Shows general corrosion associated with a pit.

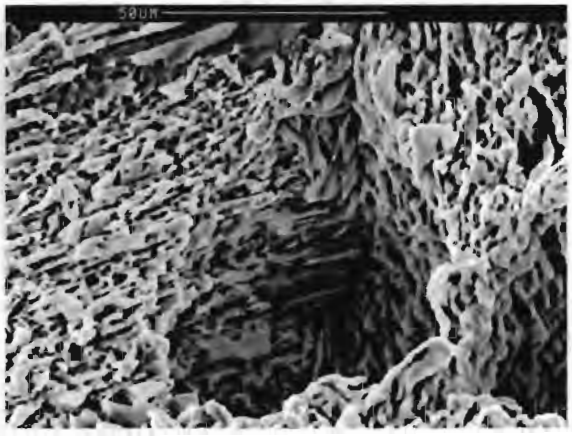

Tempered at 700°C. Higher magnification within pit.

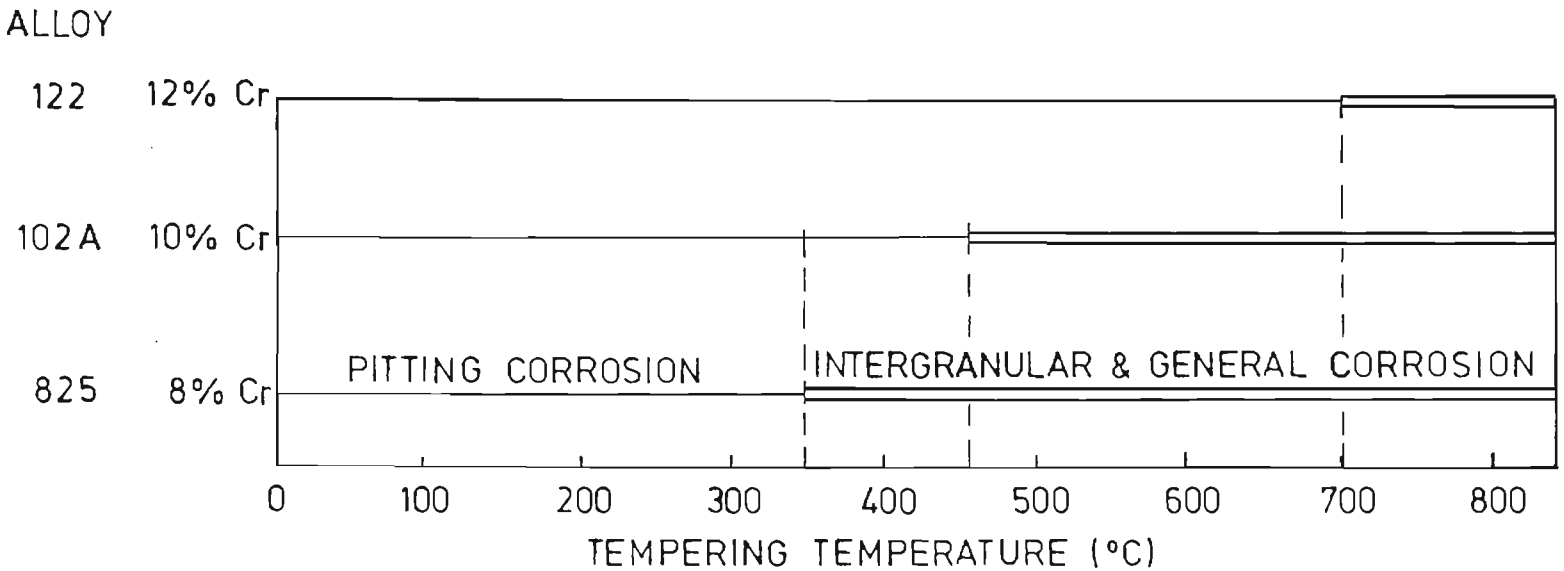

FIGURE 4.28 : The type of corrosive attack as a function of tempering temperature for Alloys 825, 102A and 122.

CHAPTER 5

DISCUSSION

The corrosion resistance of a material is dependent primarily on its chemical composition, with microstructural and environmental factors playing secondary roles. Since microstructure can be changed by the use of heat treatment, its effect on the corrosion behaviour of a material is of great importance. The significance of this is that for a given chemical composition and environment, optimum corrosion resistance for the alloy can be achieved by appropriate heat treatments. Ideally this treatment will also provide acceptable mechanical properties.

5.1 HARDNESS AND MICROSTRUCTURE

When heated to 1100°C for 30 minutes, Alloys 825, 102A and 122 are fully austenitic. On oil quenching down to room temperature, a predominantly martensitic structure is obtained. All the alloys have small amounts of retained austenite. Alloy 825, which has the lowest Ms temperature and Mf temperature below room temperature, (refer to table 3.2) is expected to have the highest percent of retained austenite. It would appear from figs. 4.2a, 4.4a and 4.6a that not all carbon goes into solution at 1100°C and on quenching carbon precipitates are visible.

The martensite transformation is a diffusionless transformation resulting in a supersaturated solid solution of carbon in iron with a body-centered tetragonal (bct) structure. The supersaturation by the interstitial carbon atoms results in a hard metastable structure. There is therefore a driving force, on tempering, to form a thermodynamically more stable structure. This is achieved by the precipitation of carbon.

The following discussion relates to figures 4.1, 4.3 and 4.5.

After tempering at temperatures between 150°C and 350°C softening of the as-quenched alloys occurs. After tempering at temperatures below 200°C, hexagonal -carbide precipitates from the martensitic matrix relieving internal strain. The depletion of carbon from the matrix results in softening.

Specimens which have received tempering treatments at temperatures between 200°C and 300°C undergo the decomposition of any retained austenite as well as the replacement of ϵ-carbide by cementite. The retained austenite is expected to decompose to bainitic ferrite and cementite (Honeycombe (1981)).

At these tempering temperatures the ϵ-carbide interfaces with the matrix become the most likely sites for the nucleation of cementite (Fe_3C) and the ϵ-carbide particles gradually disappear as the Fe_3C particles grow. Grain boundaries, too, are nucleation sites for Fe_3C. As the tempering temperature increases, the Fe_3C particles change from being coherent, to semi-coherent, to incoherent and finally spheroidize at tempering temperatures close to 700°C. As the carbides coarsen, with the removal of carbon from the matrix, softening of the alloys occurs and a minimum hardness is reached after tempering at 350°C.

The three alloys under observation have varying alloying contents. Alloys 825 and 102A have approximately 12.5wt% alloying additions and Alloy 122 has approximately 13.7wt% alloying additions. Of these alloying additions, there are sufficient carbide-forming elements to form alloy carbides at higher tempering temperatures. The enthalpies of formation of some of the compounds are shown in fig. 5.1 in which iron carbide is the least stable compound.

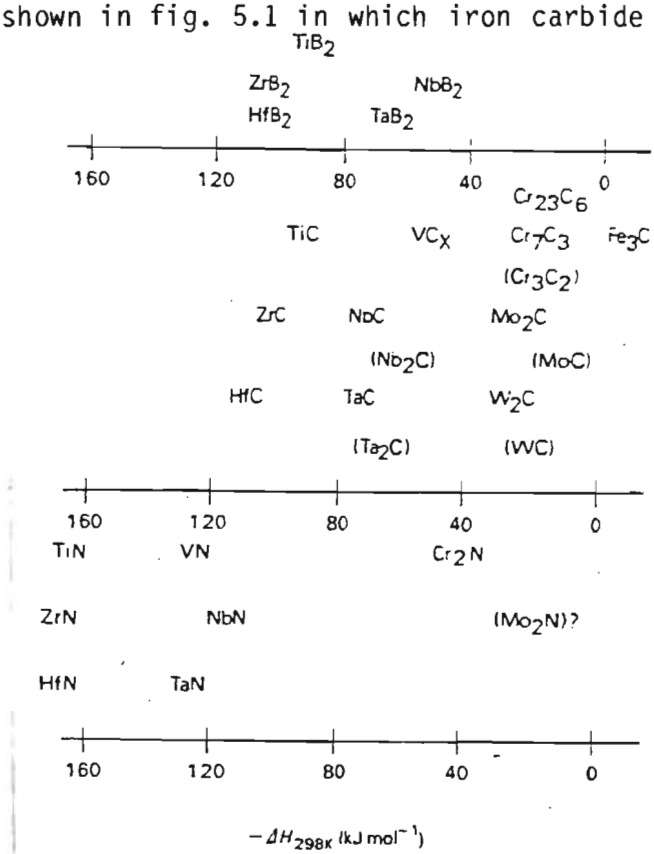

FIGURE 5.1 : Enthalpies of formation of carbides, nitrides and borides (after Honeycombe (1981)).

The alloying elements chromium and molybdenum form carbides with substantially higher enthalpies of formation and therefore form in preference to cementite but only at tempering temperatures between 500°C and 600°C. Due to the high percent of chromium in Alloys 825, 102A and 122, chromium carbides are expected to be the predominant carbide present after tempering at these higher temperatures.

Alloy carbides only form at higher temperatures because the metallic elements diffuse by substitution, in contrast to carbon and nitrogen which move through the iron lattice interstitially. Thus the diffusivities of carbon and nitrogen are several orders of magnitude greater in an iron lattice than those of the metallic alloying elements. Consequently, higher temperatures are needed for the necessary diffusion of the alloying elements and the formation and growth of alloy carbides.

Treatment of coarsening of a dispersion formulated by Lifshitz and Wagner (as discussed by Honeycombe (1981)), can be applied to the coarsening of the cementite and later the chromium carbides. They describe the coarsening of dispersion by the equation:

$$r^3_t - r^3_0 = (k/RT)V^2_m D\gamma t \qquad \text{equation 5.1}$$

where r_0 = the mean particle radius at time zero
r_t = the mean particle radius at time t
D = diffusion coefficient of solute in matrix
γ = interfacial energy of particle/matrix interface
V_m = molar volume of precipitate
k = constant

As carbon has a higher diffusion co-efficient, it is evident from Equation 5.1 that the cementite will coarsen at a greater rate than the alloy carbide does.

There are two ways in which the transformation of chromium carbide from cementite can take place:

1. By <u>in situ</u> transformation - the cementite/ferrite interfaces act as nucleation sites for the alloy carbides which then grow and replace the cementite.

2. By separate nucleation and growth - heterogeneous nucleation of alloy carbides occurs on dislocations, lath boundaries and prior austenite grain boundaries. The carbides then grow at the expense of cementite. (Porter and Easterling (1980)).

Either or both mechanisms could operate depending on the alloy composition.

The process is both time and temperature dependent, and both variables are combined in the Holloman-Jaffe parameter (as discussed by Honeycombe (1981)).

$$p = T(k + \log t) \quad \text{equation 5.2}$$

where T = absolute temperature
t = tempering time
k = constant (about 20 for alloy steels)

This parameter is then plotted against hardness to yield fig. 5.2.

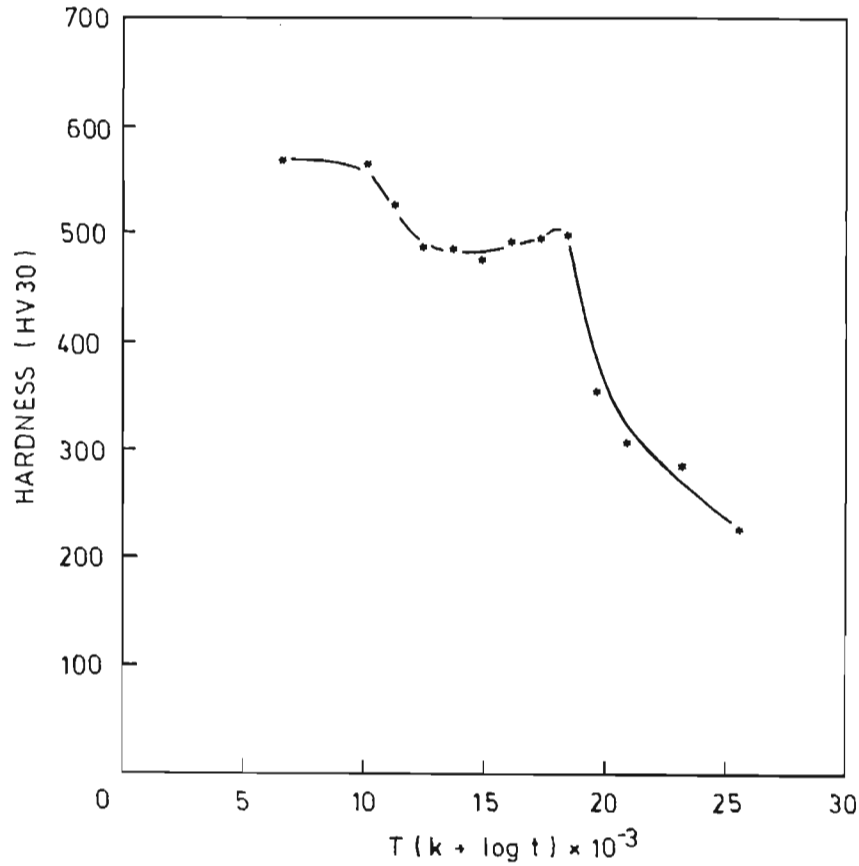

FIGURE 5.2 : Hardness versus the Holloman-Jaffe parameter for single tempered alloy 825

The formation of the chromium carbides causes an increase in hardness - a phenomenon known as secondary hardening. The normal carbide sequence which occurs as the tempering temperature is increased from 150°C through to 500°C is:

$$\underset{(150°C)}{\text{matrix}} - \underset{(200°C)}{Fe_3C} - \underset{(400°C)}{(FeCr)_3C} - \underset{(400°C)}{Cr_7C_3} - \underset{(500°C)}{Cr_{23}C_6}$$

Secondary hardening is due to the precipitation of Cr_7C_3 and $Cr_{23}C_6$ which nucleate simultaneously but at different sites. $Cr_{23}C_6$ grows at the expense of the Cr_7C_3 which eventually disappears from the microstructure, at which stage the steel has completely overaged. The effectiveness of the alloy carbides as hardeners depends on the fineness of the dispersion and the volume fraction precipitated. Orowan formulated an equation (see Smallman (1962) for a discussion) which describes this effect.

$$\tau = 2\alpha\mu b/L \qquad \text{equation 5.3}$$

where τ = shear stress

α = constant

μ = shear modulus

b = Burgers vector

L = interparticle spacing

A finely dispersed precipitate will have a small interparticle spacing and thus a high strength whereas a coarsely dispersed precipitate will have a much greater interparticle spacing and thus a lower strength. A finely dispersed precipitate will retard dislocation movement, due to its smaller interparticle spacing, more than coarsely dispersed particles. All three alloys show a maximum hardness after tempering at 500°C where finely dispersed intragranular particles are formed. These precipitates are both homogeneous (within the grains) and heterogeneous (on dislocations). After tempering at higher temperatures, a drop off in hardness occurs as a result of the coarsening of the $Cr_{23}C_6$ precipitates. This effect is observed in figs 4.2b, 4.4b and 4.6b where coarsening of the carbides leads to grain boundary decoration as well as intragranular precipitation. Figures 4.1, 4.3 and 4.5 show the resulting decrease in hardness at these tempering temperatures.

It would appear from figs 4.2c, 4.4c and 4.6c, that after tempering at 700°C for 2 hours, the chromium carbide precipitates go back into solution, with fine evenly dispersed precipitates remaining which coarsen after tempering at 800°C for 2 hours.

A schematic diagram of the various carbides which precipitate as the tempering temperature is increased is given in fig. 5.3.

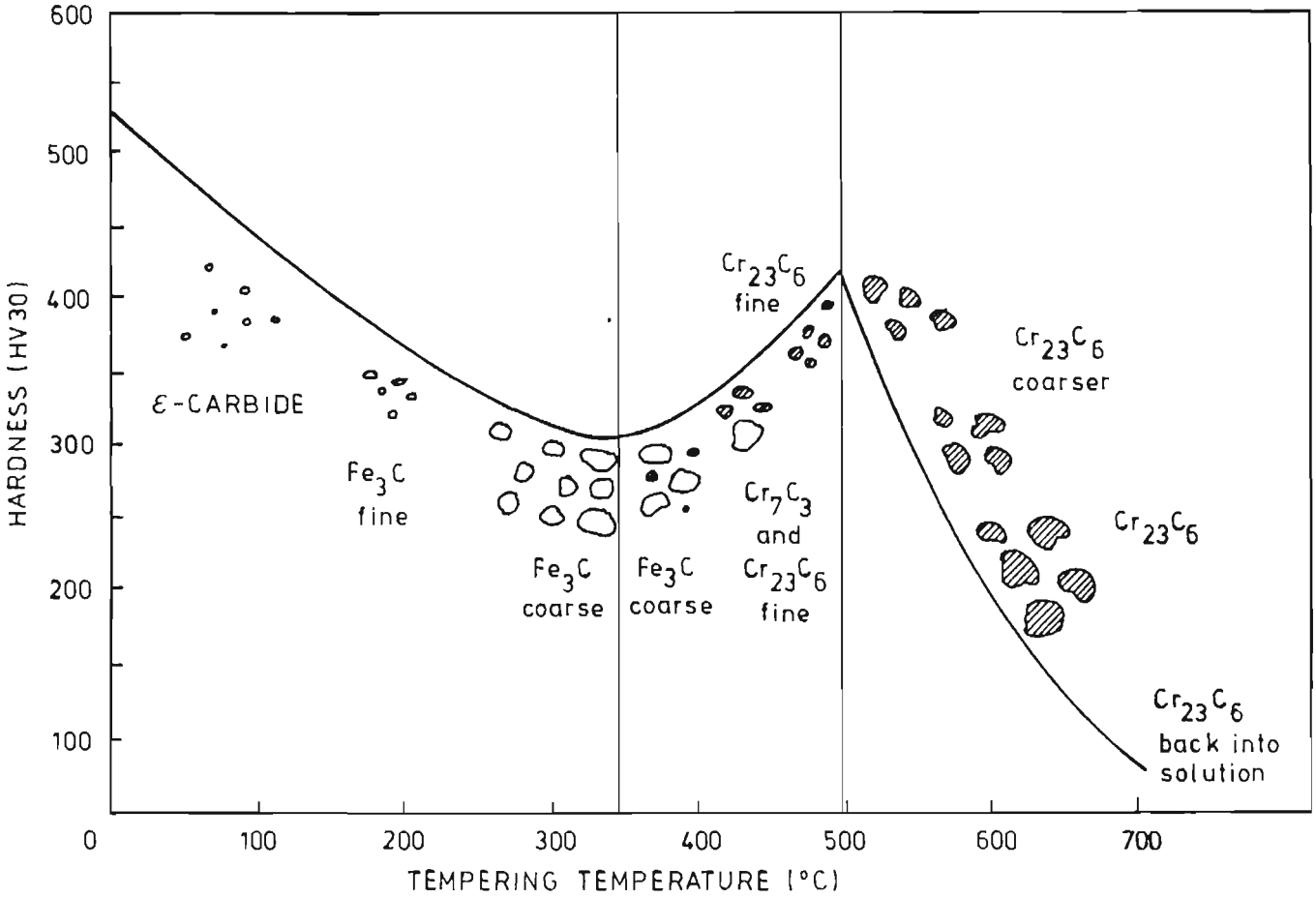

FIGURE 5.3 : A schematic diagram of the effect of the type and nature of precipitation on hardness.

The lath martensite produced in the low carbon steels by quenching contains high-angle lath boundaries and low-angle cell boundaries within the laths together with dislocation tangles within the cells. On tempering above 400°C, recovery occurs and leads to the elimination of both dislocation tangles and the low-angle cell walls and relieves internal stress. This results in softening. This effect therefore counteracts the secondary hardening effect. The final hardness is therefore the net effect of the two.

In all three alloys, the double temper generated a softer material than the single temper at lower tempering temperatures and a greater degree of secondary hardening at higher tempering temperatures. After tempering between 200°C and 300°C, the double temper ensures a complete transformation of retained austenite to martensite. Diffusion of atoms is a controlling factor in the tempering process and is governed by the Arrhenius rate equation where

$$y = Ae^{-Q/RT} \quad \text{equation 5.4a}$$

or

$$1/t = Ae^{-Q/RT} \quad \text{equation 5.4b}$$

where y = fraction transformed per unit of time
t = time to transform a unit of reactant
Q = activation energy
A = constant
R = gas constant (8.314 JK mol)
T = absolute temperature

From this equation it follows that

$$\log y = \log A - Q/RT \quad \text{equation 5.5}$$

and thus $\log y$ or $\log 1/t$ vary linearly with $1/T$

It can be deduced that, as the tempering temperature increases, the amount of time needed for a transformation to occur decreases.

A double temper allows more time for a reaction to take place. At lower tempering temperatures, a greater amount of carbon will be able to diffuse under the double tempered conditions than the single tempered conditions and thus more ϵ-carbide and later cementite particles are formed and thus a softer material results. The double temper will allow for more relaxation and recovery, also having a softening effect. After tempering at 400°C to 500°C where substitutional diffusion exceeds the rate of interstitial diffusion, chromium is given more time to diffuse under the double tempering conditions and therefore more chromium carbides should be formed. Thus, the secondary hardening peak under the double tempered conditions is more pronounced than under single tempered conditions.

With reference to figs 4.2d, 4.4d and 4.6d, a 15 minute temper at 700°C causes the decoration of grain boundaries whereas a 2 hour temper does not. These differences could be explained by the fact that a reaction could proceed further in 2 hours than in 15 minutes. Lee, Cragnolino and MacDonald (1985) conducted experiments to determine the effect of heat treatment on Inconel 600 (refer to section 2.2.3.3). It was observed that there was a change in microstructure with increasing tempering time at 700°C and a stepped increase in transformation with time was found. It is postulated therefore that while a 15 minute temper at 700°C is too short for the dissolution of grain boundary precipitates, a 2 hour temper at 700°C is sufficiently long to allow this to occur. Thus a stepped transformation with time is observed.

A comparison between the hardness of the three alloys is given in figure 4.7a and b for the single and double tempered conditions respectively. As can be seen, the hardnesses of the three alloys follow a similar trend but Alloy 122 is consistently 100HV softer than Alloys 825 and 102A. Microhardness tests were carried out on Alloy 122 to establish whether this effect was due to decarburization. It was established that decarburization had not occurred and that the edge of the sample was harder (620.6HV 200g) than the centre (593.6HV 200g) as would be expected after quenching. An alternative explanation is thus required.

Those elements which are carbide formers not only retard softening but also form the fine alloy carbides responsible for secondary hardening. The effects various levels of molybdenum have on the retardation of softening is illustrated in fig. 2.7. Alloy 122 contains no molybdenum whereas Alloy 102A contains 0.013wt% molybdenum and Alloy 825 contains 0.148wt% molybdenum. Pickering (1978) suggests that a retardation of softening, rather than pronounced secondary hardening, is produced by the formation of small precipitates of Cr_7C_3 and a M_2X phase, based presumably on $Cr_2(CN)$. The presence of nitrogren causes the amount of M_2X to increase at the expense of Cr_7C_3. Molybdenum accentuates M_2X formation resulting in increased secondary hardening. In the overaged condition, $Cr_{23}C_6$ forms progressively larger particles as M_2X is replaced by the more stable carbide. Because molybdenum stabilizes M_2X it makes M_2X's replacement by $Cr_{23}C_6$ less rapid so that the tempering resistance is increased.

Increasing the chromium content of the steels from zero to 12wt% results in increased secondary hardening. Figure 5.4 illustrates the effect the

chromium equivalent has on the secondary hardening range of the three alloys. The fact that increasing chromium content results in an increased number of chromium carbides indicates that at lower chromium contents not all carbon is incorporated as chromium carbides. As the chromium equivalent increases, the slope of the graph decreases and thus a region is expected to be reached where adding more chromium will not further increase the secondary hardening range. This results when the maximum percentage of carbon is incorporated with the chromium and no further addition of chromium will have an effect. Alloy 122 has the most chromium and therefore more carbon will be incorporated as carbides and less carbon will be in the surrounding matrix than in Alloys 825 and 102A and therefore the general level of hardness of Alloy 122 is expected to be softer.

According to Pickering (1978), an increase in the molybdenum and cobalt content increases the general level of the tempering curve. This, together with the higher nickel content explains why Alloy 825 has a tempering curve 100HV higher than Alloy 122. Alloy 102A, however, cannot be explained as simply as this. It is presumed that the obtained hardness is a result of the combination of alloying elements. Alloy 825 contains 0.024 wt% nitrogen whereas Alloy 102A contains 0.08wt% nitrogen and Alloy 122 contains 0.032wt% nitrogen. The presence of nitrogen causes M_2X to increase at the expense of $Cr_{23}C_6$. Thus the combined effect of nitrogen, cobalt and molybdenum, with a total wt% in alloy 825 of 0.306wt%, in Alloy 102A of 0.107 wt% and in Alloy 122 of 0.065wt% may account for the difference in hardness between Alloys 825, 102A and 122.

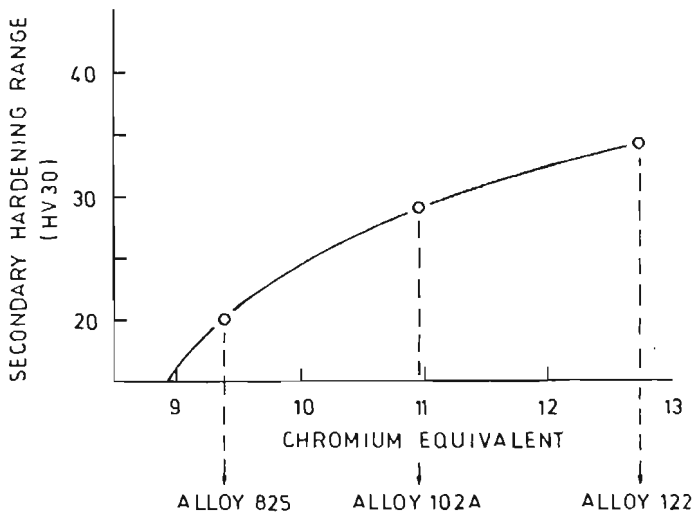

FIGURE 5.4 : The effect of the chromium content on the magnitude of secondary hardening.

5.2 ELECTROCHEMICAL ANALYSIS

The most important property of high chromium steels is their corrosion resistance. This corrosion resistance is provided by a very thin surface film, composed of chromium oxide, which is self-healing in a wide variety of environments. The corrosion resistance of stainless steels is, however, undermined by localized breakdown in the form of pitting and crevice corrosion. Factors which affect pitting corrosion include the alloy composition, the passive film characteristics, the environment and the heat treatment. Stainless steels can undergo sensitization after tempering between 500°C and 650°C which has a significant effect on the corrosion resistance. Sensitization is caused by alloy-carbides which precipitate out of solution after tempering at higher temperatures resulting in a chromium depleted zone which is susceptible to corrosion.

A comparison of the free corrosion potential versus time of Alloys 825, 102A and 122 is given in fig. 4.23. Under the ideal conditions of a clean polished surface, a fully aerated solution and no stagnant zones, the corrosion behaviour of Alloys 102A and 122 are similar, both becoming more noble with time and reaching a steady state situation after 40 hours but Alloy 122 is consistently at a more noble potential. Alloy 825, however, has a different corrosion mechanism and becomes more active with time and does not reach a steady state situation after 40 hours. The change in corrosion mechanism between Alloy 825 and the other two alloys is related to the different chemical compositions. A plot of the chromium equivalent of each alloy versus the equilibrium free corrosion potential is given in fig. 5.5.

An increase in the chromium equivalent is accompanied by an increase in the equilibrium free corrosion potential. The slope of the curve indicates that a saturation point will be reached where furtner additions of chromium (i.e. a steel with a higher chromium content) will not further increase the free corrosion potential. At chromium levels of 8%, a stable passive layer does not form and breakdown of the film occurs at the weakest spots resulting in pitting and crevicing; thus localized breakdown accounts for the decrease in the free corrosion potential with time exhibited by alloy 825.

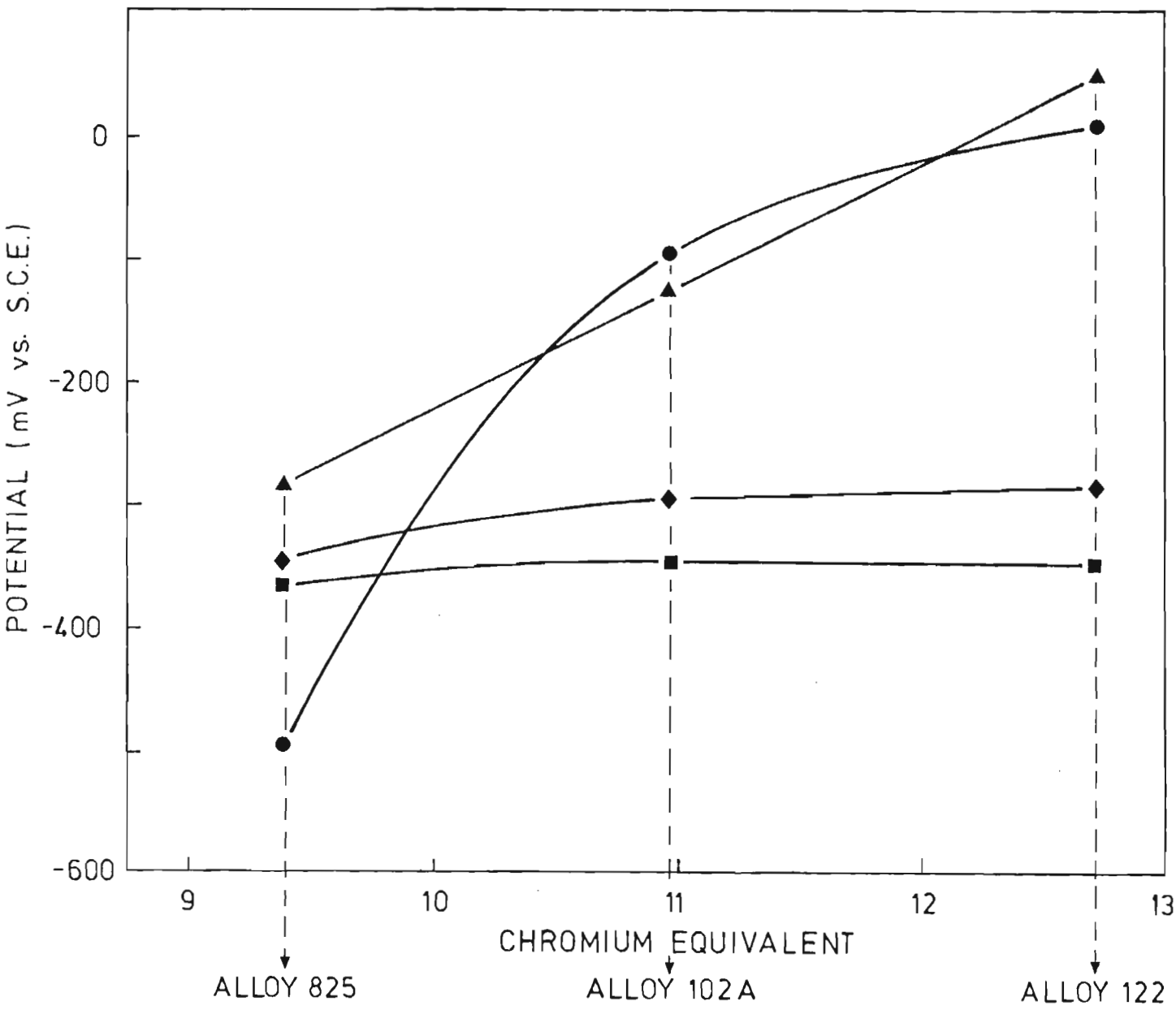

● Free corrosion potential
▲ Breakdown potential
■ Ecorr under single tempered conditions
◆ Ecorr under double tempered conditions

FIGURE 5.5 : The effect of the chromium equivalent on the free corrosion potential, the breakdown potential and Ecorr.

Alloy 102A and Alloy 122, with 10% and 12% chromium respectively, show passive behaviour with the oxide film thickening with increasing time. The free corrosion potential of Alloys 102A and 122 may be attributed to a mixed potential where:

$$E_{corr} = xE^{active} + yE^{passive} \qquad \text{Equation 5.6}$$

where x = area of the surface that is anodic

y = area of the surface that is cathodic

E^{active} = potential of anode

$E^{passive}$ = potential of cathode

Atrens (1983), when experimenting with a typical 12% chromium low-pressure steam turbine blade material in chloride solutions, found that the free corrosion potential became more active with time in aerated solutions. It was thought that the free corrosion potentials were a reflection of the actively corroding pits and crevices as is the case with Alloy 825.

A typical potentiodynamic scan for each alloy is illustrated in fig 5.6. It is observed that breakdown and repassivation do occur prior to the final breakdown of the specimen. Frankel et al (1984) suggest that this breakdown and repassivation is due to metastable pits forming as discussed in Section 2.2.1a. Briefly, the measured current increases as the pit nucleates and begins to grow. After a short growth period, the metastable pits repassivate and the current decreases rapidly to the level of the original signal.

As can be observed from fig. 5.6, all three alloys have a very similar passive current density, ipass, of approximately 1.2μA/cm^2. The size of the passive potential range is influenced by the difference in chemical composition and specifically the difference in chromium content. With increasing chromium content, an increase in the passive region range occurs.

Each steel displayed hysteresis loops on reversing the scan afer pitting had commenced. If the loops rejoin the scan in the passive region, initiated pits will repassivate. However, if the loops rejoin the scan in the cathodic region initiated pits will propagate. The protection

potential of Alloy 825, after almost all tempering treatments, rejoined the initial scan in the cathodic region and therefore initiated pits will propagate.

Superimposed on fig. 5.5 are the results from the potentiodynamic scans for E_{corr} and E_b (or E_p). Average values taken over the full range of tempering temperatures are plotted. It is observed that, in general, the E_{corr} values are more active than the equilibrium free corrosion potentials. The E_{corr} values obtained from the potentiodynamic scans reflect the value expected on a clean surface with no passive layer. The equilibrium free corrosion potentials are indicative of the value likely to be encountered in service (with a stable passive layer on the surface).

It can also be observed from fig. 5.5 that E_{corr} is more noble after double tempering than after single tempering. A possible explanation for this is that the probability and number of potentially active sites diminishes with double tempering conditions with respect to single tempering conditions and thus the chromium oxide layer is more stable after double tempering than after single tempering. This results because the double temper allows more internal strain to be relieved due to the increased time of temper. After double tempering at higher temperatures, however, it is expected that more chromium will be incorporated within the carbide leaving less chromium in solution and therefore decreasing the corrosion resistance. The final corrosion resistance is therefore the nett effect of the two.

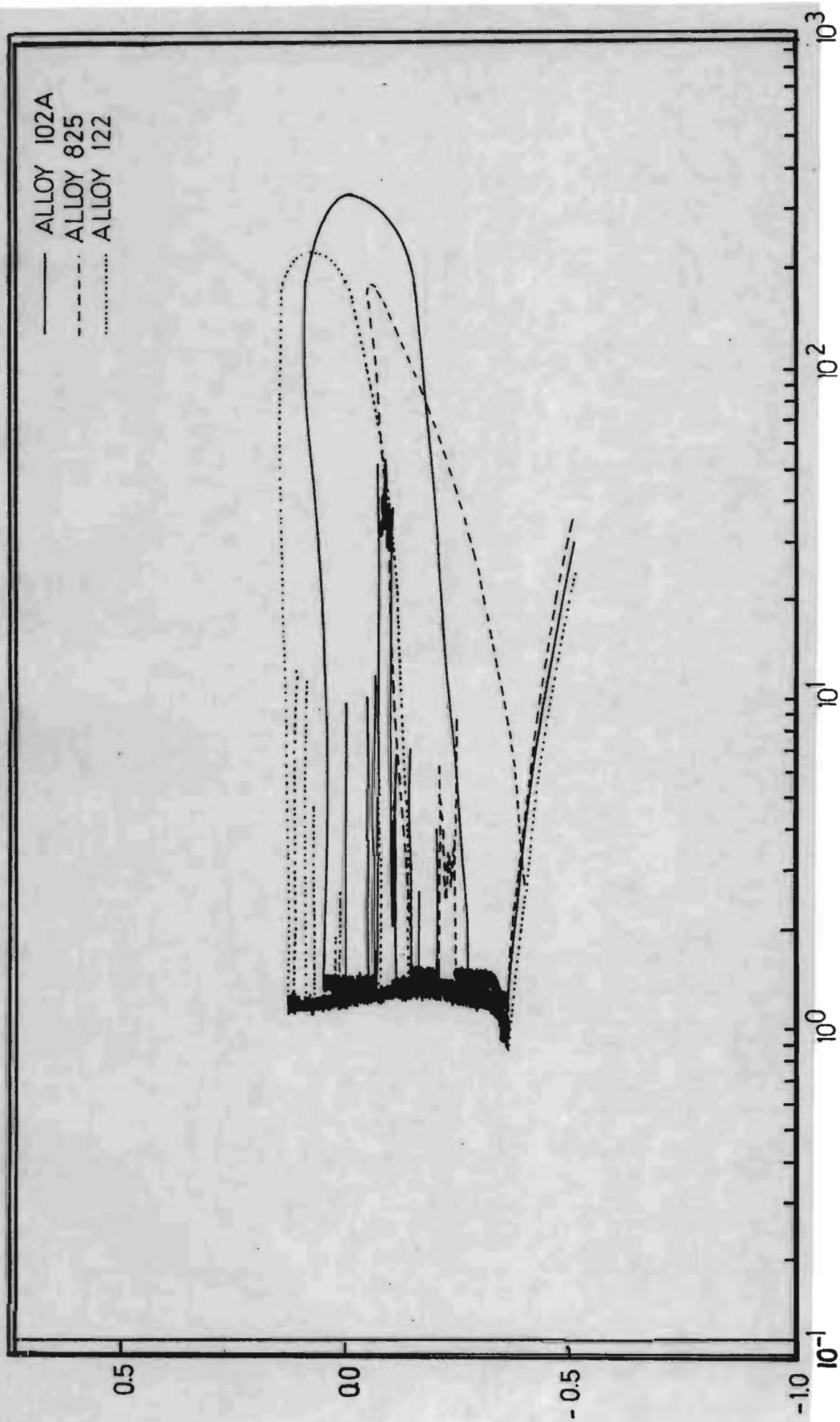

FIGURE 5.6 : A typical potentiodynamic scan of Alloys 825, 102A and 122. Double tempered at 250°C for a total of 4 hours.

The fact that samples which have undergone single tempering treatments are more susceptible to corrosion than those that have undergone double tempering treatments is substantiated by the protection potential results. All three alloys show a decrease in the number of scans where the protection potential is more active then E_{corr} for the double tempered samples with respect to the single tempered samples as is evident in a statistical analysis of the scans in Table 5.1. It is also evident from Table 5.1 that an increase in chromium content, from 8% to 10% to 12% for Alloys 825, 102A and 122 respectively, raises the transition tempering temperature above which the protection potential is more active than E_{corr}. A double temper, too, raises the transition tempering temperature.

TABLE 5.1 : Number of scans where the protection potential is below the free corrosion potential for both the single and double tempered specimens. The transition temperature is the temperature above which E_{prot} is below E_{corr}.

ALLOY	SINGLE	TRANSITION TEMP.	DOUBLE	TRANSITION TEMP.
Alloy 825	9	150°C	7	350°C
Alloy 102A	6	350°C	5	400°C
Alloy 122	1	*	0	

* only one at 400°C

Alloy 122 has protection potentials more noble than E_{corr} for all tempering temperatures in both the single and double tempered conditions which would indicate that all pits which initiate may repassivate. Mancia and Tamba (1988) found E_{prot} to vary with the intensity of local attack and thus decided that E_{prot} was not a reliable basis for predicting localized corrosion risks in stainless steels. This would account for the apparent anomaly, exhibited by Alloy 122, after tempering at 400°C.

Pits which initiate in Alloys 825 and 102A, however, after tempering at temperatures higher than 150°C or 350°C respectively in the single tempered conditions, will propagate and not repassivate.

It is also indicated on fig. 5.5 that Alloy 102A has a pitting (breakdown) potential more active than the equilibrium free corrosion potential and therefore pitting corrosion may occur in this solution tested in freely corroding conditions.

Many difficulties were experienced with determination of the corrosion rates. Other workers, too, have commented on the difficulty of only using one method to determine the corrosion rates or to quantify the extent of corrosive damage. Payer and Staehle (1975) found that "Anodic polarization curves cannot be used to predict susceptibility to intergranular corrosion due to sensitization". Heitz and Schwenk (1976) state that, "In the case of local corrosion in the passive state there is only limited applicability of the method (potentiodynamic polarization tests). If the corroding areas are large, polarization resistance measurements are useful. During pitting, intergranular corrosion rates might be measured, but they generally give no information on the rate or extent of the corrosion damage". The following discussion is written with this knowledge.

On consideration of the corrosion rates represented in fig. 4.9a (Alloy 825), fig. 4.14a (Alloy 102A) and fig. 4.19a (Alloy 122), it is apparent that a random scatter occurs when using i_{corr} for calculation of the corrosion rate. The value of i_{corr} is due to the summation of all corrosion currents over the specimen's surface. Large areas of chromium depletion will result in a greater measured i_{corr} since active general corrosion can occur at these times. Alloy 825, in both the double and single tempered condition and Alloy 102A, in the single tempered condition, show in contrast to Alloy 122, maximum corrosion rates after tempering treatments between 450°C and 550°C. This is because the precipitation of chromium carbides and the simultaneous formation of a chromium depleted zone adjacent to the precipitates at these tempering temperatures results in active general corrosion and increasing i_{corr}. This precipitation occurs intergranularly as well as on grain boundaries and so general corrosion as well as intergranular corrosion is expected to occur. This is substantiated in figs. 4.27a and b for Alloys 825 and 102A where intergranular and intragranular precipitation is observed after tempering at 500°C. Alloy 122, however, does not show this increased corrosion rate afer tempering between 450°C and 550°C and also no general or intergranular attack is observed on the surface (fig. 4.27c).

As was proposed in Section 5.1 for secondary hardening, a saturation point is reached where the maximum amount of carbon is incorporated as chromium carbide and excess chromium remains free in solid solution. It is propsed that Alloy 122, containing 12% chromium, is in the region above the saturation point and is therefore protected from general corrosive attack by the excess chromium left in solid solution. A diagrammatic model of the effect of 12% chromium, in comparison to 10% or 8% chromium, is given in fig. 5.7. It shows that the depletion profile of chromium from the adjacent zones is not as severe for steels containing 12% chromium as for steels containing 8% chromium because of the excess chromium left in solid solution in a 12% steel.

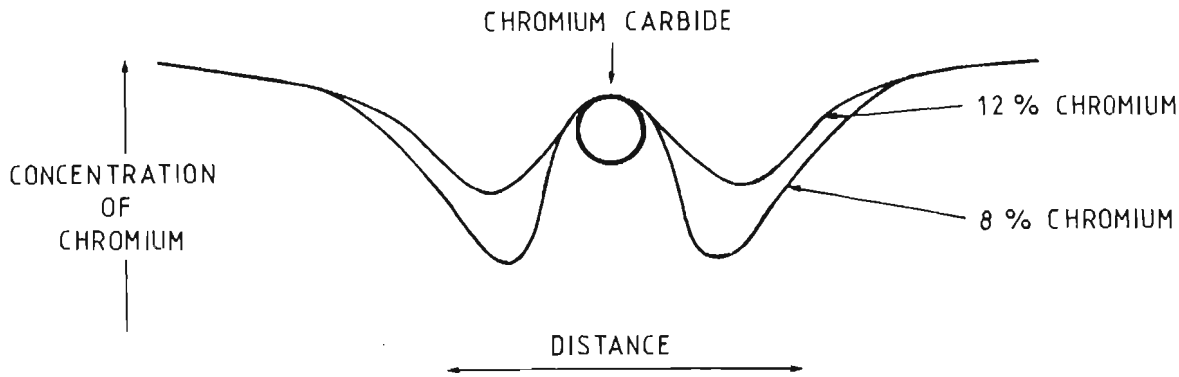

FIGURE 5.7 : Chromium concentration profile.

Truman (1976), however, obtained a very defininte increase in corrosion rate, using weight loss tests, as is indicated in fig. 2.9 for a 13% Cr.29% C steel after tempering for 16 minutes and 2.7 hours at 450°C to 700°C. Grobler and Mostert (1988) found that the corrosion rate of alloy 927 increased after tempering temperatures above 600°C. Alloy 927 has approximately 9% Cr and 0.18% C. It is expected to behave as Truman's (1976) steels did but there is a delayed effect and the equilibrium carbide $M_{23}C_6$ only replaces M_2C and M_7C_3 carbides at 600°C. They attributed the decrease in corrosion resistance to the depletion of chromium and molybdenum adjacent to chromium and molybdenum carbides.

Alloys 825 and 102A do not reflect, using ipass in the corrosion rate equation (refer to appendix A), the slight increase in corrosion rate seen for Alloy 122, when tempering at 450°C and 600°C (figs. 4.9b and 4.14b respectively). This is due to there being no passive region in these alloys at higher tempering temperatures. Therefore using i_{pass} to calculate the

corrosion rate is the incorrect method for the lower chromium steels and particularly Alloy 825. Alloys 102A and 122 are both calculated to have a a lower corrosion rate after double tempering at lower temperatures and a higher corrosion rate after double tempering at higher temperatures with respect to the single tempered samples. As discussed in section 5.1 after double tempering at lower tempering temperatures more ϵ-carbide and later more cementite is formed and after double tempering at higher temperatures more chromium carbides precipitate and increased chromium depletion takes place resulting in a decrease in the corrosion resistance.

An alternative approach is to use i_{pass} when a passive region existed on the potentiodynamic scan and i_{corr} when no passive region existed as shown in fig 4.9c for Alloy 825. A maximum corrosion rate occurs after single tempering at 500°C and after double tempering at 550°C. Again, this can be explained by the chromium depleted area surrounding the chromium carbides.

As discussed at the beginning of section 5.2.3, other workers have also commented on the difficulty of only using one method to determine the corrosion rates.

Alloys 825 and 102A both show random breakdown potentials with increasing tempering temperature as reflected in figs 4.10 and 4.15 respectively. Apart from those samples tempered between 350°C and 450°C, the single tempered samples of Alloy 102A have a lower breakdown potential than the double tempered samples. This is again explained by the double tempered sample having a more stable chromium oxide layer than the single tempered sample. The minimum breakdown potential appears to be as a result of tempering at 525°C as expected due to the incease in the number and fineness of the $Cr_{23}C_6$ and simultaneous increase in area of chromium depleted zones. The randomness of the results reflects the instability of the passivity of the material especially in the case of Alloy 825. Many problems were experienced with Alloy 825 on obtaining a "correct" scan due to this instability. There was much crevice corrosion underneath the gasket and many tests had to be repeated.

With reference to fig. 4.16 the passive region range, in Alloy 102A, shows much variation with tempering temperature up to 400°C and then stabilizes after tempering above 400°C, tending to zero. However, after tempering above 550°C, a passive region again develops. A possible explanation for this is that chromium can go back into solution at these higher tempering

temperatures. This is accompanied by a decrease in the area which is depleted of chromium and the chromium oxide layer reachieves stability.

Alloy 122 shows a stable, constant breakdown potential and passive region range for both the single and double tempered conditions within the tempering range 150°C to 550°C and then both the breakdown potential and passive region range decrease after tempering at higher temperatures as can be seen in figs. 4.20 and 4.21. The S.E.M micrographs in fig. 4.27 show that Alloy 122 does not undergo general corrosion after tempering between 150°C and 600°C. The sample tempered after 700°C, however, does show the initial stages of general corrosion. It is therefore expected that, for alloy 122, chromium carbides precipitate out of solution at higher tempering temperatures than for Alloys 825 and 102A.

The protected passive ranges of Alloys 825, 102A and 122 as a function of tempering temperature, are given in figs. 4.12, 4.17 and 4.22 respectively. In all alloys, double tempering increases the tempering temperature range over which a protected passive range exists with respect to single tempering. The tempering temperature range over which a protected passive range exists, also increases with increasing amounts of chromium as is explained in fig. 5.7.

5.3 A SUMMARY OF THE CORROSION RESISTANCE OF ALLOYS 825, 102A AND 122

It would appear from what has been discussed that alloy 825 has an extremely unstable passive layer and tends to undergo a general type of attack rather than localized pitting attack. This is supported by work of Barker (1985), Bechet (1988) and Cotterrell (1988).

Work done by Barker (1988), revealed three types of responses of an abraded surface to corrosion. This is shown in fig. 5.8.

In Region I active general corrosion predominates. Region II covers the transition from active general corrosion to spontaneous repassivation and Region III is where spontaneous repassivation occurs. It is clear after analysing the results that Alloys 825 and 102A containing 8% and 10% chromium respectively fall in Region II whereas Alloy 122 containing 12% chromium falls in Region III. Further Barker (1988) found that materials with less than 6% chromium exhibited active general corrosion over the entire surface. The materials with between 7% and 9% chromium initially

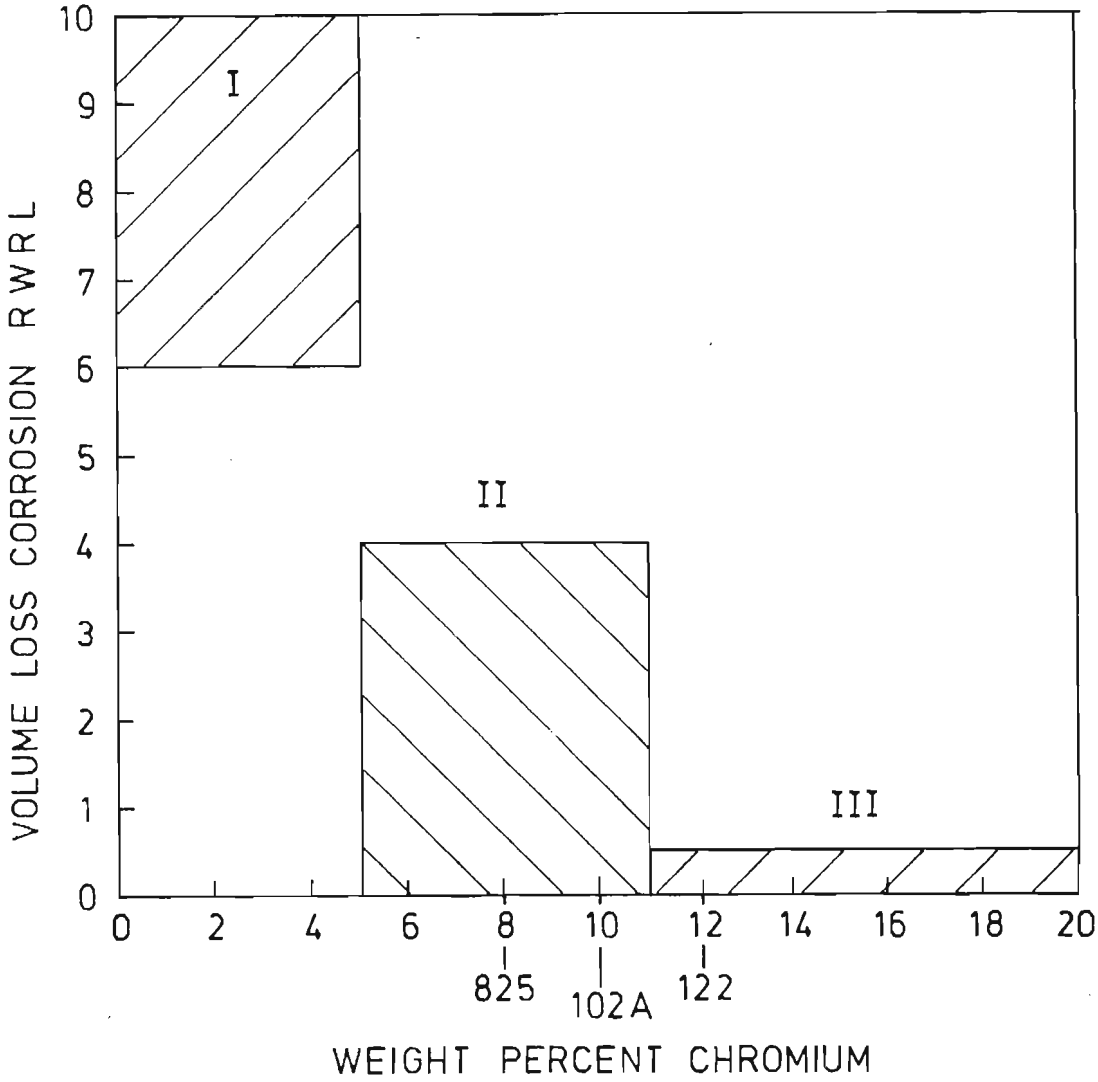

FIGURE 5.8 : The volume of material lost is dependent on the chromium content. Three types of material response are identified for the corrosion of an abraded surface at the end of an uninterrupted period of 46 hours. (Synthetic mine water was used). (Barker (1988)).

showed evidence of passivity and corroded mainly by localized anodic activity which developed into open crevices capped by oxide product. General passivity breakdown and active corrosion of the entire surface then followed. For materials with greater than 10% chromium, the localized anodic activity was more restricted. Corrosion proceeded in the form of small isolated pits and crevices. The S.E.M. micrographs of Alloys 825, 102A and 122 show that the steels generally follow this pattern (fig. 4.27).

Alloy 102A under ideal tempering conditions (a double temper at 200°C) borders on Region III and thus has a randomly stable oxide layer. Conversely, the corrosion resistance afforded by steels like Alloy 825, which fall in this transition region, is quite unstable irrespective of heat treatment. The instablility in corrosion behaviour would explain why it was very difficult to obtain reproducible results for Alloy 825.

Briefly, the results and discussion have shown that both tempering temperature and time at temperature have a significant influence on the corrosion behaviour of chrome steel because of the type and morphology of carbides precipitated after different tempering temperatures and tempering time. It should also be noted that the analyzed weight per cent chromium is not a direct indication of corrosion behaviour without a detailed knowledge of heat treatment and consequent microstructure. A model showing the effect that 12% chromium, in comparison to 8% chromium, has on the corrosion resistance has been proposed.

CHAPTER 6

CONCLUSIONS

A corrosion resistant steel will only be useful in a mining environment if it remains in the passive state during its service life. This will ensure that corrosion is maintained at a very low rate. The heat treatment that a specific alloy receives determines its mechanical as well as corrosion resistant properties. This dissertation has assessed the corrosion behaviour of the alloys designated 825, 102A and 122 after different tempering temperatures. The combination of the 0.25C 8-12Cr 2Ni + Mo steels tested and their heat treatments provides useful information about materials selection and their optimum heat treatments.

1. After tempering between 150°C and 300°C, ϵ-carbide and cementite precipitate and coarsen. This results in a softening of the material and a decrease in the corrosion rate. The predominant mode of corrosion after tempering at these temperatures is localized in the form of pitting corrosion and crevice corrosion. Although this localized corrosion contributes very little to the total volume of material lost by corrosion, it is of significance in that it is insiduous and can be precursor to environmental sensitive fracture and to a castastrophic failure. Pitting corrosion, stress corrosion cracking and corrosion fatigue are particularly serious in pipes where perforations could lead to unsafe conditions, a loss of pressure and down time while the component is being replaced.

2. After tempering above 350°C, chromium carbides begin to precipitate as very fine particles. A maximum hardness value is reached after tempering at 500°C. After tempering at higher temperatures, coarsening of the chromium carbides causes a decrease in hardness and an increase in corrosion rate. The predominant modes of corrosion after tempering at temperatures above 500°C for Alloys 825 and 102A is general and intergranular since the chromium carbides precipitate both intergranularly and intragranularly. Alloy 122 however, corroded locally after tempering at 650°C. After tempering at 700°C general corrosion as well as localized corrosion was observed in Alloy 122.

3. The corrosion rate is directly proportional to the type and morphology of carbides precipitated. After tempering at temperatures between 550°C and 650°C, the chromium carbides coarsen. This is accompanied by a zone depleted of chromium adjacent to the carbide. Coarsening of the chromium carbide results in an increase in the area depleted of chromium and thus an increase in the corrosion rate.

4. After tempering above 700°C for Alloys 825 and 102A, it is postulated that chromium goes back into solution and thus obviates chromium depletion. This results in increased corrosion resistance.

5. Increasing the chromium content proportionally from 8% to 10% to 12% increases the corrosion resistance of the alloys. A model is postulated whereby not all chromium is incorporated with carbon after tempering at higher temperatures in a steel containing 12% chromium. Thus the chromium depletion profile is less severe if there is 12% chromium than if there is 8% chromium and corrosion resistance is increased.

6. A double tempering treatment increases the corrosion resistance of a material with respect to a single tempering treatment. An explanation for this is that the probability and number of potentially active sites diminishes with double tempering conditions and thus the chromium oxide layer is more stable after double tempering than after single tempering.

7. An optimum tempering treatment for Alloys 825, 102A and 122 is a double temper at 200°C where there is maximum corrosion resistance and hardness.

8. Alloy 122 would have advantages in the mining situation where its combination of high hardness and general corrosion resistance would be of advantange.

REFERENCES

ALLEN, C., BALL, A., NOEL, R.E.J. (1984) "The Development of 3CR12 Type Steels to Resist Corrosive Abrasive Environments", Proceedings of Inaugural International 3CR12 Conference, Johannesburg, March 1984, 433-453.

ALLEN, C., PROTHEROE, B.E., BALL, A. (1981) "The Selection of Abrasion-corrosion-resistant Materials for Gold-mining Equipment", J. of S.A.I. of Mining and Metallurgy, 1981.

ASTM (1980), "Standard Reference Method for Potentiostatic and Potentiodynamic Anodic Polarisation Measurements", Annual Book of Standards, Part 10, G5 - 78, p. 816.

ATRENS, A. (1983) "Environmental Conditions Leading to Pitting/Crevice Corrosion of a Typical 12% Chromium Stainless Steel at 80°C", Corrosion-NACE, 39, p.483.

BARKER, K.C. (1988) "The Development of Abrasive-Corrosive Wear Resistance of Steels by Microstructural Control", PhD thesis, Materials Engineering Department, University of Cape Town.

BECHET, M. (1988) Pending MSc thesis.

BEE, J., PETERS, J.A., ATKINSON, M., GARRETT, G.G. (1985) "The Development of Abrasion-Corrosion Resistant Steels for Mining Applications", Paper presented at Mintek Conference, Johannesburg, May 1985.

BRIGHAM, R. (1975) "Effect of Cr on the Pitting Resistance of Austenitic Stainless Steels", Corrosion Science, 15, p.579.

CAPENDALE, A.E. (1985) "The Influence of Water Composition on the Pitting Behaviour of a Stainless Steel", MSc thesis, Materials Engineering Department, University of Cape Town.

CHADWICK, G.A. (1972) "Metallography of Phase Transformations", Butterworth and Co. (Publishers) Ltd., London.

CHANCE, R., SCHREIBER, T., FRANCIS, W. (1975) "Anomolous Effects of Temperature on the Polarization Characteristics of Type 409 Stainless Steel", Corrosion-NACE, 31, p.296.

CHARBONNIER, J., JOSSIC, T. (1983) "An Electrochemical Study of Intergranular Corrosion Related to the Chromium Depletion Mechanism in the case of 18-10 Austenitic Stainless Steels", Corrosion Science, 23, p.1191.

CHEN, W., STEPHENS, J. (1979) "Anodic Polarization Behaviour of Austentic Stainless Steel Alloys with Lower Chromium Content", Corrosion-NACE, 35, p.443.

CIESLAK, W. (1986) "The Influence of Sulphide Inclusions on the Initiation of Pits in Fe-29Ni-17Co", Corrosion-NACE, 42, p111.

CIHAL, V., HUBACKOVA, J., KUBELKA, J., MAZANEC, K. (1985) "A Study of Corrosion Electrochemical Properties of Martensite-Austenite Cri2Ni6Mo", Corrosion-NACE, 41, p.625.

COTTERRELL, M.H. (1988) "The Influence of Water Composition on the Pitting Behaviour of Newly Developed Corrosion Resistant Steels", MSc thesis, Materials Engineering Department, University of Cape Town.

DAWSON, J., FERRIERA, M. (1986) "Electrochemical Studies of the Pitting of Austenitic Stainless Steel", Corrosion Science, 26, p.1009.

DEGERBECK, J. (1973) "On Accelerated Pitting and Crevice Corrosion Tests", J.E. Electrochem. Soc, 120, p.175.

DEVINE, T., RITTER, A. (1983) "Sensitization of 12 Wt Pct Chromium, Titanium-Stabilized Ferritic Stainless Steel", Metallurgical Transactions, 14A, p.1771.

DEVINE, T., RITTER, A., DRUMMOND, B. (1981) "Influence of Heat Treatment on the Sensitization of 18Cr-2Mo-Ti stabilized Ferritic Stainless Steels", Metallurgical Transaction, 12A, p. 2063.

FLORIANOVICH, G.M. (1965) "Protection of Metals", Vol. 1., p. 131.

FLOREEN, S. (1982) "An Examination of Chromium Substitution in Stainless Steels", Metallurgical Transactions A, 13A, p.2003.

FRANKEL, G., STOCKERT, L., HUNKELER, F., BOEHNI, H. (1987) "Metastable Pitting of Stainless Steel", Corrosion-NACE, 43, p.429.

FRANKENTHAL, R., PICKERING, H. (1972) "On the Mechanism of Localized Corrosion of Iron and Stainless Steel" J. Electrochem. Soc., 119, p.1304.

GALVELE, J. (1976) "Transport Processes and the Mechanism of Pitting of Metals", J. Electrochem Soc., 123, p.464.

GREENE, N. (1962) "Predicting Behaviour of Corrosion Resistant Alloys by Potentiostatic Polarization Methods", Corrosion-NACE, 18, p.136.

GROBLER, P., MOSTERT, R. (1988) "Experience in the Laboratory and Commercial Development of Corrosion and Abrasion-Resistant Steels for the Mining Industry" ISCOR.

HARRIS, J.B. (1983) "An Investigation of Wear and the Performance of Steels in the Gold Mining Industry", MSc thesis, University of Cape Town.

HASHIMOTO, K., ASAMI, K., NAKA, M., MASUMOTO, T. (1979) "The Role of Alloying Elements in Improving the Corrosion Resistance of Amorphous Iron Base Alloys", Corrosion Science, 19, p.857.

HEINE, M.A., KERR, D.S., PRYOR, M.J. (1965) "The Specific Effects of Chloride and Sulphate Ions on Oxide Covered Aluminium", J. Electrochemical Soc., 112, p.24.

HEITZE, E., SCHWENK, W. (1976) "Theoretical Basis for the Determination of Corrosion Rates from Polarization Resistance", Br. Corros. J., 11, p.74.

HOAR, T. (1967) "The Production and Breakdown of Passivity in Metals", Corrosion Science, 7, p.341.

HOAR, T.P., MEARS, D.C., ROTHWELL, G.P. (1965) Corrosion Science, 5, p.270. As cited by Oldfield (1987).

HONEYCOMBE, R.W.K. (1981) "Steels-Microstructure and Properties", ed. Honeycombe, R.W.K., Hancock, P., Metallurgy and Materials Science Series, Edward Arnold Publishers, London.

HOSPADARUK, V., PETROCELLI, V. (1966) "The Pitting Potential of Stainless Steels in Chloride Media", J. of Electrochem. Soc., 113, p.878.

HOU, W., VAN MUYLDER, J., WINAND, R. (1983) "The Characteristics of the Pitting Corrosion of Stainless Steel Above Breakdown Potential", Corrosion Science, 23, p.1307.

HUBACKOVA, J., CIHAL, V., HULICIOUA, Z., DORDA, K., MAZANEC, K. (1984) "A Contribution to the Study of the Transformation Characteristics of type 15% Cr 6%Ni Mo Steel Under Tempering in the Intercritical Temperature Range", Acta Metallurgica, 32, p. 2131.

HULTQUIST, G., LEYGRAF, C. (1981) "Selective Oxidation of a Ferritic Stainless Steel and Its Influence on Resistance to Crevice Corrosion Initiation", Corrosion Science, 21, p.401.

JANIK-ZACHOR, M. (1981) "An Assessment of the Processes Leading to Pit Nucleation on Iron", J. Electrochem. Soc., 128, p.513.

JANIK-CZACHOR, M., SZUMMER, A., SZKLARSKA-SMIALOWSKA, Z. (1975) "Electron Microprobe Investigation of Processes leading to the Nucleation of Pits on Iron", Corrosion Science, 15, p.775.

KIESSLING, R., (1978) "Non-metallic inclusions in steel", The Metals Society, London.

KILLEEN, J., SMITH, A., WILD, R. (1976) "Chromium Depletion Profiles after preferential Removal of Chromium from Alloys", Corrosion Science, 16, p.551.

KOLOTYRKIN, J. (1961) "Effects of Anions on the Dissolution Kinetics of Metals", J. Electrochem. Soc., 108, p.209.

KRAUSS, G. (1980) "Principles of Heat Treatment of Steel", eds. Grossmann, M. and Bain, E. American Society for Metals.

KRUGER, J., RHYNE, K. (1982) "Nuclear Chemical Waste Management", 3, p.205.

LEE, K., CRAGNOLINO, G., MACDONALD, D. (1985) "Effect of Heat Treatment and Applied Potential on the Caustic Stress Corrosion Cracking of Inconel 600", Corrosion-NACE, 41, p.540.

LEE, Y., TAKEHARA, Z., YOSHIZAWA, S. (1981) "The Enrichment of Hydrogen and Chloride Ions in the Crevice Corrosion of Steels", Corrosion Science, 21, p.391.

LeROY, R. (1975) "Evaluation of Corrosion Rates from Polarization Measurements", Corrosion-NACE, 31, p.173.

LUNARSKA, E., SZKLARSKA-SMIALOWSKA, A., JANIK-CZACHOR, M. (1975) "Susceptibility of Cr-Ni-Mn Stainless Steels to Pitting in Chloride Solutions", Corrosion-NACE, 31, p.231.

MAN, H., GABE, D. (1981) "A Study of Pitting Potentials for some Austenitic Stainless Steels Using a Potentiodynamic Technique", Corrosion Science, 21, p.713.

MAN, H., GABE, D. (1981) "The Determination of Pitting Potentials", 21, p.323.

MANCIA, F., TAMBA, A. (1988) Corrosion, 44, p.88.

MANKOWSKI, J., SZKLARSKA-SMIALOWSKA, A. (1975) "Studies on Accumulation of Chloride Ions in Pits Growing During Anodic Polarization", Corrosion Science, 15, p.493.

MANNING, P. (1983) "Comparison of Several Accelerated Laboratory Tests for the Determination of Localized Corrosion Resistance of High-Performance Alloys", Corrosion-NACE, 39, p.98.

MOKKEN, A. (1979) "Pipe Maintenance and Performance in Gold and Uranium Mining", S.A. Mining and Engineering Journal,p.63.

MOREAU, R., BRISON, J. (1972). J.Men.Sci., p. 845.

NAGAKURA, S., MIROTSU, Y., KUSUNOKI, M., SUZUKI, T., NAKAMURA, Y. (1983) "Crystallographic Study of the Tempering of Martensitic Carbon Steel by Electron Microscopy and Diffraction", Metallurgical Transactions 14A, p.1025.

NARASIMHA ROA, G., THOMAS, G (1980) "Structure Property Relations and the Design of Fe-4Cr-C Based Structural Steels for High Strength and Toughness", Metallurgical Transactions, 11A, p.441.

NOEL, R.E.J. (1981) "The Abrasive-Corrosive Wear Behaviour of Metals", MSc (Eng) thesis, University of Cape Town.

NOEL, R., ALLEN, C., BALL, A. (1984) "The Development and Use of In-Situ and Laboratory Tests as a Guide to the Selection of Materials for the Gold Mining Industry".

OGURA, S., SUGIMOTO, K., SAWADA, Y. (1976) "Effects of Cu,Mo and C on the Corrosion of Deformed 18Cr-8Ni Stainless Steels in HSO/NaCl Solutions", Corrosion Science, 16, p.323.

OKADA, T. 1985) "A Theory of Perturbation-Iitiation Pitting", J. Electrochem. Soc., 132, p.537.

OLDFIELD, J. (1987) "Test Techniques for Pitting and Crevice Corrosion Resistance of Stainless Steels and Nickel-base Alloys in Chloride-containing Environments", Internationsl Materials Review, 32, p.153.

OLDFIELD, J., LEE, T., KAIN, R. (1985) "Avoiding Crevice Corrosion of Stainless Steels ", Proc. Stainless Steel '84, Chalmers University of Technology, The Institute of Metals, 1985, p.205.

PALUMBO, G., KING, P., AUST, K. (1987) "Pitting Corrosion Behaviour of Alloy 800 in Chloride-Sulphate Media", Corrosion-NACE, 43, p.37.

PARKINS, R. (1985) "Significance of Pits, Crevices and Cracks in Environment-Sensitive Crack Growth", Materials Science and Technology, 1, p.480.

PAYER, J., STAEHLE, R. (1975) "The Dissolution Behaviour of $Cr_{23}C_6$ and TiC Related to the Stainless Steels in Which They Occur", Corrosion-NACE, 31, p.30.

PESSALL, N., LIU, C. (1971) "Determination of Critical Pitting Potentials of Stainless Steels in Aqueous Chloride Environments", Electrochmica Acta, 16, p.1987.

PICKERING, F.B. (1978) "Physical Metallurgy and the Design on Steels", ed. Kelly, A., Materials Science Series, Applied Science Publishers Ltd., London.

PICKERING, H. (1983) "Characteristic Features of Alloy Polarization Curves", Corrosion Science, 223, p.1107.

PORTER, D., EASTERLING, K. (1980) "Phase Transformations in Metals and Alloys". Van Nostrand Reinhold, U.K.

POURBAIX, M. (1970) "Significance of Protection Potential in Pitting and Intergranular Corrosion", Corrosion-NACE, 26, p.431.

POURBAIX, M., DE ZOUBOV, N. (1966) Atlas of Electrochemical Equilibria, ed. Pourbaix, M., Brussels, p.97-105.

PROCTER, R., Private Communication.

PROTHEROE, B.E. (1979) "The Causes of Metallic Wear in Hard Rock Mining Conditions with Some Solutions", Paper presented at Conference of Fracture, University of Witwatersrand, Johannesburg.

PROTHEROE, B.E., BALL, A., HEATHCOCK, C.J. (1982) "The Development of Wear Resistant Alloys for the South African Gold Mining Industry", Proceeding of International Conference on Recent Development in Speciality Steels and Hard Materials, Comins, N.R. and Clarke, J.B. (eds), CSIR, Pretoria, 289-298.

RAWAT, N. (1976) "Corrosivity of Underground Mine Atmospheres and Mine Waters : A Review and Preliminary Study", Br. Corros. J., 11, p.86.

REED-HILL, R.E. (1964) "Physical Metallurgy Principles", ed Hagerty, W., D Van Nostrand Company, Inc.

ROLLASON, E.C. (1973) "Metallurgy for Engineers", Edward Arnold Publishers, London.

SATO, N. (1987) "Some Concepts of Corrosion Fundamentals", Corrosion Science, 27, p.421.

SCOTTO, V., VENTURA, G., TRAVERSO, E. (1979) "The Influence of Non-Metallic Inclusion Nature and Shape on the Pitting Corrosion Susceptibility of 18Cr9Ni and 17Cr11Ni2Mo Austenitic Stainless Steels", Corrosion Science, 19, p.237.

SEDRICKS, A.J. (1979) "Corrosion of Stainless Steels", ed. Foley, R.T., et al., The Corrosion Monograph Series, Wiley-Interscience.

SEDRICKS, A.J. (1984) "Metallurgical Aspects of Passivation of Stainless Steels", Proc. Stainless Steels '84, Chalmers University of Technology, The Institute of Metals, 1985, p. 125.

SMALLMAN, R.E. (1962) "Modern Physical Metallurgy", Butterworth and Co. (Publishers) Ltd.

STEFEC, R., FRANZ, F. (1978) "A Study of the Pitting Corrosion of Cold-Worked Stainless Steel", Corrosion Science, 18, p.161.

STERN, M., GEARY, A. (1957) "Electrochemical Polarization", J. of the Electrochem Soc., 104, p.56.

STREHBLOW, H.-H., IVES, M. (1976) "On the Electrochemical Conditions within Small Pits", Corrosion Science, 16, p.317.

SZAUER, T., JAKOBS, J. (1976) "The Pitting Corrosion of Low Alloy and Mild Steels", Corrosion Science, 16, p.945.

SZKLARSKA-SMIALOWSKA, Z. (1971) "Review of Literature on Pitting Corrosion Published Since 1960", Corrosion-NACE, 27, p.223.

TOMLINSON, W., GILES, K. (1983) "The Microstructures and Corrosion of a 0.79C Steel Tempered in the Range 100-700C", Corrosion Science, 23, p.1353.

TOUSEK, J. (1978) "The Localised Corrosion of Cr-Ni Stainless Steel", Corrosion Science, 18, p.53.

TRUMAN, J. (1976) "Corrosion Resistance of 13% Chromium Steels as Influenced by Tempering Treatments", Br. Corros. J., 11, p.92.

TRUMAN, J., PIRT, K. (1976) "Resistance to Oxidation at Elevated Temperatures of a Number of Alloy Steels", Br. Corros. J.,11, p.188.

TRUMAN, J., PIRT, K. (1979) "The Resistance of Localised Corrosion of Some Stainless Steels", Corrosion Prevention and Control, ,p.12.

TURNBULL, A. (1983) "The Solution Composition and Electrode Potential in Pits, Crevices and Cracks", Corrosion Science, 23, p.833.

VETTER, K.J., STREHBLOW, H.-H. (1970) "Localised Corrosion", ed. Staehle, R.W. et al, NACE, p.240. As cited by Oldfield (1987).

VERMILYEA, D., TEDMON, C., BROECKER, O. (1975) "Some Effects of Heat Treatment Variables on the Sensitisation of Type 304 Stainless Steel", Corrosion-NACE, 31, p.140.

WALZAK, T., SHEASBY, J. (1983) "The Effect of Heat Treatment Parameters on the Anodic Polarization Behaviour of 440C Stainless Steel", Corrosion-NACE, 39, p.503.

WANKLYN, J. (1981) "The Role of Molybdenum in the Crevice Corrosion of Stainless Steels", Corrosion Science, 21, p.211.

WILDE, B., ARMIJO, J. (1967) "Influence of Sulphur on the Corrosion Resistance of Austenitic Stainless Steels", Corrosion-NACE, 23, p.208.

WILLIAMS, D., WESTCOTT, C., FLEISCHMANN, M. (1984) "Studies of the Initiation of Pitting Corrosion on Stainless Steels", J. Electroanal. Chem., 180, p.549.

YANG, W., Ni, R., Hua, H. (1984) "The Behaviour of Chromium and Molybdenum in the Propagation Process of Localised Corrosion of Steels", Corrosion Science, 24, p.691.

APPENDIX A

ANALYSIS OF POTENTIODYNAMIC SCANS

According to the mixed potential theory for metal/electrolyte corroding systems, Wagner and Traud (as referenced in Heitz and Schwenk(1976)) showed in 1938 that there exists a simple relationship between the polarization resistance at the rest potential (free corrosion potential) and the corrosion rate. The theoretical basis together with experimental examples for the validity of the theory was published in this work. Later Stern and Geary (1957) emphasized the practical applicability of the relationship which has been given their name; it is also referred to as the linear polarization or resistance polarization method. They considered the rate equations for anodic and cathodic reactions at electrochemical equilibrium on the basis of activation control and the symmetry between the activation energies for the two processes. They found that, near the reversible potential, the applied potential and current density enhibited a closely linear relationship, which could be related to the exchange current density in terms of the Tafel slope for the process.

The ratio, the linear polarization resistance, Rp, can be related to the corrosion current density, i_{corr}, in terms of the slope βa and βc for the anodic and cathodic processes respectively according to the following relationship:

$$i_{corr} = \beta a \ \beta c / 2.3 \ (\beta a + \beta c) \ Rp$$

where i_{corr} = corrosion current density
Rp = linear polarization resistance
βa = slope of anodic process
βc = corrosion current density

The slopes of the processes are obtained as indicated in Figure A1.

i_{corr} can be defined directly at the intersection of the projections of the linear regions of the cathodic and anodic slopes (E_{corr}).

Since the resultant anodic curve reflects the combination of several different slopes caused by corrosion occurring on the changing surface in the anodic region, it is possible experimentally that the extrapolation of the linear regions of the anodic and cathodic curves will not intersect at E_{corr}. For this reason, more accurate results can be obtained by measuring i_{corr} at the point where the cathodic Tafel plot extrapolation intersects E_{corr}.

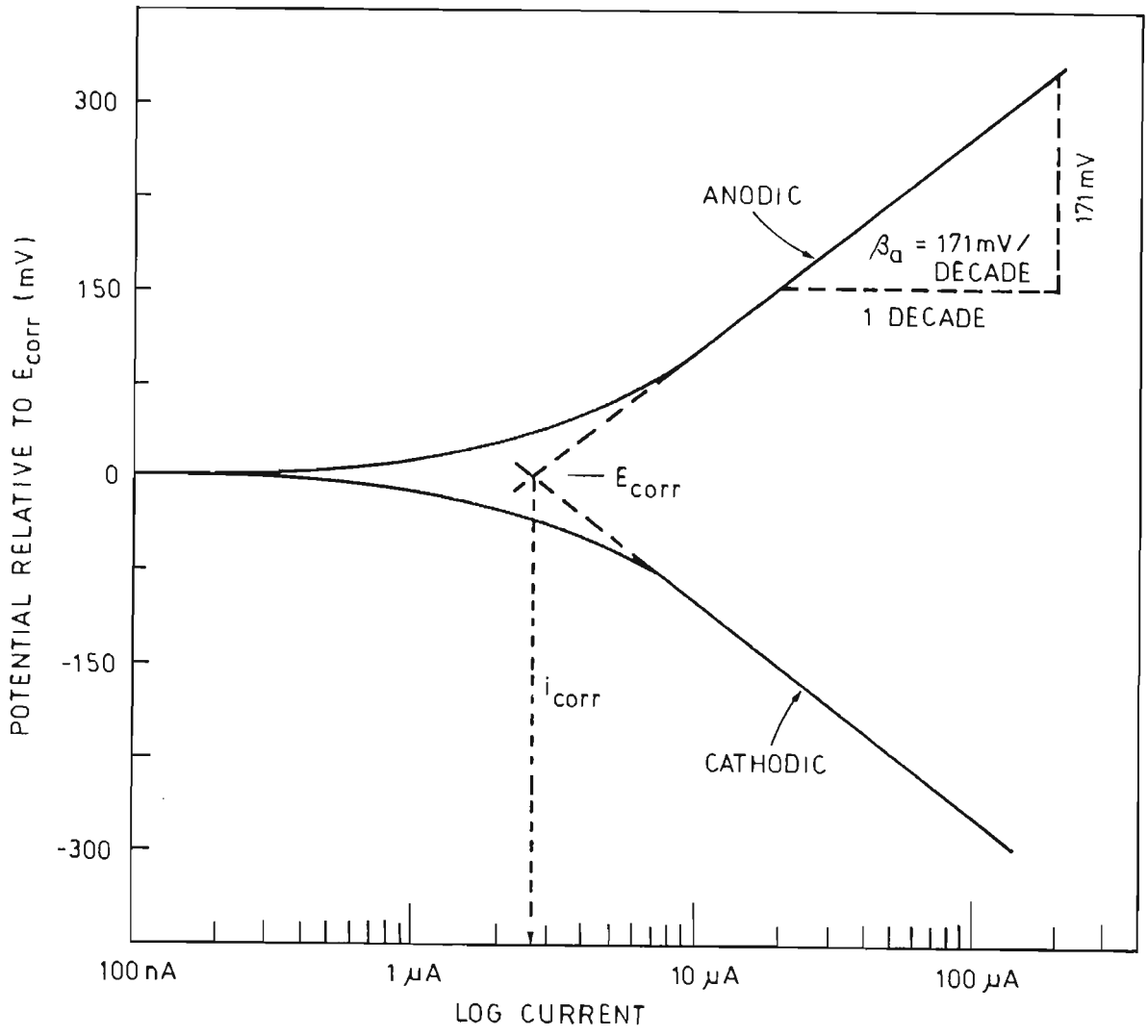

FIGURE A1 : Tafel Plot

The cathodic curve deviates from linearity due to factors such as concentration polarisation and resistance drop effects, and therefore a tangent, drawn to the cathodic curve, 50mV below E_{corr}, is used as an estimation of the linear region of the curve. (Deviation from linearity is expected up to 50mV below E_{corr}). The point of intersection of the tangent of the cathodic curve and E_{corr} defines i_{corr}. This is shown in fig. A.2.

If the material exhibits passivity, in practise the corrosion rates expected will be those associated with the behaviour of the material in the passive region. Thus values of i_{corr} obtained using the extrapolation of the cathodic curve will give corrosion rates reflecting active behaviour of this material which will differ from that found in practise. For this reason corrosion rates for those alloys are calculated using i_{pass} and not i_{corr} . i_{pass} is obtained from the intersection of the extrapolation of the slope of the passive region and E_{corr}.

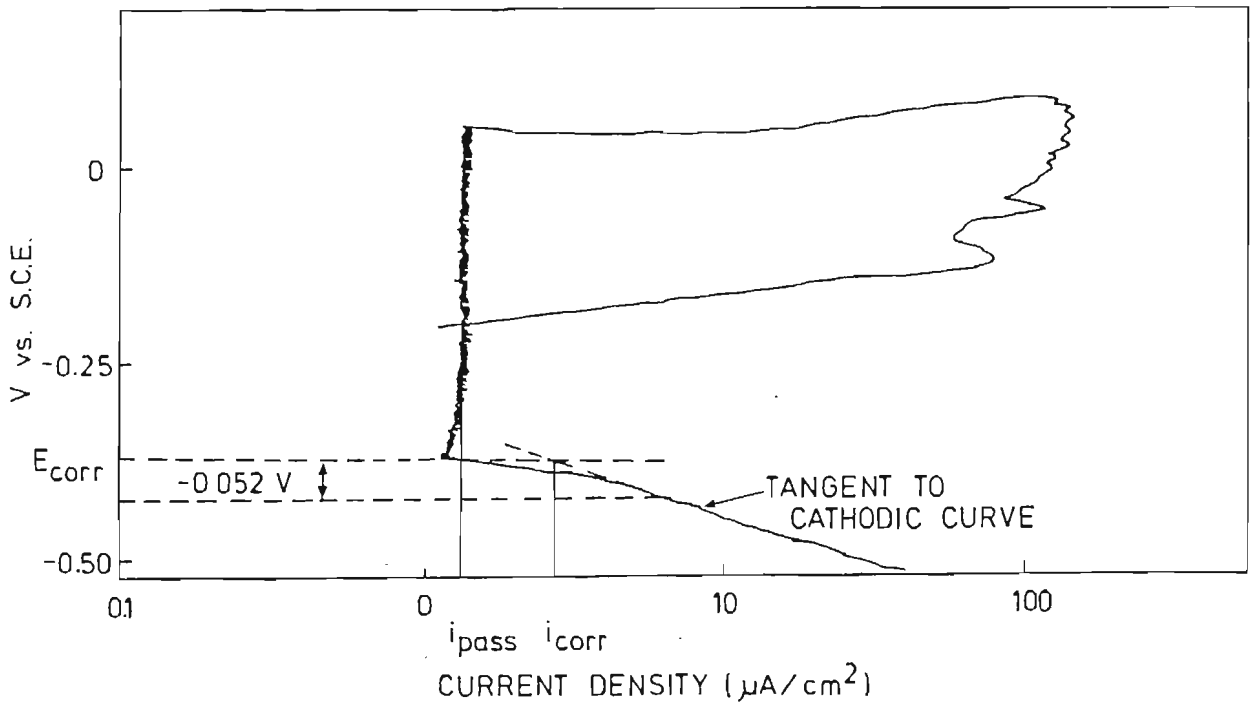

FIGURE A2 : A scan showing method of extrapolating to obtain both I_{corr} and i_{pass}

i_{corr} can then be converted into corrosion rate using Faraday's law.

According to Faraday's law:

$$Q = nFW/M$$

where Q = coulombs
n = number of electrons involved in the electrochemical reaction
F = the Farraday, 96 487 Coulombs
W = weight of electroactive species
M = molecular weight of electroactive species

From Faraday's Law:

$W = QM/nF$

Since equivalent weight (E.W.) = M/n

$W = Q \times E.W./F$

and since $Q = it$

$$W = it\ (E.W.)/F$$

therefore $W/t = i(E.W.)/F$

W/t is the corrosion rate (C.R.) in grams/second. Corrosion rate is expressed in mm/yr.

Dividing the above equation by electrode area and density gives:

$C.R.\ (cm/sec) = i(E.W.)/dFA$

After converting seconds to years, centimetres to millimetres and the Faraday (amp - sec/eq) to microamps, this becomes:

$$CR(mm/yr) = \frac{i(E.W.) \times 31.6 \times 10^7}{d\ F\ A \times 2.5 \times 10^6}$$

Expressing the terms i/A as current density and combining all the constants gives :

$$\text{Corrosion Rate (mpy)} = \frac{i_{corr} \times \text{E.W.} \times 0.0033}{d} \quad \ldots\ldots\ldots \text{equation A1}$$

where $\text{E.W.} = \dfrac{\text{volume element in alloy} \times \text{molecular weight}}{\text{valency}}$

i_{corr} = corrosion current density, A/cm^2

d = density of corroding species, g/cm^3

APPENDIX B

THE METHOD OF DETERMINING THE CHROMIUM EQUIVALENT

The most common ferrite-forming elements were used to empirically determine the chromium equivalent (Honeycombe (1981)).

$$\text{Cr equivalent} = (Cr) + 2(Si) + 1.5(Mo) + 5.5(Al) + 1.75(Nb) + 1.5\,(Ti) + 0.75(W)$$

This is demonstrated for alloy 825 where

$$\text{Cr equivalent} = 8.05 + 2(0.46) + 1.5(0.148) + 5(0) + 5.5(0.034) + 1.75(0.005) + 1.5(0.003) + 0.75(0)$$

$$= 9.392$$